Equine Endothelial Colony Forming Cells: *In Vitro* and *In Vivo* Analysis

by

Randolph Lee Winter

A Dissertation Submitted to the Graduate Faculty of
Auburn University
In Partial Fulfillment of the
Requirements for the Degree of
Doctor of Philosophy

Auburn, Alabama
August 3, 2019

Keywords: Equine, Endothelial Colony Forming Cells, Regenerative

Approved by

Anne A. Wooldridge, Chair, Professor of Clinical Sciences
Russell C. Cattley, Tyler & Frances Young Professor of Pathobiology
A. Ray Dillon, Jack O. Rash Professor of Clinical Sciences
Elizabeth A. Lipke, Mary and John H. Sanders Associate Professor of Chemical Engineering

Abstract

Endothelial colony forming cells (ECFCs) are a subset of the endothelial progenitor cell (EPC). EPCs are found in bone marrow and in peripheral blood samples, and their subset the ECFC can be isolated from these samples for use. ECFCs have a high proliferative capacity, the ability to heal damaged blood vessels, and can form *de novo* blood vessels. The ease of isolating ECFCs and the potential clinical applications of their use makes these cells an attractive therapeutic option for regenerative medicine. When used for *in vivo* studies, stem or progenitor cells may aid wound healing either directly or indirectly by paracrine mechanisms. In order to determine if equine ECFCs aid in wound healing by direct blood vessel incorporation, the ability to track cell movement and their final destination is paramount. Equine ECFCs were labeled with semiconductor quantum nanodots, and cell growth and function characteristics were then assessed. These results were used to aid study design for *in vivo* ECFC use in an equine distal limb wound model. The distal limb wound is a disease of clinical importance in equine medicine that is characterized by local ischemia, hypoxia, and poor wound healing which can lead to exuberant granulation tissue. To assess the effects of equine ECFCs on wound healing, a distal limb wound model was created in the horse. Wound healing was assessed with non-invasive analyses as well as histologic evaluation. In addition to wound healing parameters, ECFCs were labeled with fluorescent nanodots prior to injection and then

tracked with serial biopsies in order to identify their final location within the wound. Results from this and other studies show that distal limb wounds in the horse are characterized by prolonged inflammation. The effects of tumor necrosis factor alpha, a pro-inflammatory cytokine known to be present in equine distal limb wounds, were evaluated in equine ECFCs under *in vitro* conditions to understand how ECFC function is affected by this pro-inflammatory stimulus.

Acknowledgments

I thank my advisor, Dr. Anne A. Wooldridge, for her expert guidance and unwavering support throughout my research career at Auburn University. I would also like to thank my committee members, Dr. Elizabeth Lipke, Dr. Ray Dillon, Dr. Russell Cattley, and University Reader, Dr. Dean Schwartz for their time and knowledge in the preparation and critical review of this manuscript. I would also like to thank Mrs. Qiao Zhong, whose help and advice were critical for my research success. I would like to express my appreciation to Dr. Wen Seeto, Dr. Jey Koehler, Dr. David Pascoe, Dr. Fred Caldwell, Dr. Ashley Sharpe, Dr. Claudia Reyner, Yuan Tian, Kelly Himeback, Rachel Pfeifle, Kaitlyn Bello, and Caroline Parker for doing research together.

My professional and research career would not be possible without the love and support of my wife, Dr. Amanda R. Taylor. She and our perfect daughter, Giva O. Winter, have been and continue to be my motivation to aim for perfection. With them, I find it.

Table of Contents

List of Figures

List of Tables

List of Abbreviations

Ab	Antibody
ANOVA	Analysis of variance
BSA	Bovine serum albumin
CD	Cluster of differentiation
C_H	Number of cells at the time of subculture
CPDL	Cumulative population doubling level
C_S	Number of cells seeded
CLI	Critical limb ischemia
CXCR	Chemokine receptor
DAPI	4',6-diamidino-2-phenylindole
DiI-Ac-LDL	I,I-dioctadecyl-3,3,3',3'-tetramethlyindocarbocyanine perchlorate-acetylated low-density lipoprotein
DiO-Ac-LDL	3,3'-dioctadecyloxacarbocyanine-acetylated low-density lipoprotein
DMEM	Dulbecco's Modified Eagle Medium
ECFC	Endothelial colony forming cell
ECFC/MS	ECFCs encapsulated into PEG-fibrinogen microspheres
ECM	Extracellular matrix
EDTA	Ethylenediamine tetra-acetic acid
EGT	Exuberant granulation tissue
EPC	Endothelial progenitor cell
Fb	Fibrinogen

FBS	Fetal bovine serum
FFPE	Formalin fixed paraffin embedded
GFP	Green fluorescent protein
GLM	Generalized linear model
GS	Granulation scores
H&E	Hematoxylin and eosin
HLA-DR	Human leukocyte antigen-D related
IBA1	Ionized calcium-binding adapter molecule 1
IF	Immunofluorescence
IHC	Immunohistochemistry
IL	Interleukin
MMC	Mitomycin C
MRI	Magnetic resonance imaging
MS	Microspheres
MSC	Mesenchymal stem cell
NCD	Number of cell doublings
OCT	Optimal cutting temperature
P	Passage
Pax-5	Paired box protein 5
PBS	Phosphate buffered saline
PDT	Population doubling time
PDMS	Polydimethylsiloxane
PEG	Poly(ethylene glycol)

PEGDA	Poly(ethylene glycol) coupled with diacrylate
QD	Semiconductor quantum nanodots
ROI	Region of interest
SD	Standard of deviation
SPIO	Superparamagnetic iron oxide particles
TGF-β1	Transforming growth factor-beta 1
TNF-α	Tumor necrosis factor-alpha
UEA-1	*Ulex europeaus* agglutinin-1
VEGFR-2	Vascular endothelial growth factor receptor - 2
vWF	von Willebrand factor
WSA	Wound surface area

Chapter 1: Literature Review

1.1 Endothelial colony forming cells

Cell Definition – Surface Marker Expression

Endothelial progenitor cells (EPCs) are a population of cells that have been isolated both from bone marrow and from peripheral blood samples (Asahara et al., 1997; Medina et al., 2017). They originate in the bone marrow or within the lining of blood vessels, may be released from the bone marrow in response to local growth factors, and home to areas of blood vessel damage (Asahara et al., 1997; Medina et al., 2017). There have been many studies regarding how best to identify EPCs and their subset populations, the early-outgrowth EPC and the late-outgrowth EPC, sometimes with conflicting results. Late-outgrowth EPCs are also known as endothelial colony forming cells (ECFCs). EPCs were first described as cells which were isolated from peripheral blood samples, adherent to fibronectin-coated cell culture wells, and expressed CD34, CD31, vascular endothelial growth factor receptor 2 (VEGFR2), Tie-2, or E-selectin (Asahara et al., 1997). These cell surface markers are typically found on progenitor cells or endothelial cells, and therefore this specific combination of cell surface markers have been speculated by some to identify the EPC (Asahara et al., 1997; Medina et al., 2010; Pelosi et al., 2014). The cell surface markers CD34 and CD45 are thought to indicate a hematopoietic stem and progenitor cell population (Asahara et al., 1997; Case et al., 2007; Patel et al., 2016). Cells isolated from peripheral blood that express CD34 can be separated into distinct subpopulations, including EPCs and hematopoietic low and high proliferative potential colony forming

cells (Case et al., 2007). The evaluation of additional cell surface markers is used to further define each population, with cells that are CD34+ / CD45+ considered hematopoietic progenitor cells that do not have the capability for endothelial cell function (Case et al., 2007; Richardson and Yoder, 2011). The cell surface marker CD45 is also known as the common leukocyte antigen, and this is expressed on the majority of nucleated blood cells in circulation (Yoder et al., 2007). Expression of CD45 was observed in 94% of the freshly isolated cells in Asahara's original description of EPCs, but after 7 days in culture these cells became CD45- (Asahara et al., 1997). CD133 is another marker of stem and progenitor cells which has been used to identify this population (Case et al., 2007; Richardson and Yoder, 2011).

A combination of progenitor cell and endothelial cell surface markers have been used to help identify EPCs. The cell surface markers of CD31, von Willebrand factor (vWF), VEGFR-2, Tie-2, and E-selectin are all endothelial cell related markers that may help identify EPCs (Asahara et al., 1997; Kovacic et al., 2008; Richardson and Yoder, 2011). Additional mature endothelial cell surface markers studied include CD144 and CD105 (Richardson and Yoder, 2011; Timmermans et al., 2009). The cell surface marker CD31, also called platelet endothelial cell adhesion molecule 1, is found on the surface of endothelial cells but also on platelets and monocytes (Newman, 1994). The receptor VEGFR-2 is essential for the development of embryonic blood islands, a precursor for the onset of hematopoiesis and vasculogenesis, which is found on cells of endothelial lineage (Choi et al., 1998). The Tie-2 gene encodes a tyrosine kinase receptor, which is one of several tyrosine kinase receptors prominently involved in the development of endothelial cells and essential to the formation of blood vessel networks

(Sato et al., 1995). E-selectin is known as CD62E and is expressed almost exclusively on endothelial cells, with upregulation of expression occurring during activation of endothelial cells (Telen, 2014). Although there are many different endothelial-specific cell markers that can be utilized, not all cells described as EPCs demonstrate consistent positive staining with each of these markers.

Defining which cells are EPCs initially involves describing the cell surface markers positive staining characteristics, utilizing various combinations of the markers listed above. However conflicting reports of positive staining characteristics of EPCs exist, so another important aspect for characterizing the EPC is the cell surface marker negative staining characteristics. There are some reports that EPCs should not express CD45, however other reports refute this (Case et al., 2007; Timmermans et al., 2009). In part, this discrepancy may be related to the challenge of identifying early-outgrowth EPCs vs ECFCs based on cell surface markers. One study demonstrated that cells with a CD34+ / CD45+ / CD133+ profile had characteristics of early-outgrowth EPCs, whereas cells with a CD34+ / CD45- / CD133- profile also expressed VEGFR-2 and had ECFC characteristics (Timmermans et al., 2009). Most reports suggest the EPCs and their subset ECFCs do not express CD14, as CD14 is a peripheral blood monocytic cell marker (Kovacic et al., 2008; Timmermans et al., 2009). However the EPC subset early-outgrowth EPCs and a similar cell the endothelial colony forming unit cell do stain positive for CD14 (Kovacic et al., 2008; Yoder et al., 2007). There is also evidence that equine ECFCs express CD14 (Salter et al., 2015). In the study that initially characterized ECFCs in the horse, 83% of the ECFCs isolated expressed CD14 (Salter et al., 2015).

ECFC Identity – Cell Morphology and Function

To define and accurately identify the EPC subset populations, the early-outgrowth EPC and the ECFC, more information than simply the cell surface marker staining characteristics must be obtained. ECFCs are also defined by *in vitro* growth and function characteristics. The ECFC is typically observed as an adherent colony in cell culture flasks (Figure 1) anywhere from one to three weeks in standard cell culture conditions (Kovacic et al., 2008; Minami et al., 2015; Mukai et al., 2008; Sieveking et al., 2008). ECFCs have a cobblestone morphology when present as a monolayer in cell culture flasks and will stop proliferating with contact of nearby cells, a process called contact inhibition (Kovacic et al., 2008). Early-outgrowth EPCs by comparison are typically isolated within 3 - 7 days in standard cell culture conditions, and their morphology is described as spindle-shaped cells clustered around more rounded cells centrally (Kovacic et al., 2008; Timmermans et al., 2009). The early-outgrowth EPC also has a limited expansion capability *in vitro*, whereas the ECFC has a high expansion capability *in vitro* (Richardson and Yoder, 2011; Timmermans et al., 2009). Other cell function characteristics can be used to help identify the ECFC. Cell binding and uptake of the lectin *Ulex europeaus* agglutinin-1 (UEA-1) and low density lipoprotein have been used to identify the EPC, but neither necessarily helps to differentiate the early-outgrowth EPC from the ECFC (Choi et al., 1998; Richardson and Yoder, 2011). The binding of UEA-1 lectin is not specific to endothelial cells, and this binding can occur even with certain epithelial cells or certain hematopoietic cells such as platelets (Baldus et al., 1994; Richardson and Yoder, 2011). This is particularly relevant to the intended isolation of ECFCs, as platelet microparticles are commonly

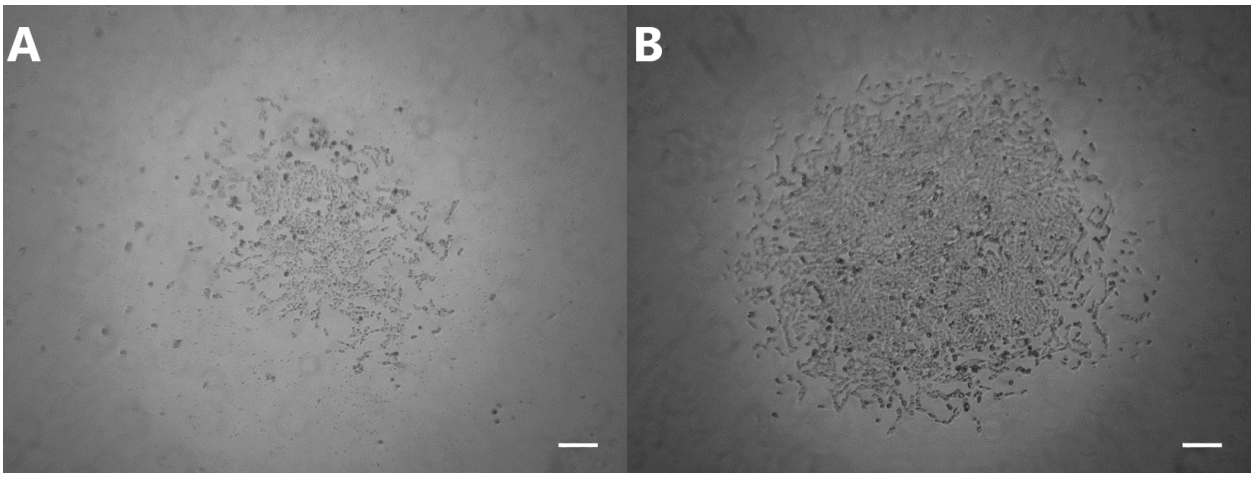

Figure 1. Appearance of ECFC colonies in cell culture flasks during isolation.
A) Representative photomicrograph of a newly-developing ECFC colony in a cell culture flask 7 days after peripheral blood sampling from a horse. B) Representative photomicrograph of a mature ECFC colony in a cell culture flask, 1 day after the image shown in (A). Scale bars are 100 μm.

found in EPC cell cultures (Prokopi et al., 2009). These microparticles contain platelet proteins such as CD31 and vWF, and they also have the ability to bind UEA-1 (Prokopi et al., 2009). Even low density lipoprotein uptake, which is considered an endothelial-specific function, may occur in non-EPC monocytes cultured in endothelial medium, as this cell culture environment has been shown to cause considerable phenotypic overlap between monocytes and EPCs (Schmeisser et al., 2001; Schmeisser et al., 2003). Both early-outgrowth EPCs and ECFCs have the ability to bind and uptake low density lipoprotein.

Arguably the function most specific to the ECFC is its ability to form new blood vessels or incorporate into existing, damaged blood vessels (Minami et al., 2015; Richardson and Yoder, 2011). A surrogate test to evaluate new blood vessel formation ability is the *in vitro* tubule formation assay performed on basement membrane matrix (BD Matrigel Basement Membrane Matrix, BD Biosciences, Bedford, MA, USA). For this assay, cells are cultured on basement membrane containing matrix under standard cell culture conditions. Cells which form organized tubules (sometime referred to as capillary-like) along the surface of the medium are considered ECFCs (Minami et al., 2015; Mukai et al., 2008; Pelosi et al., 2014; Richardson and Yoder, 2011). However, these results are not unique to ECFCs. Human monocytes, which express both endothelial and macrophagocytic cell surface markers, form tubule-like structures on basement membrane matrix after culture in endothelial culture medium (Schmeisser et al., 2001). Similar results have been found for mesenchymal stem cells isolated from mouse kidneys, where *in vitro* capillary networks develop on basement membrane matrix after these cells were cultured in endothelial medium (Chen et al., 2008).

ECFC Function – In Vivo Evaluation

The ability to form tubules *in vitro* suggests that ECFCs have the ability to form new blood vessels *in vivo*. This has been confirmed by several studies. In Asahara's original work with EPCs, his group demonstrated incorporation of these cells at areas of experimentally-induced ischemia where subsequent active angiogenesis was observed (Asahara et al., 1997). Another study utilizing a hind limb model of ischemia found that ECFCs injected near the site of ischemia migrated to the ischemic areas, increased new capillary formation and therefore blood flow, and also directly incorporated into existing blood vessels (Minami et al., 2015). When early-outgrowth EPCs were injected, new capillary formation was observed but significantly less so than in ECFC treated limbs (Minami et al., 2015). Additionally, direct incorporation into blood vessels was not observed histologically leading the authors to speculate that early-outgrowth EPCs participated via paracrine mechanisms (Minami et al., 2015).

Equine ECFCs

Cells that have the ability to promote neovascularization *in vivo* by differentiating into mature endothelial cells and directly incorporating into newly formed blood vessels are best described as ECFCs (Medina et al., 2017; Pelosi et al., 2014; Timmermans et al., 2009). To date, this evaluation has not been performed for equine ECFCs. In the two studies published on equine ECFC isolation, the time for colony emergence *in vitro* ranged from 6 – 14 days after peripheral blood sampling (Salter et al., 2015; Sharpe et al., 2016). Cells from these colonies consistently had a cobblestone morphology and

formed a confluent monolayer with evidence of contact inhibition. These cells expressed vWF, VEGFR-2, and CD34 (Salter et al., 2015; Sharpe et al., 2016), and between 83 – 98% of them expressed CD105 and CD14 in flow cytometric analysis (Salter et al., 2015; Sharpe et al., 2016). Acetylated low density lipoprotein uptake was described as occurring in 61 – 75% of these cells, and they all formed prominent and extensive *in vitro* tubules (Figure 2) after 5 – 24 hr of culture on basement membrane matrix medium (Salter et al., 2015; Sharpe et al., 2016). In many studies, cells that express CD14 are not considered ECFCs (Medina et al., 2017; Pelosi et al., 2014). However, surface marker expression has some variation among species; equine mesenchymal stem cells (MSCs) express CD14 even though MSCs from other species do not (Hackett et al., 2011). Using all available data, our group has concluded that the cells previously described and used for the experiments described in this document are ECFCs. However evaluation of the ability of these cells within *in vivo* environments to participate directly in neovascularization is warranted.

1.2 Clinical uses of ECFCs

ECFC Use – Hind Limb Ischemia Models

Based on their ability to heal damaged or form new blood vessels and their high proliferative capacity, ECFCs may be ideal for *in vivo* clinical therapy for diseases with ischemia or vascular damage

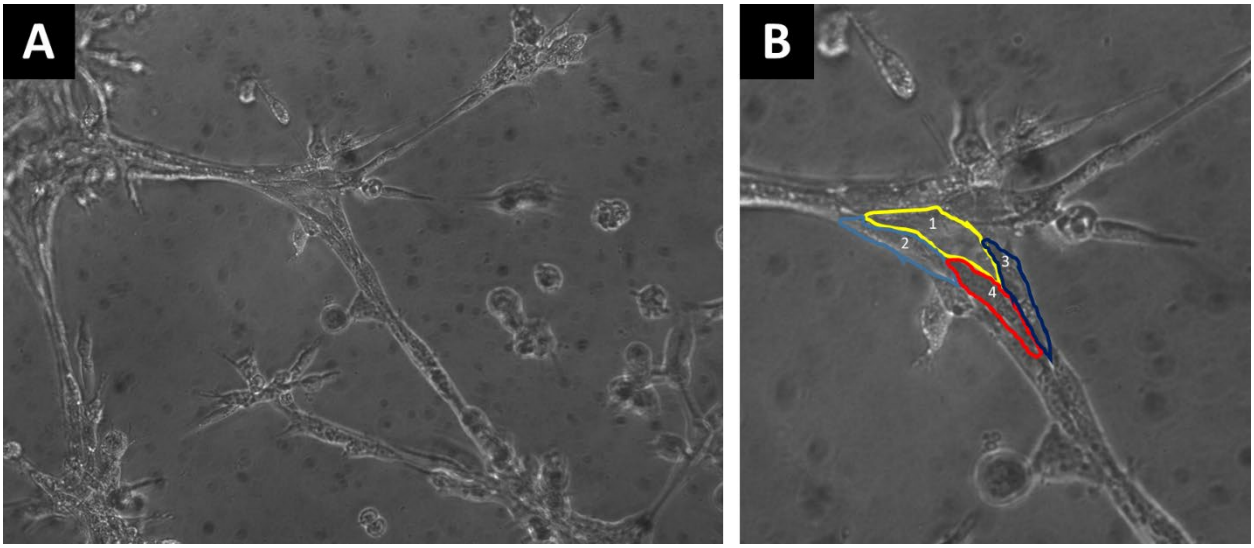

Figure 2. Equine ECFCs forming multicellular tubules *in vitro*. A) Representative photomicrograph of equine ECFCs joining to form tubules *in vitro* on basement membrane matrix medium. B) Magnified view of the cells seen in (A), with individual ECFCs outlined and numbered highlighting the multicellularity of these tubules.

(Garbuzova-Davis et al., 2017; Kim et al., 2016; Patschan et al., 2016; Pias-Peleteiro et al., 2017). Use of ECFCs for *in vivo* applications began on animal models characterized by vascular damage or ischemia (Asahara et al., 1997; Garbuzova-Davis et al., 2017; Pelosi et al., 2014). A unilateral hind limb ischemia mouse model was created by surgically ligating one femoral artery, and DiI-Ac-LDL-labeled ECFCs that were subsequently injected into the tail vein were found to be integrated into capillary vessel walls of the neovascularized hind limb tissue from one to six weeks after injection (Asahara et al., 1997). A similar finding was reported in the same study with a rabbit hind limb unilateral ischemia model, where DiI-Ac-LDL labeled ECFCs were localized exclusively to the neovascular zones of the affected limb and demonstrated incorporation into the capillary walls four weeks after injection (Asahara et al., 1997). Another study utilizing a mouse model of unilateral hind limb ischemia found that ECFCs injected into the left ventricular lumen shortly after femoral artery ligation significantly increased the perfusion to the affected leg 14 and 21 days after ligation as measured by a laser doppler perfusion image analyzer (Hur et al., 2004). By day 21, the blood flow to both hind limbs was very similar in groups treated with ECFCs. Of note, the mice treated with early-outgrowth EPCs regained a similar degree of blood flow to the affected hind limbs as those treated with ECFCs (Hur et al., 2004). The histologic assessment of new blood vessel formation was not performed in that study. However the functionality of *in vivo* ECFC-derived blood vessel formation has been documented. Using an *in vivo* vasculogenesis assay where investigators injected a mixture of cells and liquid basement membrane matrix into the subcutaneous tissue of mice, newly formed blood vessels derived from ECFCs were shown histologically to

have luminal structures containing erythrocytes (Melero-Martin et al., 2008). This demonstrated that ECFC-derived blood vessels were functional and anastomosed with existing vascular structures (Melero-Martin et al., 2008). In this study, the greatest quantity of functional, newly-formed blood vessels was observed when a combination of ECFCs and MSCs were injected together, where ECFCs remained on the luminal aspect of the blood vessels and the MSCs remained in a perivascular location around the ECFC-derived lumens (Melero-Martin et al., 2008).

ECFC Use – Disease Models without Hind Limb Ischemia

Disease models characterized by vascular damage unrelated to limb ischemia have also been studied to understand the potential benefits of EPC or ECFC therapy (Cahoon et al., 2015; Hendrickx et al., 2010; Huang et al., 2013; Kim et al., 2016; Lee et al., 2014; Zhang et al., 2013). Diabetic retinopathy has been studied using a mouse model characterized by compromised endothelial and pericyte integrity, decreased capillary density, and a breakdown of the blood-retinal barrier (Cahoon et al., 2015; O'Neill et al., 2018). Mice that received intra-vitreal ECFCs had improved retinal vascular density and integrity, decreased blood vessel permeability, decreased inflammation, and an improved neurophysiological response compared to control mice. These effects were enhanced with the addition of a bioengineered angiopoietin-1, a vascular growth factor (Cahoon et al., 2015). Vascular injury is also observed in mouse models of traumatic brain injury and myocardial infarction (Kim et al., 2016; Lee et al., 2014). Intravenous injections of ECFCs in mice with traumatic brain injuries caused reversal of neurologic disability compared to mice without ECFC treatment (Zhang et

al., 2013). ECFCs were observed at the site of brain injury after only 24 hr, and local microvessel density was improved in these areas (Zhang et al., 2013). Similar results were observed using the same disease model but with intra-cerebroventricular injections of ECFCs, and this method of ECFC delivery was associated with even greater neurologic improvements (Huang et al., 2013). ECFCs injected in mouse models of myocardial infarction improve global cardiac function, enhance capillary density at the infarction site, decrease myocardial fibrosis, and increase local production of angiogenic cytokines (Kim et al., 2016; Lee et al., 2014). ECFCs also incorporate into neo-vessels and promote a decrease in infarct size in pig models of myocardial infarction (Dubois et al., 2010). Even dermal wounds in mice treated with ECFCs show cell incorporation into blood vessels which promotes wound healing (Hendrickx et al., 2010).

Clinical Use of ECFCs in Humans – Limb Ischemia

Therapeutic uses of EPCs and ECFCs have been studied in humans with naturally occurring diseases characterized by limb ischemia (Arici et al., 2015; Kawamoto et al., 2009; Kinoshita et al., 2012). Peripheral artery disease has a prevalence of around 3 – 10% in the total human population, and the prevalence increases further with advancing age (Norgren et al., 2007). The worst clinical outcome of peripheral artery disease is a condition known as critical limb ischemia (CLI), which often leads to gangrene and partial limb amputation (Arici et al., 2015; Norgren et al., 2007). In one study of 8 human patients with CLI, intramuscular injections of autologous EPCs (defined as CD133+ / CD34+ / VEGFR-2+ / CD45- cells isolated from

peripheral blood samples) improved resting pain scores significantly, which is thought to be a surrogate suggesting improved perfusion of the leg muscles (Arici et al., 2015; Norgren et al., 2007). Seventy-five percent of these patients had complete healing of their wounds and improved mobility, whereas 2/8 patients did not have a favorable response and ultimately required major amputation (Arici et al., 2015). Another study evaluated autologous EPCs (defined as CD34+ / CD45- cells isolated from peripheral blood samples with endothelial cell culture enrichment) as a treatment for CLI in 17 human patients for a phase I/IIa clinical trial (Kawamoto et al., 2009). Twelve weeks after multiple, local, intramuscular injections in the affected limbs, all patients experienced a decrease in pain level, increase in pain-free walking distance, and a decrease in ischemic ulcer size (Kawamoto et al., 2009). Long-term evaluation of these patients was also encouraging. Only one patient required a minor amputation at week 104 (Kinoshita et al., 2012). The number of patients without clinical signs attributable to CLI was 88.2% at week 104, 92.3% at week 156, and 84.6% at week 208 (Kinoshita et al., 2012). These results represent significant improvements in local blood flow in a disease process which has a major amputation rate of 50% at one year after diagnosis of CLI (Arici et al., 2015). Another important aspect of CLI treatment involves recanalization of peripheral artery occlusions. One study assessed the peripheral arterial blood flow characteristics of patients with CLI using computed tomography angiography (Mutirangura et al., 2009). Six patients had autologous ECFCs (defined as CD34+ / CD133+ / VEGFR-2+ / Tie-2+ / CD144+ / CD31+ / vWF+ cells isolated from peripheral blood samples which had positive uptake of acetylated low density lipoprotein and formed *in vitro* tubules) injected intramuscularly in affected limbs, and then a repeat

computed tomography angiographic study was performed three months after the baseline study. Five of the six patients had a significant increase in arterial blood flow, with three patients demonstrating recanalization of the previously occluded artery and two additional patients demonstrating enhanced collateral circulation to the affected limb (Mutirangura et al., 2009).

Clinical Use of ECFCs in Humans – Vascular Damage Unrelated to Limb Ischemia

Evaluation of naturally occurring diseases in humans characterized by vascular damage unrelated to limb ischemia is limited. Early clinical trials utilizing EPCs or ECFCs focused on treating patients with acute myocardial infarction, however after multiple clinical trials there have been mixed results (Michler, 2018). ECFCs were used in a clinical trial for end-stage liver cirrhosis in humans (D'Avola et al., 2017), a disease in part characterized by dysfunctional hepatic endothelial cells and perivascular fibrosis (Zhou et al., 2014). In this clinical trial, patients had autologous ECFCs (defined as CD133+ / CD34+ / VEGFR-2+ / CXCR4+ / vWF+ cells isolated from peripheral blood that formed tubules *in vitro* and had acetylated low density lipoprotein uptake) delivered directly into the hepatic artery. Ninety days after ECFC injection, liver function tests showed improvement with a slight decrease in severity of portal hypertension (D'Avola et al., 2017). Endothelial damage and dysfunction are also prominent components of pulmonary arterial hypertension. Autologous, intravenously injected ECFCs (defined as CD144+ / VEGFR-2+ / CD34+ / CD133+ cells isolated from the peripheral blood that had positive uptake of acetylated low density lipoprotein) caused significant improvements in clinical signs and pulmonary hemodynamic parameters in adult and

pediatric patient populations compared to traditional medical treatment alone (Yang et al., 2013). These beneficial effects were thought to occur from reversal of pathologic vascular remodeling (Yang et al., 2013). In addition to the CLI-related ulcer wounds described above, ECFCs have been shown to aid healing of traumatic bone injuries (Vasyliev et al., 2017). Devitalized allogeneic bone scaffolds were combined with autologous ECFCs (defined as CD105+ / CD73+ / CD105+ / CD34+ / CD45- / HLA-DR- cells that formed *in vitro* tubules) prior to transplantation, and new bone growth with increased local bone integrity was observed in over 90% of the patients in that study (Vasyliev et al., 2017).

Although the methods to define cells as EPCs or ECFCs differ amongst these and other clinical trials for human patients, the results thus far are promising. A more uniform characterization of cells used in clinical trials may be of benefit in the future (Keighron et al., 2018; Medina et al., 2017). The utility of ECFC therapy for diseases with vascular damage and ischemia has been demonstrated, in both disease models and naturally occurring disease states classified as wounds (Hendrickx et al., 2010; Vasyliev et al., 2017). Although not studied in humans due to its rarity in the human population, distal limb wounds with excessive granulation tissue occur commonly in horses and are fraught with complications. Keloids are an analogous wound that occurs in human patients, and both keloids in humans and distal limb wounds in the horse are characterized by excessive fibroproliferation and poor wound healing. The equine distal limb wound is a disease process which involves ischemia and vascular damage, and this condition may also benefit from ECFC therapy.

1.3 Pathophysiology of equine distal limb wounds

Normal Wound Healing

Wound healing of the skin is typically described in terms of four phases, each of which has a specific process yet is also inter-woven with the other phases (Portou et al., 2015). The four phases of wound healing are: coagulation, inflammation, proliferation, and remodeling. After traumatic damage to the skin, the coagulation phase is characterized by hemostasis of the damaged area with local vasoconstriction, platelet aggregation, and subsequent formation of a fibrin clot (Guo and Dipietro, 2010; Portou et al., 2015). This clot releases multiple pro-inflammatory cytokines and growth factors, such as platelet-derived growth factor, fibroblast growth factor, and transforming growth factor beta (Dipietro, 1995; Guo and Dipietro, 2010). These cytokines help to facilitate the initiation of the inflammatory phase.

The inflammatory phase is characterized by migration of neutrophils from the peripheral blood to the site of injury within minutes and the presence of chemokines / cytokines (Portou et al., 2015). The early arrival of neutrophils is important for clearance of cellular debris and bacteria. After this early part of the inflammatory phase, monocytes are recruited to the wound and differentiate to become mature macrophages. Macrophages are the predominant inflammatory cell type in the wound by day three to five, and these cells perform clearance of apoptotic cells, tissue debris, and microbial invaders (Dipietro, 1995). Macrophages also help with debridement of devitalized tissue by releasing proteases and metalloproteinase enzymes (Dipietro, 1995). As macrophages begin to clear apoptotic cells including early neutrophils, they experience a phenotypic change and begin stimulating fibroblast and keratinocyte

growth as well as angiogenesis via release of keratinocyte growth factor, TGF-b, and vascular endothelial growth factor (Guo and Dipietro, 2010; Portou et al., 2015). Infiltration of T-lymphocytes occurs next, and this marks the last part of the inflammatory phase and simultaneous initiation of the proliferation phase. T-lymphocytes exert a regulatory effect on inflammation and formation of fibrosis (Jameson and Havran, 2007).

Formation of granulation tissue occurs during the proliferation phase. Migration and proliferation of dermal fibroblasts and their differentiation into myofibroblasts occur as inflammation subsides (Portou et al., 2015). Fibroblasts produce extracellular matrix such as type III collagen, and endothelial cells migrate into this newly formed extracellular matrix to form new capillaries (Dipietro, 1995; Guo and Dipietro, 2010). Myofibroblasts, identified as staining positive for the protein alpha smooth muscle actin, contribute to wound contraction (Dipietro, 1995; Portou et al., 2015). Bone marrow-derived mesenchymal stem cells and EPCs are thought to migrate to the wound during this phase and contribute to wound healing (Guo and Dipietro, 2010). Epidermal keratinocyte migration is initiated by local cytokines and production of proteases, and then proliferation and differentiation occur to cover the granulation tissue in a process called re-epithelialization (Guo and Dipietro, 2010; O'Toole, 2001; Portou et al., 2015).

The fourth phase of wound healing is the remodeling phase, characterized by a reduction in wound inflammation and granulation (Portou et al., 2015). The type III collagen produced by fibroblasts during the proliferation phase is replaced by type I collagen with the aid of collagenases and matrix-metalloproteinases (O'Toole, 2001; Portou et al., 2015). This reorganization of the extracellular matrix occurs alongside regression of newly formed capillaries as the wound requirement for nutrients begins to

decrease (Dipietro, 1995; Portou et al., 2015). Collagen becomes more organized, and the extracellular matrix begins to more closely resemble that of normal skin (Guo and Dipietro, 2010). Differentiation of keratinocytes leads to keratin production as the epidermal barrier is restored (Portou et al., 2015; Usui et al., 2008). This phase may take weeks to months.

Wound Healing in Equine Distal Limbs

Equine dermal wounds on the distal limb may have poor and incomplete healing. This is not observed in ponies, which have a stronger initial inflammatory response when compared to horses for distal limb wounds (Wilmink et al., 1999). Despite an initial weaker inflammatory response compared to ponies, horses have a prolonged duration of inflammation which may contribute to a prolonged proliferation phase of wound healing (Wilmink et al., 1999). Perhaps for these reasons, ponies are also much more likely to heal more rapidly or have successful primary closure of distal limb wounds compared to horses (Bertone et al., 1985; Wilmink et al., 2002). When compared to dermal wounds on the body, equine distal limb wounds have significantly lower local oxygen saturation levels acutely which may also promote poor wound healing (Celeste et al., 2011). Many other differences exist in wound healing characteristics between body wounds and distal limb wounds in the horse, but there is a stronger and shorter duration of inflammation in body wounds (Wilmink and van Weeren, 2005). Ultimately, there are many contributing factors for the development of poor wound healing in the equine distal limb, and this often leads to formation of exuberant granulation tissue (EGT).

Granulation tissue is an important aspect to wound healing, but when fibroproliferative granulation tissue protrudes above the skin edges it is defined as exuberant and can cause delayed wound healing (Bertone, 1989). EGT is very fibrous and can result in large masses (Maher and Kuebelbeck, 2018). Further, EGT may require surgical resection, sometimes repeatedly, in order for wound contraction and epithelialization to occur (Theoret and Wilmink, 2013). Myofibroblasts are a prominent presence in wounds with normal healing and in those with EGT, however a marked lack of myofibroblast organization is noted in wounds with EGT (Theoret and Wilmink, 2013; Wilmink et al., 1999). This abnormal and disorganized orientation may suggest that a deficient contractile ability exists in wounds that develop EGT (Theoret and Wilmink, 2013). Persistent inflammation may also cause a deficient contractile ability in these wounds (Wilmink and van Weeren, 2005). Epithelial hyperplasia exists at the wound edges, and yet there is slowed epithelial migration and lack of epithelialization of the wound (Theoret and Wilmink, 2013). These findings characterize EGT in the horse. The characteristic predisposing factors leading to EGT in the horse include abnormal inflammation, local hypoxia and ischemia, lack of epithelialization, and abnormal vasculature (Maher and Kuebelbeck, 2018; Wilmink and van Weeren, 2005).

The acute inflammation observed in distal limb wounds of horses is described as starting with a relatively weak infiltration of neutrophils, with a persistence of these neutrophils up to five weeks after wound creation (Wilmink et al., 1999). The majority of neutrophils are found in the superficial dermis of wounds with EGT, but neutrophils could also be found in smaller numbers in the deep dermis layer (Theoret et al., 2013). Neutrophils remain the most prominent cell type, but other inflammatory cells present

include macrophages, eosinophils, mononuclear lymphocytes, and mast cells (Wilmink et al., 1999). Eosinophils are prominently observed in the superficial dermis of wounds with EGT, and macrophages are mostly observed in perivascular locations (Theoret et al., 2013). Activated neutrophils and macrophages release a variety of pro-inflammatory cytokines and growth factors, many of which interact with cells in the wound and affect healing. Some cytokines such as tumor necrosis factor alpha (TNF-α) and interleukin-1 (IL-1) promote fibroblast proliferation, collagen synthesis, and may also promote an activated state of local keratinocytes (Dipietro, 1995; Usui et al., 2008). Activated fibroblasts produce extracellular matrix and differentiate into myofibroblasts (Guo and Dipietro, 2010; Theoret and Wilmink, 2013). In addition to the prolonged inflammation, distal limb wounds of the horse may have persistence of pro-fibrotic growth factors such as transforming growth factor beta 1 (TGF-β1) which promotes excessive fibroproliferation (Theoret and Wilmink, 2013). An overexpression of a mutant p53 protein has been found in distal limb wounds of horses, which may indicate that a local dysregulation of cell apoptosis may contribute to the accumulation of extracellular matrix in wounds with EGT (Lepault et al., 2005). Excessive production of fibrous tissue interferes with epithelial cell migration and prevents complete re-epithelialization (Maher and Kuebelbeck, 2018; Theoret and Wilmink, 2013). At the margins of wounds with EGT there is epithelial hyperplasia, and the keratinocytes which are activated from local growth factors and cytokines show poor wound migration and lack of differentiation into keratin-producing mature keratinocytes (Usui et al., 2008).

In addition to protracted inflammation and excessive fibroproliferation, wound vascularization is also abnormal in distal limb wounds of horses. Equine distal limb

wounds with EGT have prominent angiogenesis, as these wounds can be supplied by large blood vessels (Maher and Kuebelbeck, 2018). Angiogenesis is promoted by many growth factors present during the inflammation and proliferation stages of wound healing (Portou et al., 2015). However in distal limb wounds of the horse, there is excessive angiogenesis described as new capillary formation when compared to wounds on the equine body (Lepault et al., 2005). These new microvessels that are formed have significant occlusion compared to microvessels on the equine body, and microvessels in an EGT model were found to be 3.37 times more likely to be occluded compared to those in thoracic wounds (Lepault et al., 2005). Endothelial cell hypertrophy of these newly formed microvessels has been demonstrated in equine distal limb wounds, and this is thought to contribute to the observed occlusion (Dubuc et al., 2006). The presence of endothelial cell hypertrophy and microvessel occlusion is likely clinically relevant, as the following have been observed in equine wounds that develop EGT: dysregulation of cell apoptotic signals which prevents adequate apoptosis and allows accumulation of extracellular matrix; lower cutaneous wound temperatures compared to thoracic wall wounds and compared to distal limb wounds without EGT; and relative hypoxia in wounds acutely that develop EGT compared to thoracic wall wounds (Celeste et al., 2011; Celeste et al., 2013; Lepault et al., 2005). The *in vitro* effect of hypoxia on equine dermal fibroblasts has also been evaluated and found to induce extracellular matrix production via hypoxia-inducing factor signaling (Deschene et al., 2012).

Cellular regenerative therapy using stem or progenitor cells in wounds with vascular damage or ischemia has demonstrated promising results. Challenges that

exist with this approach include cell emigration away from the area of interest after injection and cell death near the time of injection. In order to address these challenges, some researchers have combined cells with various biomaterials in order to optimize therapeutic success. Given the overtly inflammatory environment of the equine distal limb wound, use of a biomaterial may provide support and protection for therapeutic cellular therapy for these wounds.

1.4 Biomaterials for cell delivery

Cell Therapy – Effect of Injection

Many different cell types including mesenchymal stem cells (MSCs) and EPCs have been used for cell transplantation intended for tissue regeneration, and early studies utilized direct injection for delivery (Aguado et al., 2012; Rafii and Lyden, 2003). Retention of viable cells at the site of injection has been reported as low as 1 – 32% post-transplantation (Zhang et al., 2001), and this survival post-injection seems to be cell type-independent (Aguado et al., 2012). One study evaluated the effects of different mechanical forces on cells during *in vitro* injection through a needle at clinically relevant flow rates (Aguado et al., 2012). Cell membrane disruption and subsequent cell death occurred prominently, and it was observed that the leading contributor to cell death during injection through a syringe and needle was mechanical disruption caused by extensional flow at the entrance of the needle (Aguado et al., 2012). This is an important consideration for clinical applications of cellular regenerative therapy, as

several studies have shown that better clinical outcomes are associated with greater cell survival at the time of transplantation (Laflamme et al., 2007; Zhang et al., 2008).

Cell Therapy – Retention and Survival

In addition to cell damage and death during injection, poor retention at the site of injection and poor survival post-injection limit efficacy of transplanted cells. One study evaluated the retention of rat aortic smooth muscle cells after injection into normal and infarcted myocardium. Only 50% of the smooth muscle cells remained at the site of injection in the myocardium one hour after transplantation, and this percentage progressively decreased over the course of the study (Yasuda et al., 2005). Roughly 8% of the cells transplanted into the myocardium were found in the lungs, and cells were also found in the kidneys (Yasuda et al., 2005). A significantly greater number of live cells were observed in normal myocardium compared to infarcted myocardium, and this may be related to the cell microenvironment (Robey et al., 2008; Yasuda et al., 2005). Cells injected into diseased tissue may be negatively affected by local ischemia. Ischemia may occur in diseases characterized by compromised blood supply such as myocardial infarction or limb wounds, but this can also be related to clumping of the injected cells as they are forced into the interstitium (Robey et al., 2008). Inflammatory microenvironments compromise the health of transplanted cells, as both neutrophils and macrophages produce oxygen-derived free radicals and inflammatory cytokines which can cause cell membrane damage or negatively impact cell function (Dipietro, 1995; Portou et al., 2015; Robey et al., 2008).

Hydrogel Biomaterials

To overcome the limitations of cell transplantation via direct injection as described above, studies have been performed evaluating biomaterial scaffolds in combination with cells. Synthetic scaffolds are commonly used in tissue engineering applications, in part because the mechanical properties and size of the material can be controlled (Almany and Seliktar, 2005). Biological scaffolds such as de-cellularized ECM can provide biofunctional motifs to regulate cell proliferation, adhesion, and enzyme activity (Almany and Seliktar, 2005; Hubbell, 2003). However, both types of scaffolds have inherent limitations which may be mitigated by their combination into a biomaterial. Many biomaterials are partly composed of a hydrogel, which is a three-dimensional scaffold of cross-linked hydrophilic polymer chains (Seliktar, 2012). These hydrogels can be manipulated into almost any shape or size, can absorb water and have the ability to readily undergo dissolution by hydrolysis (Seliktar, 2012). Hydrogels are compatible with cells, and the cross-linking reaction can be carried out in non-toxic conditions (Almany and Seliktar, 2005; Lutolf and Hubbell, 2003; Seeto et al., 2017). When combined with a cross-linked alginate hydrogel, human umbilical vein endothelial cells had a significant increase in cell survival percentage (58% without biomaterial, 89% with biomaterial) during *in vitro* injection through a syringe and needle (Aguado et al., 2012).

Poly(ethylene glycol) Coupled with Fibrinogen

Although many different synthetic and biological materials have been combined for biomedical research, a notable combination involves the use of a composite polymeric hydrogel made of poly(ethylene glycol) (PEG) combined with fibrinogen (Fb) fragments. The process of combining the PEG with the ECM protein Fb does not alter the biological compatibility of Fb nor does it alter the physical properties of the hydrogel (Seliktar, 2012). Hydrogels made of PEG are highly biocompatible and can be designed to have a wide range of physical characteristics (Almany and Seliktar, 2005; Temenoff et al., 2002). The Fb fragments provide protease degradation substrate and cell-adhesion motifs (Herrick et al., 1999; Werb, 1997). Fibrinogen fragment use within the hydrogel biomaterial provides additional degradability to the biomaterial *in vivo*, as cell-specific protease activity and adhesion sites are present on the Fb (Almany and Seliktar, 2005). Cell signaling motifs promote cellular ingrowth into the biomaterial (Gobin and West, 2002; Lutolf and Hubbell, 2005). These properties of PEG hydrogels combined with Fb (PEG-Fb) may allow for optimal cell function and biomaterial retention once injected into tissue.

The biomaterial PEG-Fb has been used to encapsulate cells in order to facilitate cell delivery and to study cell microenvironments. A three-dimensional tumor microsphere model has been studied to compare cell characteristics of multiple cancer cell lines using cell encapsulation by PEG-Fb. This microsphere model was compared to the traditionally-described gold standard for *in vitro* cancer cell line research, the multi-cellular tumor spheroid model (Pradhan et al., 2017). In contrast to cells within tumor spheroids, cancer cells within PEG-Fb microspheres displayed characteristics of

their native tumor microenvironment by demonstrating hallmarks of malignant transformation and tumorigenic progression (Pradhan et al., 2017). Human embryonic kidney cells had high viability and enhanced function when supported in a PEG-Fb encapsulated microenvironment (Cohen et al., 2018). Another *in vitro* evaluation of the interaction between cells and PEG-Fb revealed that mouse dorsal root ganglionic cell outgrowth and morphogenesis of neurites and glial cells were supported by this semi-synthetic biomaterial (Berkovitch and Seliktar, 2017). The characteristics of PEG within PEG-Fb hydrogels can be altered to promote ideal cell-to-hydrogel interactions that are specific to distinct cell types. Dental pulp stem cells that were encapsulated in PEG-Fb hydrogels had good cell viability, cell morphology, odontogenic gene expression, and mineralization (Lu et al., 2015). The degree of PEG-Fb hydrogel cross-linking was experimentally varied, and the cells encapsulated in PEG-Fb with the greatest degree of cross-linking had the greatest enhancement of odontogenic gene expression and degree of mineralization (Lu et al., 2015).

PEG-Fb Hydrogels – Animal Use

PEG-Fb hydrogels have been used in animal models of disease. Segmental bone defects were created in mice tibias, and PEG-Fb hydrogels of varying degradation properties were implanted into the defects. After five weeks, significant cellular ingrowth was observed within the PEG-Fb implants (Peled et al., 2007). Radiographic and histologic evaluation revealed newly formed bone in these defects, which conferred healing characteristics significantly better than control animals (Peled et al., 2007). When the growth factors vascular endothelial growth factor and angiopoietin-1 were

encapsulated into an injectable PEG-Fb hydrogel and then injected into infarcted mice hearts, both growth factors were retained locally at the site of injection and released gradually over a 30-day period (Rufaihah et al., 2017). Mice treated with these PEG-Fb hydrogels demonstrated the greatest improvement in cardiac function, cardiac muscle preservation, and angiogenesis (Rufaihah et al., 2017). The benefit of PEG-Fb hydrogels for murine myocardial infarction was further demonstrated when PEG-Fb hydrogels were seeded with induced pluripotent stem cells (iPSCs) bioengineered to secrete placental growth factor and matrix metalloproteinase 9. The hemodynamic parameters and degree of revascularization of infarcted cardiac muscle were significantly better than the cells or PEG-Fb (without cells) alone (Bearzi et al., 2014). Additionally, the host cardiac tissue and the injected cells were observed to be functionally integrated after 30 days (Bearzi et al., 2014). Cell survival and engraftment of cells was enhanced when combined with PEG-Fb as an injectable hydrogel in mouse models of acute and chronic skeletal muscle degeneration (Fuoco et al., 2012). The combination of mesoangioblasts and PEG-Fb were injected into areas of skeletal muscle damage, and enhanced differentiation of transplanted cells was observed with acute and chronic skeletal muscle damage (Fuoco et al., 2012). Research performed with *in vitro* and *in vivo* models demonstrates that combining cells with a PEG-Fb hydrogel may provide protection from damage related to injection. Combining PEG-Fb hydrogel with cells and other therapeutic agents may aid in local retention, resulting in prolonged interaction of host tissue and transplanted cells or therapeutic agents. In order to accurately determine cell location and local retention, successful cell labeling techniques must be employed.

1.5 *In vivo* cell tracking

As cellular therapy is used with increasing frequency for diseases in clinical and disease model settings, questions regarding the exact nature of the cell's contribution to healing arise. Results from research in disease models suggest that stem or progenitor cells may not participate in wound healing by direct incorporation into newly formed tissue, but rather participate indirectly via paracrine mechanisms. One report described that healing was significantly improved by treating decubitus ulcers in a septic neonatal foal with a combination of MSCs and platelet-rich plasma gel (Iacono et al., 2012). However, determining whether these cells participated directly in tissue regeneration or by a paracrine mechanism could not be performed as the cells were not labeled or tracked after transplantation (Iacono et al., 2012). Knowing the location of transplanted cells and whether they demonstrate prominent migration is essential to understanding exactly how transplanted stem or progenitor cells contribute to wound healing (Bulte and Daldrup-Link, 2018; Chen et al., 2018; Lopez and Jarazo, 2015; Qadura et al., 2018). Many protocols for cell labeling have been employed, but commonly utilized types of cell labeling include transducing cells with viral vectors in order to produce a fluorescent protein, labeling cells with iron oxide particles detectable by either magnetic resonance imaging or histology, or labeling cells with fluorescent molecules (Burk et al., 2016; Peterson GF, 2014; Slotkin et al., 2007; Yukawa et al., 2009).

Viral Transduction – Green Fluorescent Protein

Viral cellular transduction refers to the introduction of a foreign gene into a cell's genome (called a transgene). This newly introduced gene is translated into a protein product, and this product is typically used to identify the transduced cells. Common viruses used for this purpose are the lentiviruses, which has been used over the past several decades for delivery of transgenes into a wide variety of cells (Chatterjee and De, 2014). Lentiviruses are able to transduce cells that are either rapidly dividing or quiescent. This results in stable integration into the host cell genome, which ultimately provides the cell with long-term expression of this transgene (Chatterjee and De, 2014; Petersen et al., 2014). As a member of the Retroviridae family of viruses, lentiviruses have the potential to begin replication and disrupt host cell functions (Chatterjee and De, 2014). To minimize this possibility in the lentiviruses used for viral transduction, self-inactivating vectors have been created that have a deletion of the viral replication promoter (Petersen et al., 2014).

Cells from many species have been successfully transduced with viral vectors, and specific cell lines from the horse include equine adipose-derived stromal cells, equine adipose-derived MSCs, equine chondrocytes, equine synovial cells, and equine bone marrow-derived MSCs (Donofrio et al., 2010; Ishihara et al., 2006; Petersen et al., 2014). Although many genes can be inserted into cell genomes via viral vectors, a common gene product for cell tracking is green fluorescent protein (GFP). When cells express GFP, the exact location of that transplanted cell can readily be obtained *ex vivo* or even *in vivo* for certain animals (Chatterjee and De, 2014). The addition of GFP transgenes via transduction allows for the expression of GFP throughout the life of the

cell. This provides dynamic and long-term imaging and tracking capabilities (Chatterjee and De, 2014). However, the main side effect of the *in vitro* transduction process prior to transplantation is cytotoxicity with resultant diminished cell function (Ishihara et al., 2006; Petersen et al., 2014).

Iron Oxide Cell Labeling

Another method of cell labeling involves intracellular uptake of superparamagnetic iron oxide (SPIO) particles. SPIO nanoparticles are one type of magnetic resonance imaging (MRI) contrast agent which are readily taken up into many different cell types by micropinocytosis or phagocytosis (Bourzac et al., 2014; Bulte and Daldrup-Link, 2018; Burk et al., 2016). Cells labeled with SPIO can be detected and localized by multiple modalities. They can be detected with MRI studies, as the SPIO nanoparticles cause magnetic field perturbations and are typically visualized as signal void susceptibility artifacts (Bulte and Daldrup-Link, 2018; Burk et al., 2016). The SPIO nanoparticles are not degraded to any appreciable degree, and this allows relatively long-term tracking of transplanted cells. Using low-field MRI, tracking of equine MSCs labeled with SPIO was successful over a period of 8 weeks in nine horses with acquired tendon disease (Berner et al., 2016). Cells labeled with SPIO nanoparticles can also be tracked histologically. Prussian Blue stain binds iron, and by using Prussian Blue stain on fixed tissues, cells previously labeled with SPIO can be identified histologically (Burk et al., 2016). This has been described in an ovine model of tendon disease, where the Prussian blue-positive cells within tendons corresponded to the areas of signal void on MRI studies (Scharf et al., 2015). Unfortunately, Prussian Blue staining may occur at

sites of injury regardless of SPIO labeling due to red blood cell degradation and hemosiderophages (Burk et al., 2016).

The benefits of using SPIO labeling for multimodal cell tracking are clear. However, there are some studies that suggest cell function may be impaired after labeling with SPIO nanoparticles. MSCs isolated from human patients had impaired chondrogenic differentiation after SPIO labeling (Bulte and Daldrup-Link, 2018; Kostura et al., 2004). Cell viability and proliferation was not altered in these cells, but they were not able to form extracellular proteoglycan matrix as well as MSCs that were not labeled with SPIO (Bulte and Daldrup-Link, 2018; Kostura et al., 2004). Altered cell function after SPIO nanoparticle labeling has also been observed in other cell types. The migration ability of swine and rat EPCs were negatively affected after labeling with SPIO nanoparticles (Yang et al., 2010).

Labeling Cells with Fluorescent Quantum Dot Nanocrystals

Cells of many different types can be labeled with intracellular fluorescent molecules, and one of the most commonly utilized is the fluorescent quantum dot (QD) nanocrystal label. QD labeling particles are fluorescent over a wide range of emission frequencies and are internalized into cells via a mechanism believed to be independent of any specific enzymatic process (Tholouli et al., 2008). Since QD are readily internalized by an enzyme-independent mechanism, they are able to be taken up by many different cells across different species (Matea et al., 2017; Zhao et al., 2018). Cells labeled with QD maintain some QD label and also pass QD label on to progeny

cells during proliferation. Cell function is commonly unaffected by QD label (Molnar et al., 2010). Since most cells do not metabolize the QD label, *in vitro* and *in vivo* detection can be achieved over a relatively long time frame (Li et al., 2016; Sugaya et al., 2016; Tholouli et al., 2008).

One study evaluated the QD label in human MSCs and found that a strong fluorescent QD signal was still observed after seven days of cell culture. This same study observed that MSCs labeled with QD could be identified via fluorescent emission of the QD label three weeks after transplantation into the subcutaneous tissue of mice (Li et al., 2016). Rabbit MSCs were also labeled with QD label in an osteonecrosis model, and the differentiation and location of transplanted MSCs could be observed as late as 24 weeks post-transplantation (Sugaya et al., 2016). This was verified within osteoblasts in newly regenerated tissue by electron microscopy, thus proving that the regenerated tissue was derived from the transplanted QD-labeled MSCs (Sugaya et al., 2016). Cell function was unaffected by the QD label in these MSCs, a similar finding with rat EPCs labeled with QD (Molnar et al., 2010). The use of QD labels with various alterations has been used in human medicine. A specific cell type, such as neoplastic cells, may be detected in human tissue or blood using QD labels as biosensors. Using a graphene QD label functionalized with an aptamer that binds to neoplastic cell receptors, circulating tumor cells could be detected in human blood samples with a sensitivity as high as ten tumor cells in a whole blood sample (Cui et al., 2019). Functionalized QD labels have also been used for detection of cancer cells in human tissue. A QD label conjugated to a prostate stem cell antigen monoclonal antibody was able to detect the presence of human urothelial cancer cells in cell culture, and the

investigators of that study speculated that this QD-based detection probe could be used for early diagnosis of this cancer from surgical biopsies taken from patients (Yuan et al., 2018).

Cell labeling with QD has also been performed in multiple disease models in the horse. In one study, four horses had bilateral tendonitis lesions created by injecting collagenase into the superficial digital flexor tendons (Carvalho et al., 2014). Adipose-derived equine MSCs labeled with QD were implanted into one tendon lesion per horse, and QD-labeled MSCs were detected two weeks later in the tendons which received the MSC injections as well as within the circulating peripheral blood (Carvalho et al., 2014). However, no QD-labeled MSCs were observed in the contralateral tendonitis lesion. Another study evaluated QD-labeled MSCs combined with an alginate hydrogel as therapy for experimental equine carpal bone lesions (Santos et al., 2019). QD-labeled MSCs were observed in the cartilage and common joint capsule for seven days and in the synovial fluid in very low numbers at 21 days post-injury (Santos et al., 2019).

Further evaluation of QD label in equine ECFCs is warranted, because the effects of QD label on cell function differs between cell types and is unknown for equine ECFCs. Regenerative therapy using MSCs has demonstrated benefit in the horse, but knowing if therapeutic cells can be safely and accurately tracked *in vivo* using a QD label is a crucial first step for the clinical use of MSCs or ECFCs in equine wounds.

1.6 Equine regenerative therapy

Regenerative cellular therapy with and without biomaterials has been investigated in equine medicine. Although bone defects, ligament damage, and joint damage have been investigated, the majority of studies utilizing regenerative cellular therapy in the horse involve using MSCs for tendinopathies (Lopez and Jarazo, 2015; Ortved and Nixon, 2016). Equine MSCs have been isolated from many different anatomic locations, but due to ease of sampling as well as osteogenic and chondrogenic capacity, bone marrow-derived MSCs are most commonly used (Ortved and Nixon, 2016; Toupadakis et al., 2010; Vidal et al., 2008). These cellular populations are important for direct tissue regeneration in connective tissue disorders, however MSCs have also demonstrated the ability to promote wound healing by regulating local inflammation (Yamada et al., 2016). The use of autologous, culture-expanded MSCs has been associated with improved healing of connective tissue diseases in many animal models in addition to the horse (Fortier et al., 2010; He et al., 2015; Lee et al., 2017; Romero et al., 2017).

Stem cell therapy has also demonstrated improved healing of naturally-occurring tendon injuries in the horse. In one study of 12 horses with naturally-occurring injuries to their superficial digital flexor tendons, horses were administered either saline (control) or autologous bone marrow-derived MSCs injected into the damaged tendon (Smith et al., 2013). Horses treated with autologous MSCs had significant improvements in the biomechanical, morphological, and composition characteristics of the tendons compared to the control group (Smith et al., 2013). Another study evaluated the re-injury rate of race horses treated with MSCs after overstrain injuries of their superficial

digital flexor tendons (Godwin et al., 2012). This study found that horses given intra-lesional injections of autologous MSCs had a significantly lower re-injury rate compared to published historical re-injury rates for the same tendon disease (Smith et al., 2013). Improved tendon healing has been observed with MSCs and with embryonic stem cells (ESCs). One study found that horses with collagenase-induced tendinopathy treated with intra-lesional fetal-derived ESCs had a smaller tendon lesion size and improved tendon tissue architecture based on ultrasound and histology compared to control horses (Watts et al., 2011).

Research in the field of equine regenerative medicine has shown that equine MSCs and other cells can improve tissue healing in disease models and naturally-occurring diseases. However, challenges regarding cell delivery and local cell retention remain (Guest et al., 2010; Lopez and Jarazo, 2015; Ortved and Nixon, 2016). Equine MSCs injected into tendon lesions are observed at the site of injection but are also observed circulating in the peripheral blood up to seven days after intra-lesional injection (Carvalho et al., 2014). In some equine models of bilateral superficial digital flexor tendinopathy or metacarpal ostectomy, MSCs and ESCs have been observed to migrate from the local injection site to the lesion on the contralateral limb (Guest et al., 2010; McDuffee et al., 2012). As studies performed *in vitro* have documented, there is low cell survival when delivered through a syringe and needle (Aguado et al., 2012; Guest et al., 2010). Equine MSCs that were injected into a superficial digital flexor tendon lesion demonstrated only a 5% survival at 10 days post-implantation (Guest et al., 2010). To improve cell survival and local cell retention at site of implantation, some equine studies have combined cells and biomaterials. An alginate hydrogel biomaterial

was used to encapsulate equine MSCs for injection into horses with experimentally induced osteoarthritis lesions (Santos et al., 2019). These cells were observed to have good survival post-implantation; cell migration into the surrounding synovial fluid and peripheral blood was minimal (Santos et al., 2019). Results of these studies are encouraging for the use of a combination of biomaterial and stem or progenitor cells in equine regenerative medicine. However, the use of equine ECFCs has not been investigated.

1.7 Justification for study

The use of MSCs is attractive for connective tissue diseases, as MSCs can undergo chondrogenic and osteogenic differentiation to regenerate ligaments, tendons, or bone. The MSC may not be the ideal cell type to use for other wounds, such as those primarily characterized by vascular damage or dysfunction. As described above, the equine distal limb wound may have poor healing due to protracted inflammation and vascular dysfunction. Based on the observed success treating connective tissue disorders with a cell such as MSCs that can differentiate into connective tissue, treating a wound with significant vascular compromise such as equine distal limb wounds with ECFCs is promising.

Equine distal limb wounds have microvessel occlusion, endothelial hypertrophy, and vascular damage, all of which contribute to local tissue hypoxia (Dubuc et al., 2006; Lepault et al., 2005). Local tissue ischemia and hypoxia may provide a stimulus for inflammatory cell presence, as a persistent pro-inflammatory state is observed in these

wounds (Theoret et al., 2013; Wilmink et al., 1999). Restoration of adequate tissue blood supply with functional microvessels should be achieved with local endothelial cell repair and *de novo* blood vessel formation, known attributes of the ECFC (Asahara et al., 1997; Minami et al., 2015). Our research group has optimized the isolation of equine ECFCs (Salter et al., 2015; Sharpe et al., 2016) and does so routinely with peripheral blood sampling. Equine ECFCs form prominent tubules *in vitro*, and ECFCs have been described as directly incorporating into newly formed blood vessels in wounds and ischemic conditions. Therefore, equine distal limb wounds may benefit from local implantation of equine ECFCs.

Certain challenges exist for the clinical use of equine ECFCs, and these should first be addressed using *in vivo* wound models. Determining how injected ECFCs contribute to wound healing in the horse will be accomplished by being able to track the location and migration of cells over the course of a study. Many different cell types readily take up QD label with no ill affects on cell growth or function (Matea et al., 2017; Zhao et al., 2018), but this should be evaluated in equine ECFCs prior to *in vivo* use. Injected cells may experience cell death or emigrate away from the site of injection (Aguado et al., 2012; Zhang et al., 2001). Combining injected cells with a hydrogel biomaterial has proven protective effects for these cells during the injection (Aguado et al., 2012), and both improved cell survival and local retention has been documented for equine MSCs combined with a hydrogel biomaterial (Santos et al., 2019).

The combination of equine ECFCs with the biomaterial PEG-Fb has been investigated by our group. ECFCs have the ability to differentiate into mature endothelial cells and assist in vascular repair, both characteristics which should be

beneficial to the equine distal limb wound. This benefit should be optimized with the improved cell viability and local retention of injected ECFCs by use of the biomaterial PEG-Fb. Tracking the injected cells' location and understanding the effect of local inflammation on injected ECFCs will also help define the utility of using ECFCs in equine distal limb wounds.

Chapter 2: Study aims and hypotheses

Specific aims

1) Equine ECFCs have characteristics which make them an attractive therapeutic option for distal limb wounds in the horse. In order to more completely understand the role that ECFCs play once implanted in distal limb wounds, a method for tracking the cells' location and migration must be identified. Techniques for labeling equine ECFCs should be evaluated to identify a cell label which will assist cell tracking but not interfere with cell function *in vivo*. The aim of the first part of this study was to evaluate the feasibility of labeling ECFCs with semiconductor quantum nanodots (QD) and subsequently analyze ECFC growth and function post-labeling *in vitro.*

2) Equine distal limb wounds have been characterized by vascular damage and dysfunction, which suggest that therapy with ECFCs may be of benefit. The aim of the second part of the study was to utilize equine ECFCs, alone and in combination with an injectable format of the biomaterial PEG-Fb, in a distal limb wound model in the horse. Additional aims were to track the location of injected cells and understand the role that ECFCs encapsulated in PEG-Fb had on wound healing.

3) Distal limb wounds in the horse have protracted inflammation locally, which is thought to negatively affect wound healing. Various stem and progenitor cells have been evaluated in environments containing inflammatory cytokines, and the function of these cells can be negatively impacted during this exposure. The aim

of the third part of this study was to study the effects of tumor necrosis factor alpha exposure on equine ECFC function.

Hypotheses

1) Equine ECFCs can be effectively labeled with semiconductor quantum dots.

2) Once labeled with QD, equine ECFCs will not have a decline in cell growth or function.

3) Tracking QD-labeled ECFCs, both with and without PEG-Fb encapsulation, post-injection into an equine distal limb wound model will be feasible, and injected ECFCs will incorporate into and form new blood vessels *in vivo.*

4) ECFCs injected into an equine distal limb wound model will increase wound vascularization, decrease wound inflammation, and decrease granulation tissue compared to control injections, effects enhanced when ECFCs are combined with PEG-Fb.

5) Equine ECFCs will demonstrate a decline in cell growth rate, migration rate, and ability to form *in vitro* tubules and uptake LDL with exposure to tumor necrosis factor alpha.

Chapter 3: Growth and function of equine endothelial progenitor cells labeled with semiconductor quantum dots

3.1 Introduction

Quantum dot (QD) nanocrystals are fluorescent cell labeling particles composed of semiconductor nanocrystals typically consisting of a heavy metal core such as CdSe coated with a high band-gap semiconductor such as ZnS (Tholouli et al., 2008). QD nanocrystals are internalized into the cytoplasm of cells with an enzyme-independent mechanism; therefore, they are used to label a variety of cell types *in vitro* (Pi et al., 2010). QD nanocrystals have a high fluorescent efficiency and minimal tendency to photobleach making them desirable for cell labeling with *in vitro* and *in vivo* applications (Pi et al., 2010; Tholouli et al., 2008). The use of QD labeling also has the advantage of multiple color spectra for labeling different cell types and longevity of the label for *in vivo* cell tracking. Both short-term tracking of QD-labeled cells over 7-10 days, as well as longer term tracking of QD-labeled cells up to 24 weeks have been demonstrated in multiple different cell types (Lee et al., 2015; Mannucci et al., 2017; Rosen et al., 2007; Sugaya et al., 2016). In addition to the imaging advantages, QD labeled cells do not transfer their QD label to surrounding cells with cell death (Molnar et al., 2010; Pi et al., 2010; Tholouli et al., 2008; Wu et al., 2003). Although the mechanism of QD label loss differs between cell types and must be tested for each new cell type, typically cells do not metabolize the QD label, meaning that labeled cells retain the QD and also pass the QD on to subsequent progeny cells during cytoplasmic partition with cell division (Molnar et al., 2010; Pi et al., 2010).

Tracking of stem and progenitor cells is essential to determine engraftment after administration. Multiple types of cell labeling strategies have been employed for *in vitro* and *in vivo* tracking including cell transduction with subsequent green fluorescent protein expression, superparamagnetic iron oxide (SPIO) nanoparticles, and QD nanocrystals (Burk et al., 2016; Hardman, 2006; Peterson GF, 2014). Important criteria when assessing the potential of a cell labeling strategy for use include ease of use, efficacy of label, and ability to maintain cellular phenotype after label. Outcomes frequently differ between cell types and between species. Therefore, detailed *in vitro* investigation is critical prior to use with *in vivo* cell tracking experiments. Concerns exist over the possibility of replication-competent lentivirus with transduction, and identification of SPIO containing cells *ex vivo* using Prussian blue stain has specificity problems (Burk et al., 2016; Peterson GF, 2014). In recent years, QD labeling has gained prevalence for use and has been used in many different cell types (including human endothelial progenitor cells) and species (Lee et al., 2015; Mannucci et al., 2017; Molnar et al., 2010; Pi et al., 2010). Different mechanisms of label loss exist among the cell types studied (Molnar et al., 2010; Pi et al., 2010). In the mouse, one study showed that embryonic fibroblasts lost QD label from cell proliferation, but embryonic stem cells lost QD label at least in part from label degradation and excretion (Pi et al., 2010). In another study of mouse embryonic stem cells labeled with QD, a loss of QD label was suggested to occur from either cell division or leaking of the label from the cell (Burk et al., 2016; Lin et al., 2007). A study using human endothelial progenitor cells suggested that QD label loss occurred primarily from cell division (Molnar et al., 2010).

The recent isolation and *in vitro* work with equine endothelial progenitor cells (EPCs) and their subset endothelial colony forming cells (ECFCs) is promising for the *in vivo*, regenerative use of ECFCs as therapeutic agents (Hardman, 2006; Peterson GF, 2014; Salter et al., 2015; Sharpe et al., 2016). Although QD labeling has been used for cell tracking of equine mesenchymal stem cells (Carvalho et al., 2014; Falomo et al., 2015), there are no studies evaluating the effects of this label on function of equine ECFCs or mechanism of label loss. Prior to *in vivo* vascularization studies using these QD-labeled ECFCs, it is important to know how ECFCs function after QD label, the duration of ECFC label retention and how these cells lose their label. Thus, the objectives of this study were to evaluate cell growth and cell function in equine ECFCs *in vitro* after QD-label. Additionally, the mechanism of QD label loss in equine ECFCs was investigated.

3.2 Methods

3.2.1 Isolation, storage, and classification of ECFCs

Whole blood was collected from three, healthy, university-owned adult horses aged 15-26 from either the cephalic vein or the jugular vein for ECFC isolation using either a whole blood isolation or density gradient centrifugation isolation method as previously described (Salter et al., 2015; Sharpe et al., 2016). The ECFCs were cryopreserved at a concentration of 100,000 cells / mL in a freezing medium containing 95% equine serum and 5% dimethyl sulfoxide and then stored in liquid nitrogen as passage 2 cells. ECFCs were thawed and used for all experiments at passage 3 – 5.

ECFCs were cultured in either 25 cm^2 or 75 cm^2 tissue culture polystyrene flasks in endothelial cell growth medium with manufacturer-supplied growth factors and anti-microbials (EGM-2 with Bullet Kit, Lonza, Visp, Switzerland) with equine serum at a final concentration of 10% (HyClone Laboratories Inc, Logan, UT, USA) at standard cell culture conditions (37° C, 5% CO_2, 95% humidity). ECFCs were defined as late-outgrowth EPCs based on characteristic cobblestone morphology (Figure 3) and rapid *in vitro* cell division (Salter et al., 2015). The ECFCs used in this study expressed CD34, CD105, VEGFR-2, vWF, and CD14, formed vascular tubules on basement membrane (Figure 4) and also had receptor-mediated uptake of fluorescently-labeled acetylated low-density lipoprotein (DiO-Ac-LDL) (Biomedical Technologies Inc, Stoughton, MA, USA), consistent with our group's previous work (Salter et al., 2015).

3.2.2 Cell labeling

Preliminary work was performed to assess the signal intensity of QD fluorescence in ECFCs. ECFCs were labeled with fluorescent quantum dots (QD) with an emission maximum at 655 nm (Qtracker® 655 Cell Labeling Kit, Invitrogen, CA, USA) based on manufacturer instructions for labeling adherent cells. Briefly, the Qtracker® nanocrystals were added to the Qtracker® carrier of phosphate buffered saline (PBS) and incubated at room temperature for 5 min. Fresh complete growth medium was then added, and this was vortexed for 30 sec. Cell culture medium was removed from adherent cells in a 25 cm^2 cell culture flask, the cells were washed with PBS, and then the QD containing mixture was added to the cell culture flask. The cells

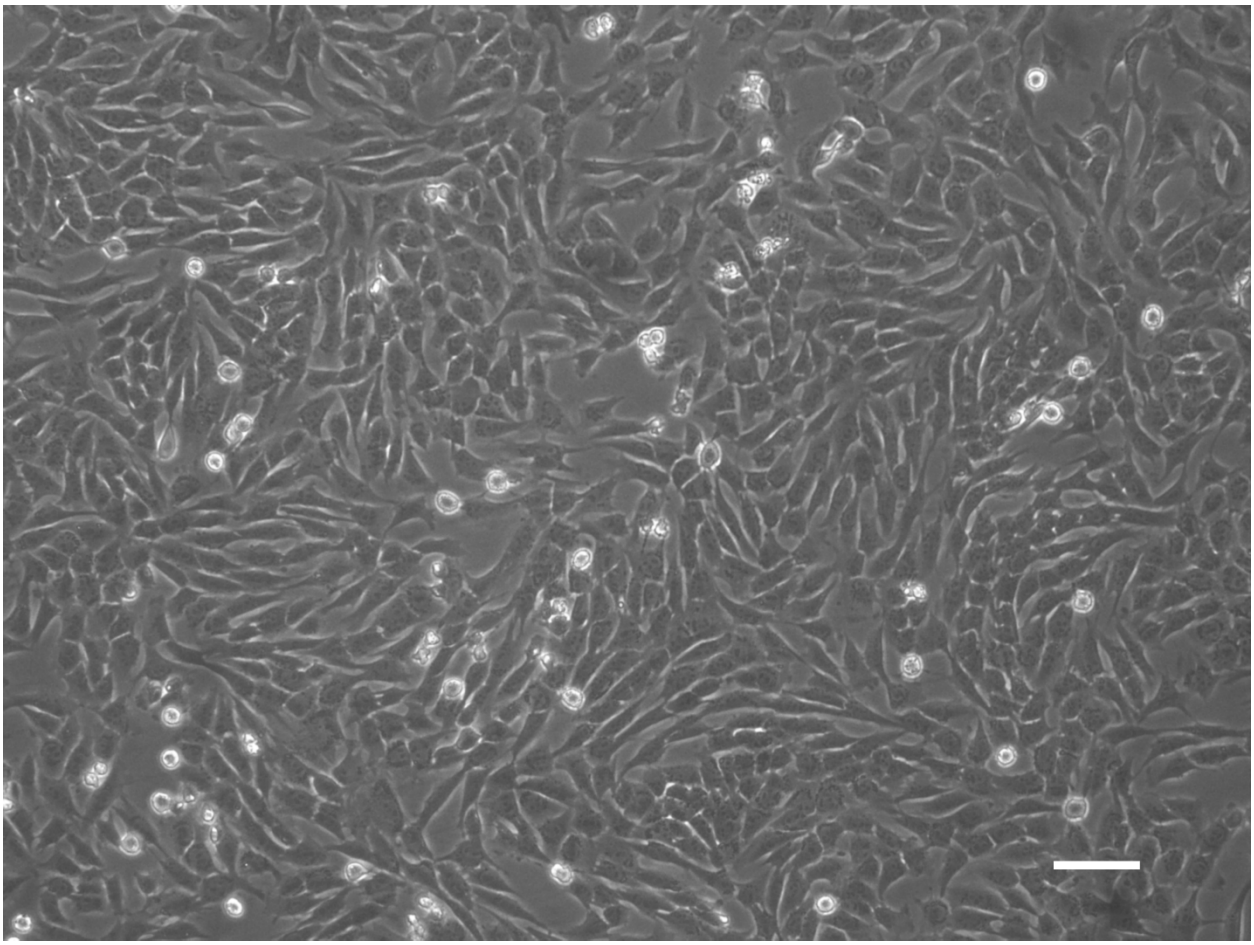

Figure 3. ECFC monolayer in culture. Photomicrograph of endothelial colony forming cells adherent to a cell culture flask demonstrating the characteristic “cobblestone” morphology. Scale bar is 100 μm.

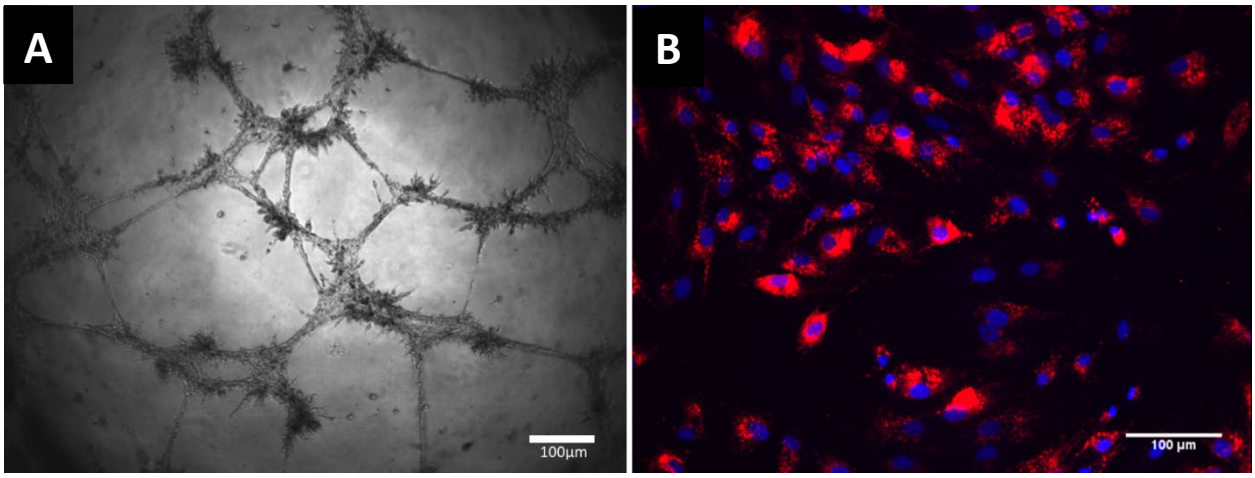

Figure 4. *In vitro* ECFC functional assays. A) Photomicrograph of ECFCs forming tubules *in vitro* throughout the entire field of view. B) Fluorescent photomicrograph demonstrating uptake of acetylated low density lipoprotein (red color) by ECFCs *in vitro*. Nuclei are stained blue with DAPI. Scale bars are 100 µm.

were then incubated at standard cell culture conditions. In a preliminary study, concentrations of QD ranging from 2 – 20 nM were used with QD label contact time of 12 hr and 24 hr used for each concentration. Fluorescent intensity was subjectively assessed with fluorescent microscopy. Cells were labeled with 5 nM and 20 nM with a label contact time of 24 hr for this study.

3.2.3 Measurement of cell growth after QD labeling

For cell growth experiments, ECFC lines from 3 horses (N=3) were tested individually. ECFCs from passage (P)3 were seeded into collagen-coated (50 µg/mL) 25 cm^2 cell culture flasks with 75,000 cells (3,000 cells/cm^2) for each QD-labeled and control condition. Once the cells were ~50% confluent, they were labeled with 20 nM QD or left unlabeled for 24 hr. After reaching 80% confluency, cells were subcultured by adding trypsin-EDTA at 0.25 mg/mL (Lonza, Visp, Switzerland) and incubating at 37° C for 1 min. Trypsin was neutralized with an equal volume of fresh ECFC culture medium, followed by centrifugation at 200 x g for 5 min. Cells were then reseeded onto collagen-coated 75 cm^2 cell culture flasks with 225,000 cells per flask (3,000 cells/cm^2). Cell seeding density after each subculture, cell number at the time of subculture, and time (hours) between subcultures were recorded and used to determine the number of cell doublings (NCD) in each 24 hr period as well as the population doubling time (PDT) in hours. Additionally, the cumulative population doubling level (CPDL) was determined from the cell count. Cell counts were performed using standard cell culture protocol where 4 fields were counted on the hemocytometer and then averaged before applying

the dilution multiplier to obtain the final cell counts. This was performed in triplicate at all subcultures. NCD was calculated as: $\mathrm{NCD} = [\frac{\log 2 \frac{\mathrm{CH}}{\mathrm{CS}}}{\text{Number of days}}]$, where C_H was the number of cells at the time of subculture and C_S was the number of cells seeded. PDT was calculated as: $\mathrm{PDT} = \frac{\text{Total number of hours}}{\mathrm{NCD}}$. The CPDL was calculated as: $\mathrm{PDL} = \frac{\log 10(\mathrm{CH}) - \log 10(\mathrm{CS})}{\log 10(2)}$. The calculated PDL for each subculture was then added to the previous subculture PDL to determine CPDL. Cells were subcultured at 80% confluency to ensure that the cells remained in log growth. Cells were subcultured until P10.

3.2.4 Quantification of QD label

To quantify the amount of QD label over multiple cell passages using flow cytometry, each of the ECFC cell lines at P3 from three horses were subjected to the same labeling procedures as described above and the following conditions: unlabeled cells, 5 nM, and 20 nM QD. Subculture procedures were as described above. After labeled cells reached 80% confluency, cells were reseeded onto collagen-coated 25 cm^2 cell culture flasks at a 1:4 ratio. Cells were subcultured in this manner out to P10.

At each passage, cells that were not used to seed the cell culture flasks were washed with 10 mL of calcium-free, magnesium-free PBS solution and then centrifuged at 200 x g for 5 min. The PBS solution was removed, 1 mL of 4% paraformaldehyde solution was added, and the cells were incubated at room temperature (25° C) for 20 min. Cells were then centrifuged at 200 x g for 5 min, washed with PBS solution, resuspended in 1% Bovine serum albumin (BSA) solution (OmniPur, Gibbstown, NJ,

USA), and kept at 4° C. Immediately prior to flow cytometry analysis, the fixed cells were filtered through a 35 μm mesh. Using a 675-25-H flow cytometry filter, a total of 15,000 events were collected for each sample, with forward scatter versus side scatter plots used for imaging (BD Accuri C6 flow cytometer, BD Biosciences, Brea, CA, USA). Gates were set to select for live cultured cells, with elimination of doubled cells, dead cells, and debris (BD Accuri C6 software, BD Biosciences, Brea, CA, USA).

3.2.5 Assessment of cell function after QD label

ECFCs from P3 from each horse cell line (N=3) were seeded at 75,000 cells per flask into two 25 cm^2 cell culture flasks, cultured until 50% confluent, and then left unlabeled or labeled with 20 nM QD. Once cells were ~80% confluent, they were subcultured using trypsin-EDTA as described above and used in either tubule formation assays or DiO-Ac-LDL uptake assays. A 96-well cell culture disk was prepared with 75 μL/well of solubilized basement membrane (BD Matrigel Basement Membrane Matrix, BD Biosciences, Bedford, MA, USA), which was incubated for 30 min at 37° C prior to cell seeding. Each well was seeded with 10,000 cells and then incubated at 37° C. Vascular tubule formation was assessed at 24 h post seeding. Three replicates of duplicate assays were performed for each horse cell line. The presence or absence of tubule formation was noted using light microscopy. Tubule quality score was subjectively scored as previously described (Salter et al., 2015) (1 = no tubule formation, 2 = tubules projecting from cells but no connections between cells, 3 = vascular tubule formation with connecting tubules in $\leq$ 50% of the field, and 4 = vascular

tubule formation with connecting tubules in > 50% of the field). Tubule quality scores were assessed by one investigator (RLW) who was blinded to cell labeling conditions.

ECFCs labeled with 20 nM QD and unlabeled ECFCs were seeded in duplicate at a density of 50,000 cells / well into 12-well cell culture plates that had been previously coated with collagen. Once cells were ~50-80% confluent, DiO-Ac-LDL, diluted in pre-warmed supplemented medium, was added to a final concentration of 50 μg/mL. Cells were incubated with DiO-Ac-LDL for 4 hr at standard cell culture conditions. After incubation, the cells were washed three times with fresh cell culture medium. Cells were then harvested with a trypsin-EDTA solution and centrifuged at 200 x g for 5 min. Cells were washed with PBS solution and fixed with 4% paraformaldehyde as described above. Cells were then washed with PBS, resuspended in 1% BSA solution, and filtered through a 35 μm mesh immediately prior to flow cytometric analysis. DiO-Ac-LDL has an emission peak at 507 nm, so a FLH-1 flow cytometry gate was used for analysis. A total of 15,000 events were collected for each duplicate sample, with forward scatter versus side scatter plots used for imaging. Gates were set to select for live cultured cells, with elimination of doubled cells, dead cells, and debris.

3.2.6 Determining mechanism of QD label loss

ECFCs from each horse cell line (N=3) were seeded as P4 in a 25 cm^2 cell culture flask and labeled with 20 nM of QD or left unlabeled as described above. Once these cells were ~80% confluent, they were subcultured at 150,000 cells/well (40,000 cells/cm^2) into 12-well cell culture plates previously coated with collagen. Four wells

were seeded for each test condition which included: unlabeled cells with and without a growth inhibitor and 20 nM QD labeled cells with and without a growth inhibitor, mitomycin C (MMC) (Sigma-Aldrich, MO, USA). At initial seeding of the wells, the growth-inhibited wells contained supplemented cell culture medium with 20 µg/ml MMC (Appendix A). After 24 hr in standard cell culture conditions, the cell culture media was removed and replaced with either standard cell culture medium or MMC-containing supplemented cell culture medium as appropriate. Cells were harvested from two wells per condition after 24 hr using trypsin-EDTA. These cells were prepared for flow cytometry and analyzed for QD quantification as described above. After an additional 24 hr in standard cell culture conditions, the remaining cells were harvested and analyzed with flow cytometry.

3.2.7 Statistical analysis

All statistical analyses were performed with commercially available statistical software (JMP®, Version 13.0.0 SAS Institute Inc., Cary, NC, USA). Data were assessed for normality using a Shapiro-Wilk test. Cell growth data with a normal distribution were expressed as mean +/- SD and compared using either a Student's t-test or ANOVA. The decline in QD fluorescence data and CPDL with a nonparametric distribution were expressed as median (range) and compared using a Wilcoxon rank sums or Kruskal Wallis test. Tubule formation categorical data were analyzed by a Fischer's exact t-test. Significance was assessed as a P value <0.05.

3.3 Results

3.3.1 Preliminary assessment of QD labeling

ECFCs were readily labeled with QD at concentrations as low as 2 nM (Figure 5), with an increase in fluorescent emission intensity as label concentrations increased to 20 nM. Label concentrations of 2 nM, 5 nM, 10 nM, and 20 nM were evaluated in duplicate, with each label concentration having one condition with a 12 hr contact time and another condition with a 24 hr contact time. For each label concentration, the 24 hr label contact time had a subjectively brighter fluorescent emission intensity than the 12 hr label contact time condition (Figure 5). ECFCs labeled with 5 nM QD were imaged while adherent immediately before fixation and immediately after fixation (Figure 6), and 4% paraformaldehyde did not diminish the fluorescent emission intensity of QD within the ECFCs. Additionally, after fixation, these QD labeled ECFCs were exposed to light for 24 hr and then imaged again. After 24 hr of exposure to light, the fluorescent emission intensity was not diminished, but rather was brighter (Figure 6).

Flow cytometric analysis of QD labeled ECFCs was successful, and a strong positive signal in the 675-25-H filter immediately after fixation was observed (Figure 7). To evaluate the QD fluorescent emission over time, these same QD labeled ECFCs were evaluated again by flow cytometric analysis two weeks later with no decline in fluorescent emission intensity (Figure 7).

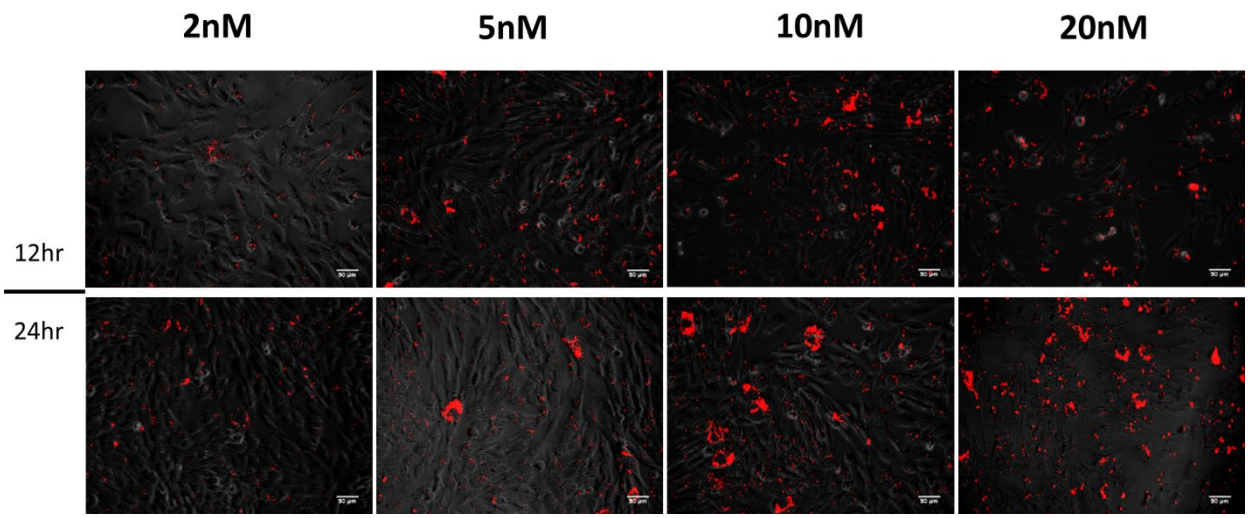

Figure 5. ECFCs labeled with quantum dots *in vitro*. ECFCs labeled with concentrations of QD of 2 nM, 5 nM, 10 nM, and 20 nM, with 12 hr label contact time (top row) and 24 hr label contact time (bottom row). Scale bars are 50 μm.

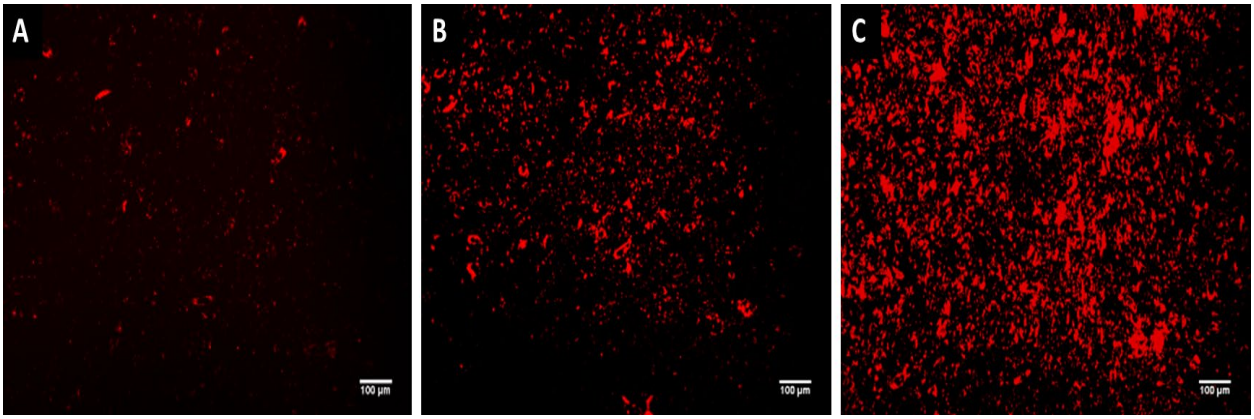

Figure 6. Effect of paraformaldehyde fixation and light exposure on QD fluorescence. Fluorescent photomicrographs of ECFCs labeled with 5 nM QD, A) pre-fixation; B) immediately after fixation; and C) after 24 hr of light exposure after fixation. These images demonstrate that fluorescent emission of QD does not decline with fixation or with light exposure. Scale bars are 100 µm.

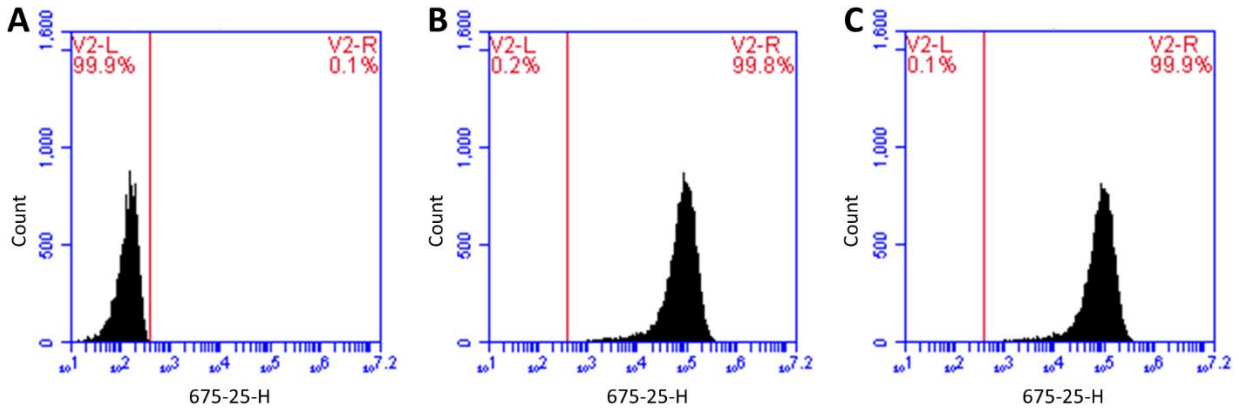

Figure 7. Flow cytometric analysis of the effects of paraformaldehyde fixation and light exposure on QD fluorescence. Flow cytometric data demonstrating fluorescent intensity in a 675-25-H filter of non-labeled ECFCs (A), ECFCs labeled with 5 nM QD immediately after fixation (B), and ECFCs labeled with 5nM QD 2 weeks after fixation (C). This demonstrates there is no decline in fluorescent emission intensity over a 2 week period.

3.3.2 QD effects on cell growth

Cell growth parameters were not different between QD labeled and unlabeled cells at any passage. NCD, PDT, and CPDL data were assessed in QD labeled P4 – P10 ECFCs for all horse cell lines (N=3). NCD for unlabeled ECFCs were not significantly different compared to QD-labeled ECFCs (*P*=0.95), indicating that QD label did not affect the NCD. PDT for unlabeled ECFCs was not significantly different compared to QD-labeled ECFCs (*P*=0.91), indicating that QD label did not affect the PDT. The maximum CPDL at P10 for unlabeled ECFCs (27.9, 26.14 – 28.48 cell doublings) was not different compared to QD-labeled ECFCs (28.27, 25.97 – 28.3 cell doublings, *P*=0.83). NCD and PDT in both labeled and unlabeled cells by passage number are shown in Figure 8.

3.3.3 Quantification of QD over cell passages

ECFCs labeled with 20 nM QD had a greater fluorescent signal intensity at multiple time points compared to ECFCs labeled with 5 nM QD, but the percent of ECFCs still labeled declined at a similar rate in each label concentration. Flow cytometry was used to determine the percentage of QD labeled ECFCs by passage and the mean fluorescent signal intensity from P3-P10 (Figure 9). ECFCs labeled with 5 nM had a similar decline in the percentage of labeled cells as ECFCs labeled with 20 nM (Figure 9) with 100% labeled at P3 and almost 0% labeled at P10. Although there were no differences in the percentage of cells labeled between 5 nM and 20 nM QD, the 20

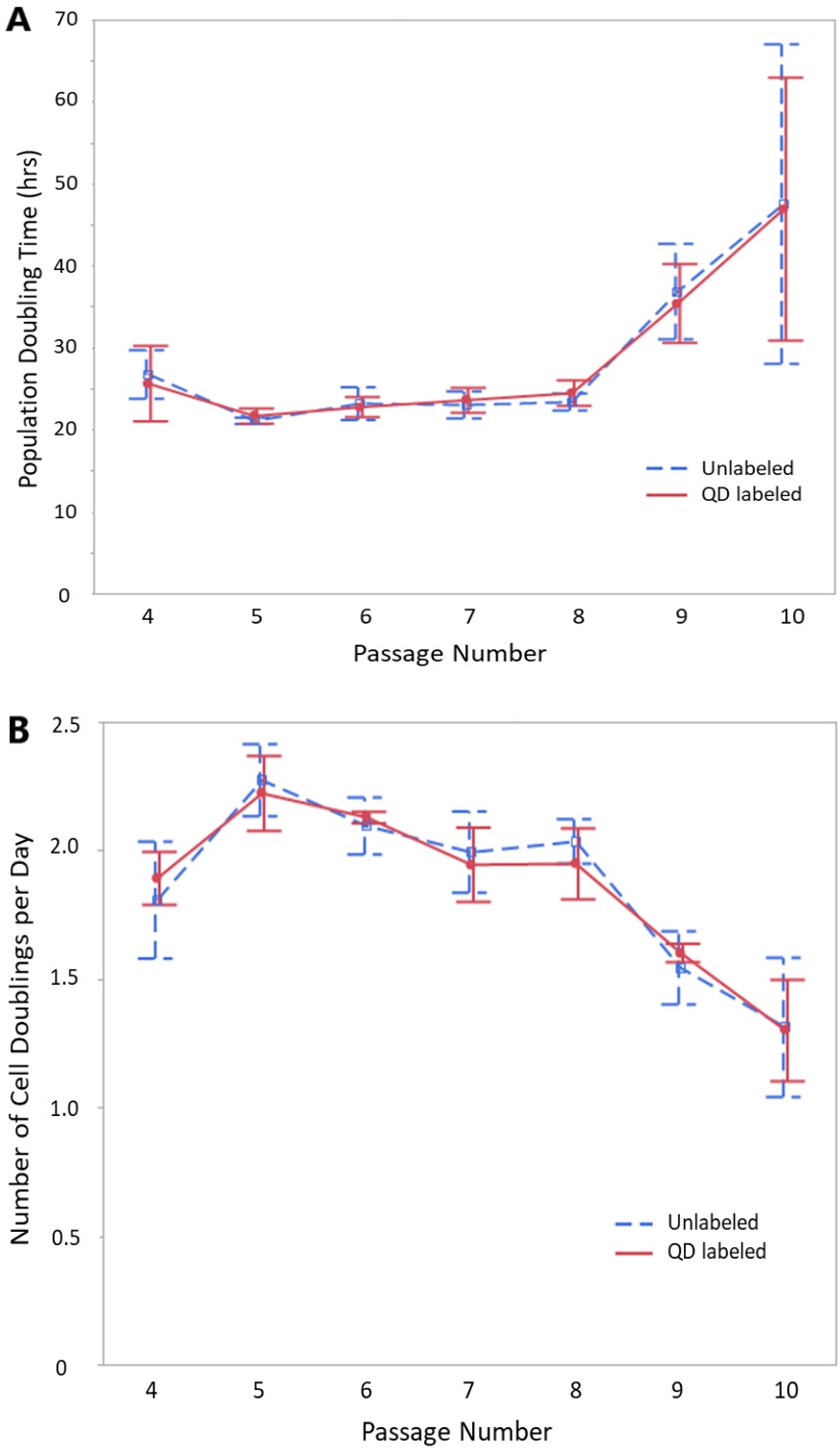

Figure 8. Influence of QD labeling on cell growth. (A) Population doubling time in hours and (B) number of cell doublings per day by passage for unlabeled ECFCs and ECFCs labeled with 20 nM QD. Each time point is the mean ± SD of data from 3 horses.

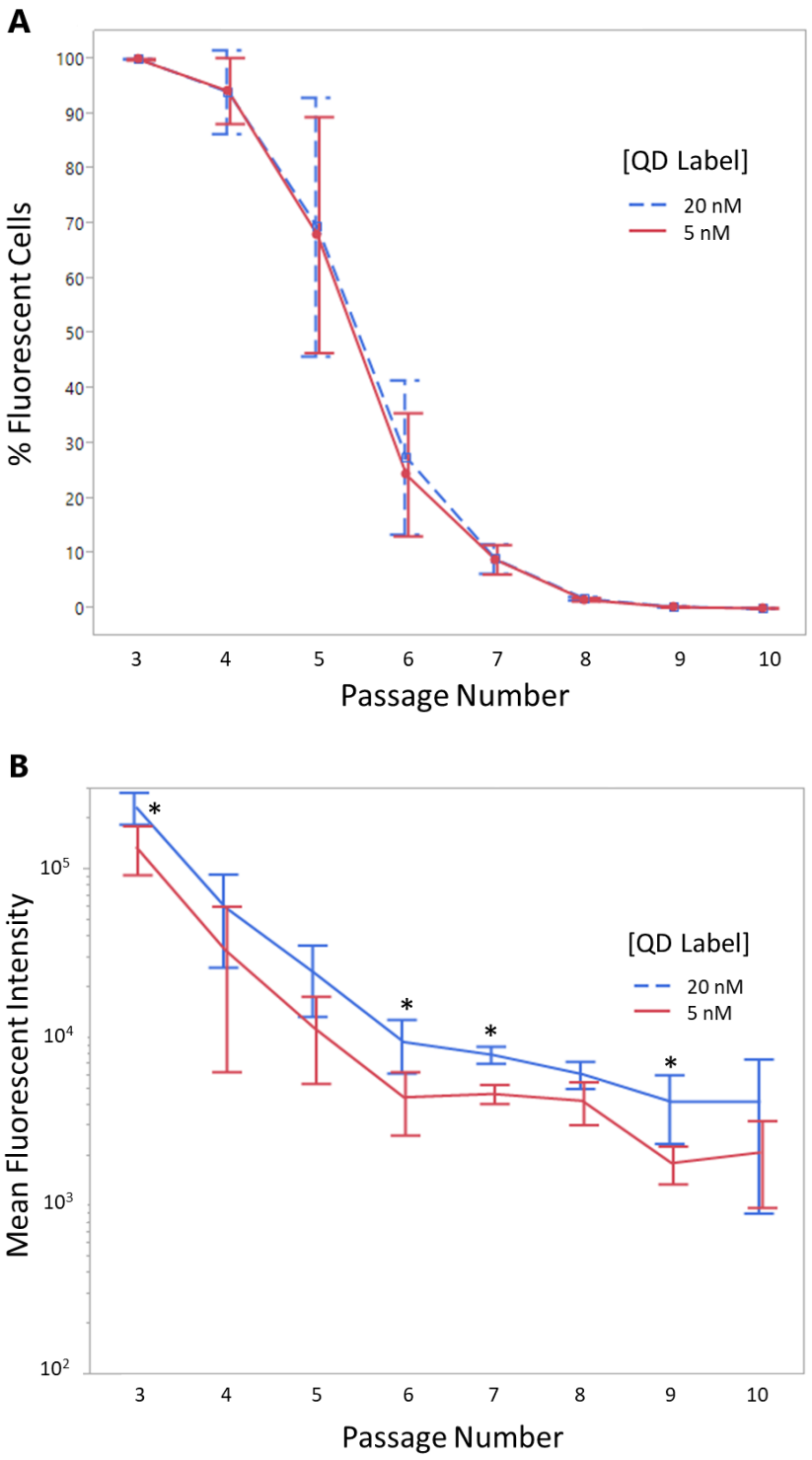

Figure 9. Decrease in percent fluorescent cells and fluorescent intensity over consecutive passages. A) Percentage of fluorescent labeled ECFCs (n=3) over time for 5 nM and 20 nM QD label concentrations. B) Decrease in mean fluorescent intensity in ECFCs (n=3) over time for 5 nM and 20 nM QD label concentrations. Data is displayed as mean +/- SD. * indicates significant differences (P<0.05).

nM QD labeled ECFCs had a significantly greater mean fluorescent signal at P3 (flow cytometric analysis performed immediately after the 24 hr label contact period at the initial labeling), P6, P7, and P9 (*P*=0.035, *P*=0.031, *P*=0.003, *P*=0.27, respectively) compared to the 5 nM QD labeled ECFCs (Figure 9). A representative flow cytometric analysis for one horse in Figure 10 shows the percentage of cells labeled by each individual passage for both 5 nM and 20 nM label concentrations (Figure 10). Regardless of initial label concentration, the decline in percentage of labeled cells over consecutive passages is similar (Figure 10).

3.3.4 Cell function after label

The ability of ECFCs to uptake LDL and form tubules *in vitro* was not affected by the QD label. Flow cytometry was used to assess the percentage of unlabeled ECFCs and of 20 nM QD-labeled ECFCs that had DiO-Ac-LDL uptake in all horse cell lines (N=3) at P4. The percentage of ECFCs with DiO-Ac-LDL uptake was 99.17% +/- 0.45% for unlabeled cells and 98.93% +/- 0.68% for QD labeled cells, with no significant differences between these two groups (*P*=0.33). A representative photomicrograph of the uptake of DiO-Ac-LDL by unlabeled ECFCs and QD-labeled ECFCs is shown in Figure 11, and the cytoplasmic localization of QD label is also evident in this figure.

ECFCs, both unlabeled and QD-labeled, were seeded onto basement membrane matrix as described above, and photomicrographs were used to score tubule quality in all horse cell lines (N=3). Three replicates of duplicate assays were performed for each horse cell line. The range of tubule scores in both groups was 3 - 4, and there was no

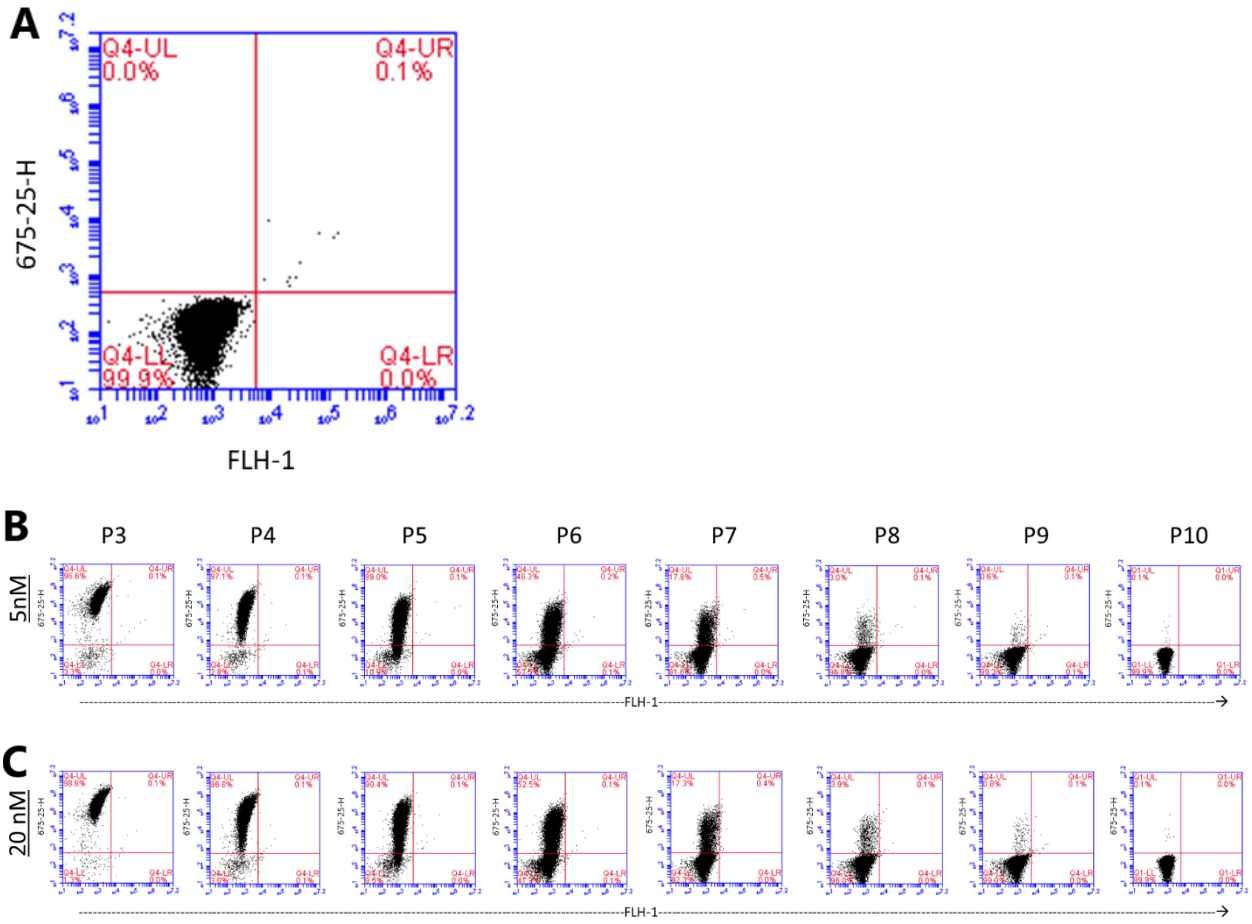

Figure 10. Decline in percentage of fluorescently labeled cells over consecutive passages. A) Flow cytometric analysis of unlabeled ECFCs of passage 3 and representative flow cytometric analysis showing decline in fluorescence over continued cell passage in ECFCs with (B) 5 nM QD and (C) 20 nM QD label concentrations.

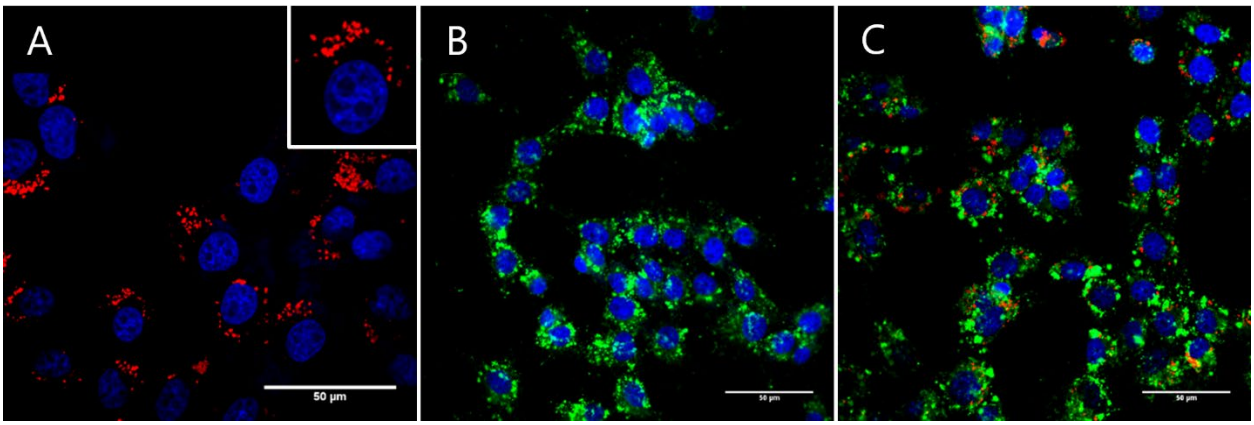

Figure 11. Influence of QD label on DiO-Ac-LDL uptake. A) Equine ECFCs labeled with quantum dots but not exposed to DiO-Ac-LDL. Representative photomicrographs (merged images) showing cellular uptake of DiO-Ac-LDL (green) in (B, C) equine ECFCs previously labeled with (B) and without (C) semiconductor quantum dots (red). Equine ECFCs labeled with quantum dots but not exposed to DiO-Ac-LDL are shown on the left. Nuclei are stained with DAPI (blue). An enlarged image of one cell is in the upper right corner of A. Scale bars are 50 µm.

significant difference in tubule quality score between unlabeled and QD-labeled ECFCs (*P*=0.524), indicating that the presence of QD label does not inhibit tubule formation (Figure 12).

3.3.5 Mechanism of label loss

ECFCs seeded with a growth inhibitor maintained QD label longer than uninhibited cells showing that cell proliferation is the primary cause of QD label loss in ECFCs. Treatment with the cell division inhibitor MMC caused a significantly lower cell count in both unlabeled (*P*=0.0005) and QD labeled (*P*=<0.0001) cells versus untreated cells.

There was no difference in cell counts on day 2 between unlabeled ECFCs and QD labeled ECFCs with (*P*=0.99) or without (*P*=0.252) MMC. The quantity of QD label was significantly higher (*P*=0.007) in MMC treated cells versus untreated QD labeled cells (Figure 13). The flow cytometry data shows the decline in the QD label in cells undergoing cell division versus those that are not (Figure 14.)

3.4 Discussion

Using labeled cells for cell tracking studies for *in vitro* or *in vivo* disease models is essential for cell localization and evaluation (Lopez and Jarazo, 2015; Ortved and Nixon, 2016; Sorice et al., 2016; Zubin et al., 2015). The engraftment and differentiation of an injected / implanted stem cell can then be specifically determined rather than just speculated (Iacono et al., 2012; Smith et al., 2013). This *in vitro* study of equine ECFCs

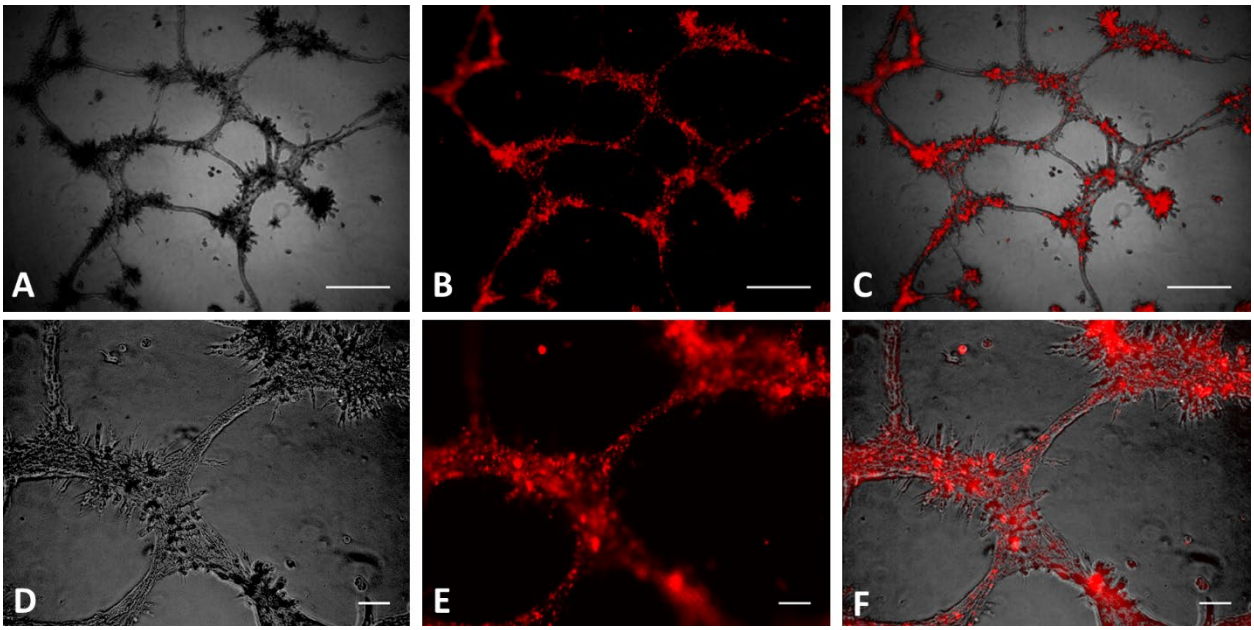

Figure 12. Influence of QD label on *in vitro* tubule formation. Representative photo micrographs of *in vitro* tubule formation in QD-labeled ECFCs (red). Panels A and D are light photo micrographs. Panels B and E are fluorescent photo micrographs. Panels C and F are merged images. Scale bars are 500 μm.

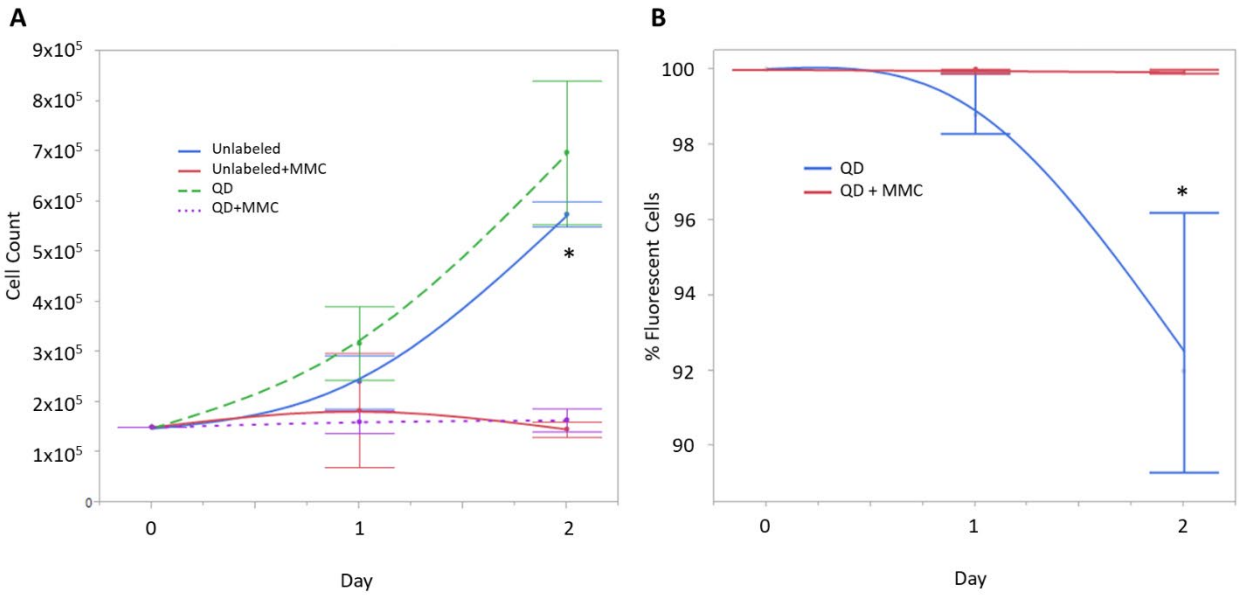

Figure 13. Inhibition of cell proliferation and QD label loss with mitomycin C. A) Cell counts for control cells and QD-labeled cells with and without mitomycin C (MMC) added. B) Decline in percentage of QD-labeled cells in groups with and without MMC. * indicates a significant difference between groups (P<0.05).

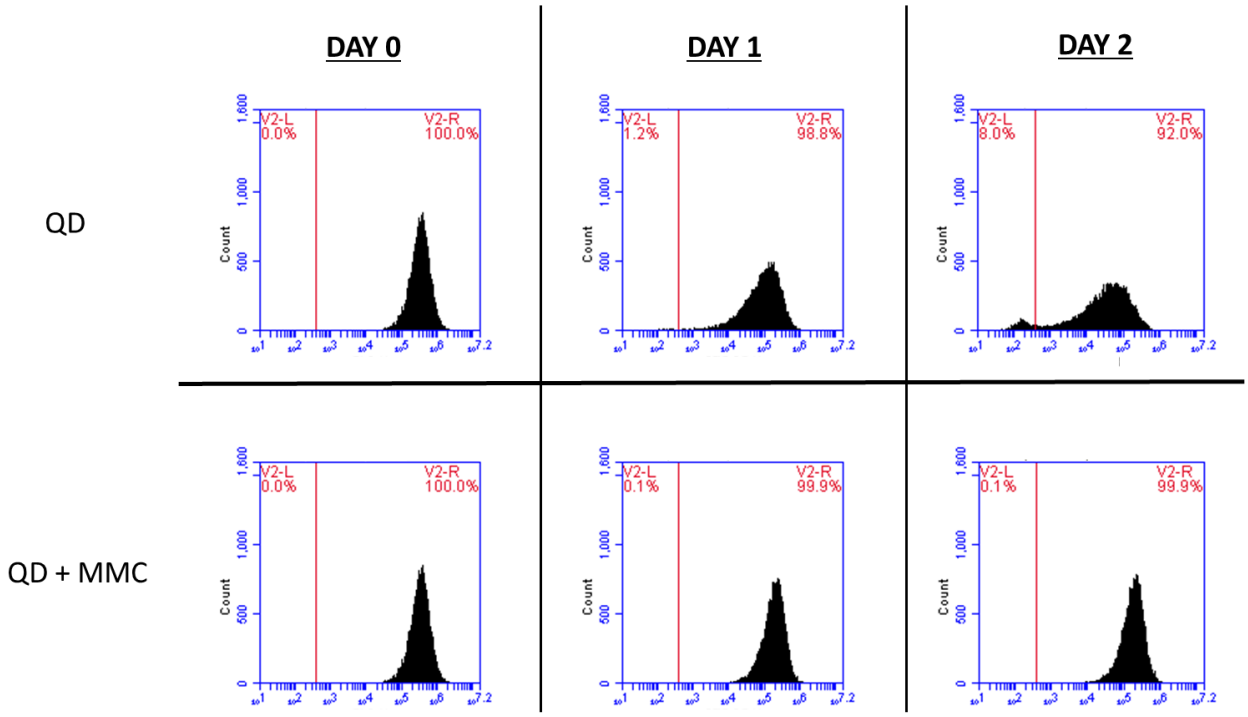

Figure 14. Quantification of QD label loss during inhibition of cell proliferation. Flow cytometric analysis of QD-labeled cells with and without mitomycin C. QD-labeled cells without mitomycin C (top row) have a decline in the % labeled cells over two days of cell division compared to cells not undergoing cell division (bottom row).

labeled with QD revealed that there are no adverse consequences of the label on cell growth or function. Using QD label on cells intended for injection into an animal should be considered a reliable way to monitor the location and activity of the ECFCs (Mannucci et al., 2017; Rosen et al., 2007; Sugaya et al., 2016). As cellular therapy and regenerative medicine continues to advance, understanding the activity and location of injected cells is paramount to understanding the true effectiveness of these cells (Burk et al., 2016). Good study design which includes appropriate control groups will assist in this assessment, but the value of being able to objectively identify the location of a previously injected cell, either *in vivo* or *ex vivo*, cannot be understated. Based on the strong fluorescent signal emitted at many time points subsequent to the labeling process, using a QD label in equine ECFCs should be considered a reasonable option to investigators.

A range of concentrations of QD label can be used according to the QD manual, from 1 nM to greater than 20 nM. ECFCs isolated from humans have had function evaluated after a QD label concentration of 8 nM with a 24 hr contact time (Molnar et al., 2010). No adverse effects on the ECFCs ability to form *in vitro* tubules and no adverse effect on cell morphology up to three generations after label were observed (Molnar et al., 2010). We subjectively assessed the label procedure of using 2 nM, 5 nM, 10 nM, and 20 nM concentration with a 12 hr and 24 hr label contact time (Figure 5) in order to find label procedure ideal for use in equine ECFCs. For each concentration, the 24 hr label contact time resulted in subjectively brighter fluorescence than the 12 hr label contact time. Based on this preliminary investigation, the 20 nM concentration with a 24 hr label contact time had the brightest fluorescent signal. In the present study,

the 20 nM QD labeled cells had a significantly higher mean fluorescent signal than the 5 nM label at the time of label and also at three, four, and six passages after the time of label. This may be an important consideration for *in vivo* studies in which identification of the injected cells post injection is planned. Although a brighter fluorescent signal would be expected with label concentrations of greater than 20 nM, based on this study we could only assure adequate function of the labeled ECFCs up to 20 nM.

In regenerative cellular therapy investigations, QD labels are used extensively in animal models for human and veterinary medicine (Lin et al., 2007; Mannucci et al., 2017; Slotkin et al., 2007; Sugaya et al., 2016). Other methods of cell labeling have been used in equine disease models such as transduction with lentivirus to induce green fluorescent protein production or *in vitro* labeling with SPIO (Burk et al., 2016; Hardman, 2006; Peterson GF, 2014). QD labels are easy to apply, have been shown to be safe in multiple cell lines, and are readily identifiable in cells long after the label is applied. Some studies suggest that the outer coating used in QD formation as well as the concentration used may affect how toxic QD is to cells (Hardman, 2006; Pelley et al., 2009). Lower concentrations of QD label are generally thought to be less toxic, which is why some studies use relatively lower concentrations of QD label (Hardman, 2006; Molnar et al., 2010). The coating for the QD nanocrystals used in this study is a CdSe coating, similar to many other commercially-available QD labels. We assessed cell function immediately after the 24 hr incubation with the QD label in equine ECFCs, which would be the time point at which the QD label concentration was greatest. No adverse effects on cell function, cell growth, or cell morphology up to P10 were observed in QD labeled cells in this study. Therefore, using a QD label concentration of

up to 20 nM in equine ECFCs would allow these cells to be tracked without adversely affecting cell behavior. The concentrations of QD used in this study were chosen based on preliminary work in the authors' lab subjectively evaluating intensity of fluorescence of QD label concentrations. The QD concentrations of 5 nM and 20 nM were chosen based on the ability to subjectively differentiate the fluorescence intensity of these concentrations, which was considered useful for *in vivo* applications of tracking cells in tissues, and using concentrations over 20 nM was unlikely for *in vivo* applications. However, comparison of proliferative capacity and cell function at multiple other doses was not performed in the current study.

In order to monitor the loss of QD label over multiple cell divisions, we chose to passage at a 1:4 ratio. This allowed fewer cell divisions to occur at each passage compared to standard cell culture conditions. Under standard cell culture conditions for ECFCs, during each passage the new cell culture flask would be seeded with 3,000 cells / cm^2 (Burk et al., 2016; Kovacic et al., 2008). This would cause the QD label to decrease progressively over time, as the QD label is partitioned to daughter cells with division (Molnar et al., 2010; Pi et al., 2010). Using a QD label of 8 nM on human ECFCs at standard cell culture seeding and cell division conditions, less than 20% of the QD label remained after three passages (Molnar et al., 2010). In our study using a 20 nM QD label concentration on equine ECFCs, we observed that 27.5% +/- 14% label remained after three passages. These cultured cells have an optimal environment for cell division. Quantification of the differences between *in vitro* and *in vivo* cell growth conditions is not straightforward, and there are many microenvironments that may not be optimized for ECFC division. For instance, *in vivo* cells experience reduced nutrients

and space compared to *in vitro* standard cell culture environments (Carvalho et al., 2014; Falomo et al., 2015; Ortved and Nixon, 2016; Sharpe et al., 2016). This may be particularly true for pro-inflammatory *in vivo* environments where tissue oxygen and metabolite levels are decreased (Carvalho et al., 2014; Falomo et al., 2015; Ortved and Nixon, 2016). Cell function has been shown to be compromised for EPCs and other cells within inflammatory conditions (Carvalho et al., 2014; Falomo et al., 2015). Therefore, ECFCs would divide less over a given amount of time compared to that same time *in vitro* cell culture conditions. For this reason, we chose to passage QD labeled ECFCs at a 1:4 ratio, to somewhat emulate the number of divisions these cells may have if injected *in vivo*. Thus, the percentage of cells that remain labeled at each passage may provide relevance for understanding the QD label of ECFCs injected *in vivo*.

Some studies using a QD label report a variable labeling efficiency in different cell lines, but this study shows that equine ECFCs from multiple lines are all labeled efficiently with QD. For studies investigating autologous cells for regenerative therapies, consistency of QD labeling between lines is critical to obtaining meaningful results. The mechanism of label loss varies by cell type. One study demonstrated that QD label was rapidly degraded by murine embryonic stem cells, with 15.8% +/- 2.9% of embryonic stem cells maintaining QD label only 48 hr after label (Pi et al., 2010). This is in contrast with murine embryonic fibroblasts which maintained high levels of QD-labeled cells 48 hr after label, with almost 95% of embryonic fibroblasts maintaining QD label after 72 hr when MMC was added to cell culture media (Pi et al., 2010). Mouse embryonic stem cells were also found to excrete QD label into the surrounding cell

culture media (Pi et al., 2010). Human EPCs may lose QD label from cell division, and mouse embryonic stem cells lose QD label by cell division or leaking of the QD label (Lin et al., 2007; Molnar et al., 2010). In our study, we investigated the mechanism of label loss by blocking cell division through the addition of MMC. If QD label leakage or metabolism was the major mechanism of label loss in equine ECFCs, then the percentage of cells labeled with QD or the fluorescent intensity would have decreased over time in cells with and without MMC added. However, a substantial label loss was not observed when MMC was present. Therefore, our study shows that equine ECFCs have substantial loss of QD label over time due to cell division.

3.5 Conclusion

This study demonstrated that equine ECFCs were labeled effectively with QD nanocrystals, but label loss occurred as the label was partitioned to daughter cells during division. Equine ECFCs do not have their growth or functional characteristics altered with QD label, thus making this *in vitro* labeling procedure favorable for *in vivo* cell tracking of this cell type in horses.

Chapter 4: Evaluation of cell engraftment, vascularization, and inflammation after treatment with endothelial colony forming cells encapsulated within hydrogel microspheres in an equine distal limb wound model

4.1 Introduction

Wounds, especially of the distal limb, are costly and complicated problems for equine veterinary medicine (Theoret and Wilmink, 2013). In the 2015 Needs Assessment Survey conducted by the National Animal Health Monitoring System for Equine health, one of the top priorities for further focus was leg / hoof problems leading to lameness (NAHMS, 2014). Approximately 7% of all injuries leading to retirement of a racehorse are the result of a limb wound (Perkins et al., 2005). A common consideration of wound healing in the horse is that primary closure of limb wounds is often unsuccessful. In a retrospective study evaluating more than 500 ponies and horses, primary closure of limb wounds was successful in only 26% of the horses in which it was attempted (Wilmink et al., 2002). Without healing by primary closure, healing with second intention repair by granulation tissue formation is the only option.

Poor or delayed healing of equine distal limb wounds is one of the most common problems faced by equine practitioners and horse owners. Distal limb wounds in the horse may have physical disruption of blood supply, excessive inflammation, and local ischemia and hypoxia, all of which contribute to the formation of exuberant granulation tissue (EGT) and slow wound healing times (Bertone, 1989; Celeste et al., 2011; Lepault et al., 2005; Theoret and Wilmink, 2013). Distal limb wounds have protracted inflammation and slower epithelialization compared to body wounds, in part due to poor wound oxygenation (Bertone, 1989; Celeste et al., 2011; Lepault et al., 2005; Theoret

and Wilmink, 2013). Wounds with EGT have an abundant vascular supply, with new blood vessels sprouting within the EGT for rapid granulation tissue volume growth (Celeste et al., 2011; Theoret and Wilmink, 2013); however, these vessels may be dysfunctional and occluded, thus promoting fibroproliferation (Lepault et al., 2005). Based on their ability to heal damaged blood vessels and form new vessels *in vivo*, ECFCs may be an attractive option for promoting wound healing in distal limb wounds of the horse.

Although promising for use as an injectable treatment, there are important barriers to consider for ECFCs and other cellular therapies for tissue regeneration and repair. Direct injection of ECFCs or other cells into the wound or wound periphery is the most straightforward way to deliver these cells. However, the mechanical shear stress that these cells encounter during the injection through the needle is often enough to damage or kill many of the injected cells (Aguado et al., 2012). When human umbilical vein endothelial cells were injected through a syringe and needle *in vitro*, only 58.7% survived the injection (Aguado et al., 2012). Additionally, there are other challenges for cell survival once the cells are injected into tissue *in vivo*. Cells that are injected into or around damaged areas such as inflamed wounds or infarcted areas experience a harsh environment with reactive oxygen species or damaging inflammatory cytokines (Robey et al., 2008). The low retention rate of injected cells of ~5-9% in animal models of disease may be caused by cell death associated with either the injection or the harsh environment into which they are injected (Freyman et al., 2006; Yasuda et al., 2005).

One possible remedy to the problem of low cell retention and cell death during injection involves the use of a biomaterial for cell delivery, specifically a material readily

broken down by the body and unlikely to elicit an inflammatory reaction once injected. Hydrogels are 3-dimensional scaffolds composed of hydrophilic polymer chains and can be cross-linked into any desired shape (Seliktar, 2012). These hydrogels can also be coupled with oligopeptides or proteins to more strongly mimic extracellular matrix (Lutolf and Hubbell, 2003; Seliktar, 2012). Cells that are encapsulated in biomimetic hydrogels experience a microenvironment similar to the native extracellular environment (Lutolf and Hubbell, 2005). This may in part explain why stem or progenitor cells that are encapsulated into hydrogels demonstrate proliferation and long-term survival (Rafii and Lyden, 2003). One hydrogel biomaterial that has been investigated with cell therapy is poly(ethylene) glycol coupled with fibrinogen (PEG-Fb). Injecting cells that are surrounded by PEG or other hydrogels has been shown to enhance immediate survival of injected cells (Aguado et al., 2012; Zhang et al., 2008). Our group can consistently create cell laden PEG-Fb microspheres (MS) for injection (Seeto et al., 2017). The equine ECFC viability post-encapsulation was 97%, and cell marker expression and function was normal (Seeto et al., 2017). Encapsulated cells survived after injection through 18 – 23 gauge needles, and were detected in equine skin 1 week after injection (Seeto et al., 2017).

Given the potential beneficial effects of using ECFCs on wounds with vascular damage and the potential benefits of coupling ECFCs with the biomaterial PEG-Fb, we hypothesized that: 1) ECFCs injected into an equine distal limb wound model would participate in vascularization of the wound and form *de novo* blood vessels; and 2) wound healing and vascularization would be enhanced in wounds where ECFCs are injected and this effect would be augmented with PEG-Fb biomaterial encapsulation.

We aimed to evaluate these hypotheses by non-invasive wound assessment, immunohistochemical (IHC) evaluation of vascularization and inflammation, and *in vivo* tracking of ECFCs that were labeled *in vitro* prior to injection in an equine distal wound model. The overall aim of this study was to evaluate the influence of ECFCs with and without PEG-Fb encapsulation on healing time, vascularization and inflammation of distal limb wounds in the horse.

4.2 Methods

4.2.1 Horses

All procedures involving animals were approved by the Auburn University Institutional Animal Care and Use Committee (# 2014-2637). Six, healthy university-owned, adult horses (ages 9 – 26 years) were utilized for autologous ECFC isolation and to create the distal limb wound model. Five were geldings and one was a mare. Breeds included warmblood (N=2), quarter horse (N=1), Tennessee walking horse (N=1), thoroughbred (N=1), and a thoroughbred cross (N=1). They underwent general physical examinations before recruitment into the study. Horses were kept free in individual box stalls in an environmentally-controlled building for the duration of the study (4 weeks) and allowed *ad libitum* access to grass hay and water. Horses were examined daily for signs of discomfort, lameness, and systemic illness. At the termination of the study, the animals were monitored until all wounds were completely healed, and then returned to their herds.

4.2.2 Autologous ECFC isolation and labeling

Whole blood was collected from either the cephalic vein or the jugular vein for autologous ECFC isolation using either a whole blood isolation or density gradient centrifugation isolation method as previously described (Salter et al., 2015; Sharpe et al., 2016). ECFCs were characterized based on cell surface markers (positive staining for von Willebrand factor, vascular endothelial growth factor receptor-2, CD34, CD105, and CD14) and *in vitro* formation of tubules on basement membrane and uptake of low density lipoprotein (Salter et al., 2015; Sharpe et al., 2016). ECFCs were cryopreserved in freezing medium (5% DMSO, 95% FBS), and then thawed for use as passage 3 – 5. ECFCs were cultured in 75 cm^2 cell culture flasks with 12 mL endothelial cell growth medium at standard cell culture conditions (37° C, 5% CO_2, 95% humidity) with manufacturer-supplied growth factors and anti-microbials (Lonza, Visp, Switzerland) and 10% equine serum (HyClone Laboratories Inc, Logan, UT). Adherent ECFCs of passage 3-5 were labeled with 4 nM QD, where the QD label remained in contact with the cells for 1 hour (Winter et al., 2018). ECFCs were then rinsed three times and fresh endothelial cell growth medium was added.

4.2.3 Encapsulation of ECFCs

PEG-fibrinogen was synthesized using a previously published method (Almany and Seliktar, 2005). Fibrinogen was dissolved in 8 M urea (Sigma-Aldrich, St. Louis, MO, USA) in PBS (Lonza) solution to obtain a final concentration of 7 mg/mL and a pH of 7.4. Tris (2-carboxyethyl) phosphine (Acros Organics, Geel, Belgium) was then

added to the solution, and it was reacted at a pH of 8. PEGDA was dissolved in urea-PBS to obtain a final concentration of 280 mg/mL. The fibrinogen solution was then slowly added to react for 3 hr in the dark at room temperature. After this reaction, PEGylated fibrinogen was extracted with acetone, which was followed by centrifugation in order to remove the acetone, and then this was dissolved in urea-PBS again for the purpose of dialysis. This product was then dialyzed in sterile PBS over 24 hr in the dark at a temperature of 4° C and then stored at -80° C. The protein content was determined to be 12.5 mg/mL using a Pierce BCA protein assay kit (Thermo Fisher, Dublin, OH, USA). The PEGylation yield was calculated as 98.1%.

Cell encapsulation in PEG-fibrinogen hydrogel was achieved using a custom microfluidic polydimethylsiloxane (PDMS) system (Seeto et al., 2017). The PDMS mold was created using a Sylgard 184 silicone elastomer kit (Dow Corning, Midland, MI, USA) by mixing the base and cure component into a polystyrene dish which contained the pre-assembled microfluidic channel mold. This mixture was degassed and heat-cured at 60° C for 2 hr. The microfluidic channel mold was disassembled after curing. The microfluidic PDMS mold was then sonicated in 70% ethanol for purposes of cleaning and sterilization before and after each use.

Before cell encapsulation, polymer precursor solution was prepared by mixing PEG-fibrinogen with 0.1 w/v% of Pluronic P68 (Sigma-Aldrich, St. Louis, MO, USA) solution, 0.1 mM of EosinY photoinitiator (Fisher Scientific, Pittsburgh, PA, USA) solution, 1.5 v/v% triethanolamine (Acros Organics, Geel, Belgium), and 0.39 v/v% of N-vinylpyrrolidone (Sigma-Aldrich, St. Louis, MO, USA). ECFCs were detached from the

tissue culture flask, centrifuged, and then resuspended in the crosslinking precursor solution to a cell density of 10 million cells/mL.

A biosafety cabinet was used for cell encapsulation and hydrogel photo-crosslinking to maintain sterility. The PDMS custom device had two inlets and one outlet where cells and polymer precursor mixtures flowed from the top inlet, and the mineral oil flowed from the bottom inlet using syringe pumps (Figure 15). When the streams met at the junction, MS were formed by emulsification. The cell-encapsulated MS were cross-linked by a 2.7 W full spectrum visible light (Prior Scientific, Rockland, MA, USA). A mirror was placed behind the microfluidic device near the outlet in order to aid the crosslinking process by reflecting light that passed through the device. The MS were washed from the outlet using pre-warmed Dulbecco's Modified Eagle Medium (DMEM) aided by a third syringe pump (set at 22 mL/hr). The resulting cell-laden PEG-Fb MS (ECFC/MS) were then washed twice with Dulbecco's Modified Eagle Medium (DMEM) by centrifugation (200 g for 3 min) to remove residual mineral oil, and MS were cultured in endothelial cell growth medium at 37° C and 5% CO_2. Preliminary studies assessed the impact of encapsulation on ECFC survival, cell surface marker expression, growth, and ability to form tubules in tissue after being injected (Seeto et al., 2017). Cell viability after encapsulation was tracked in subset of ECFC/MS used in this study by utilizing an XTT cell viability assay (Biotium, Fremont, CA, USA) and microplate reader (BioTek, Winooski, VT, USA).

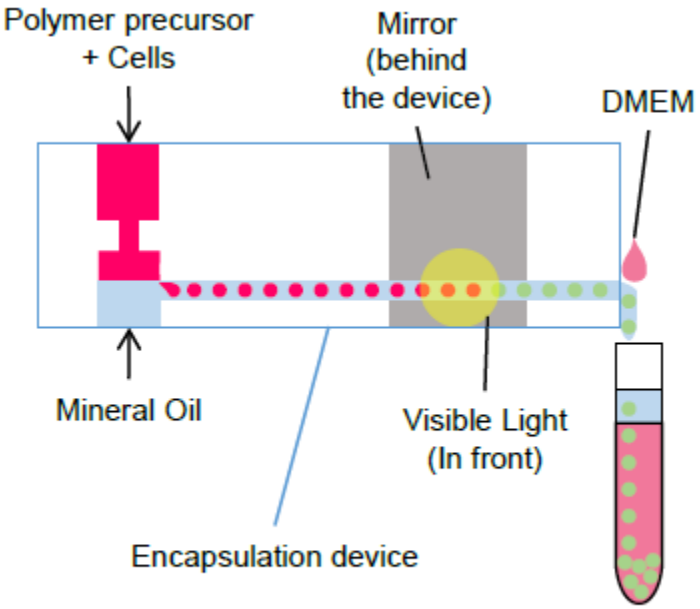

Figure 15. Formation of microspheres containing ECFCs. Schematic of how the PDMS mold was used to encapsulate ECFCs into microspheres. The polymer precursor with ECFCs was mixed with mineral oil, which formed microspheres due to emulsification. The microspheres were then cross-linked with a 2.7 W full spectrum light.
DMEM = Dulbecco's Modified Eagle Medium.

4.2.4 Creation of distal limb wounds

On day 0, horses were restrained in stocks and sedated with detomidine hydrochloride (0.01 mg/kg; IV) and butorphanol tartrate (0.04 mg/kg; IV). Hair was clipped from the dorsolateral surfaces of both metacarpi and metatarsi. Perineural anesthesia of the median cutaneous antebrachial nerve, deep and superficial peroneal nerves and ring blocks was performed using 2% mepivacaine hydrochloride. The surgical sites were aseptically prepared, and 2 full-thickness wounds of 2.5 cm X 2.5 cm (6.25 cm^2) area were created on each metacarpus and metatarsus using a sterile wound template and a #15 scalpel blade (Figure 16); this skin was kept as the baseline sample for immunohistochemistry. Each horse had 2 wounds created per limb (fore and hind) for a total of 8 wounds per horse (Figure 17). The wounds were bandaged for approximately 24 hr for hemostasis and then left to heal by second intention for the duration of the 4-week study. Bandaging consisted of a non-adherent gauze dressing, covered with a cotton wool roll held in place with a tertiary adhesive layer. Horses were examined daily for signs of discomfort, lameness, and systemic illness. Wounds were monitored until healed.

4.2.5 Experimental phases

Wounds were injected with 4 different treatments with two phases of the study (Figure 17). Treatments included equine serum, ECFCs suspended in serum, acellular PEG-Fb MS suspended in serum, and ECFCs-laden PEG-Fb MS (ECFC/MS) suspended in serum. Each wound was randomly assigned to one of the 4 treatments

Figure 16. Creation of distal limb wound. A sterile template was used to create two 6.25 cm^2 full-thickness skin wounds on each equine distal limb.

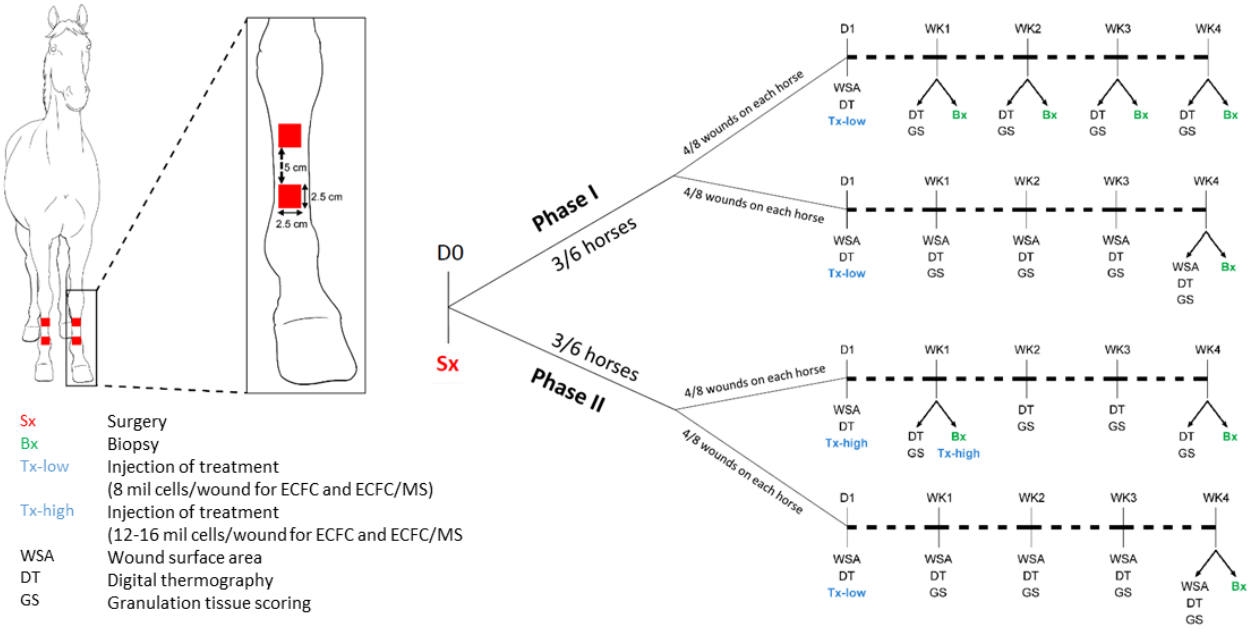

Figure 17**.** Schematic of study design. Two wounds were created on each metacarpi/metatarsi. Tissues from biopsies were formalin fixed and paraffin embedded for immunohistochemistry or frozen in optimum cutting temperature media and imaged with confocal microscopy for cell tracking.

Horse	Limb	Wound location on limb	Right limb Treatment	Left limb treatment
1	Forelimb	Proximal	ECFC	MS-bx
		Distal	Serum-bx	ECFC/MS-bx
	Hind limb	Proximal	Serum	ECFC-bx
		Distal	ECFC/MS	MS
2	Forelimb	Proximal	ECFC	Serum-bx
		Distal	ECFC/MS-bx	MS
	Hind limb	Proximal	MS-bx	Serum
		Distal	ECFC/MS	ECFC-bx
3	Forelimb	Proximal	MS-bx	ECFC/MS
		Distal	ECFC-bx	Serum
	Hind limb	Proximal	Serum-bx	ECFC/MS-bx
		Distal	ECFC	MS
4*	Forelimb	Proximal	MS-bx	Serum
		Distal	Serum-bx	MS
	Hind limb	Proximal	ECFC-bx	ECFC
		Distal	ECFC/MS-bx	ECFC/MS
5*	Forelimb	Proximal	ECFC	MS
		Distal	ECFC/MS	ECFC-bx
	Hind limb	Proximal	MS-bx	ECFC/MS-bx
		Distal	Serum-bx	Serum
6*	Forelimb	Proximal	Serum	ECFC-bx
		Distal	ECFC/MS-bx	ECFC/MS
	Hind limb	Proximal	MS	ECFC
		Distal	Serum-bx	MS-bx

Table 1. Treatment assignments for all 6 horses. All wounds were biopsied at the completion of the study, and some wounds had biopsies also taken prior to the completion of the study (indicated with “-bx”). *Indicates horse was injected twice.

using a random number generator, resulting in 2 wounds per treatment per horse. All investigators involved in wound assessment or daily care of the horses were blinded to the treatment assignments. Treatment and biopsy designation were randomly assigned (Table 1).

In Phase 1, three horses had treatments injected around the wound periphery at a single time point (24 hr after wound creation, day 1). ECFC and ECFC/MS treated wounds were injected at the mid-point of each wound edge with 2 million cells for a total of 8 million cells/wound. For the 2 wounds with the same treatment, one wound was biopsied weekly, and the other wound was only biopsied at the end of the study. Phase 1 horses had the following biopsy schedule: 4 wounds (1 from each treatment) had biopsies collected at the medial leading edge and at the center of the wound at 4 weeks. The other 4 wounds (one from each treatment) had biopsies collected from one wound leading edge each week (order of biopsy location was: medial, lateral, ventral, then dorsal) for 4 consecutive weeks and from the center of the wound at week 4.

In Phase 2, three horses had treatments injected into 4 wounds at a single time point (24 hr after wound creation, the same as described in phase 1) and into 4 wounds at 2 time points (24 hr and 1 week post wound creation). Four wounds (1 per treatment) were injected once with 8 million cells/wound (LOW) for ECFC and ECFC/MS groups (day 1), and the medial leading edge and the center of the wound were biopsied at 4 weeks. The other 4 wounds (one per treatment) were injected twice with a higher dosage of cells: once at 24 hr with 16 million cells/wound (4 injections on 4 edges with 4 million cells/injection), and then again at week 1 with an additional 12 million cells/wound (3 injections on 3 edges with 4 million cells/injection, 1 biopsy on 1 edge)

(HIGH). Syringes were numbered, and only the investigators that prepared the syringes knew what they contained. Everyone doing procedures with or evaluating the horses was blinded to the treatment that the horse received, but could not be blinded to the number of injections (once versus twice). For the 4 wounds with 2 treatment injections, biopsies were collected from the medial leading edge of the wound at week 1 (before the second injection) and then from the lateral leading edge and the wound center at 4 weeks.

Wounds were analyzed non-invasively each week of the study, and biopsies were analyzed by IHC for vascular formation and inflammation and by indirect immunofluorescence (IF) for cell tracking.

4.2.6 Treatments

To perform injections of treatments for each wound, horses were sedated and perineural anesthesia was administered as described above. The treatments were injected subcutaneously at the mid-point of each edge of the wound. The different treatments were loaded into 1 mL syringes at a volume of 600 (LOW) – 1000 (HIGH) µL. These syringes were kept on ice for 0.5 – 2 hr prior to injection. Syringes with ECFCs in suspension and ECFC/MS had either 2 million cells (LOW) or 4 million cells (HIGH) total per syringe. There were approximately 2800 ECFCs per MS. Wounds with LOW treatments were injected with approximately 750 MS, whereas wounds with HIGH treatments were injected with approximately 1500 MS. Injections were performed using an 18 gauge x 1” needle on a 1 mL syringe.

4.2.7 Wound biopsies

Surgical biopsies were obtained using a 6 or 8 mm punch biopsy instrument. For the surgical biopsy procedure, horses were sedated and local anesthesia administered as previously described. Wounds were cleaned with water and sterile 0.9 % NaCl. Debris was removed from the wound periphery and center with gentle, manual extraction. Biopsies were obtained at the leading edge of the wound with the punch instrument overlapping the visual epithelization and the granulation bed, or biopsies were obtained at the center of the wound, depending on the time point (Figure 18). Two biopsies were taken from each location. One biopsy sample was fixed in 10% neutral buffered formalin for 24-48 hr prior to processing and paraffin embedding (FFPE) for IHC, and the other sample was embedded in optimal cutting temperature (OCT) compound within a 15 mm X 15 mm X 5 mm disposable vinyl specimen mold (Sakura Finetek, Torrance, CA, USA). The cryomold was submerged in liquid nitrogen-cooled isopentane (2-methyl butane) to achieve a temperature of -176° C, and molds were stored at -80° C until sectioning and analysis.

4.2.8 Non-invasive Wound Assessment

The wound surface area (WSA) was measured weekly with digital photography. Each wound was photographed at a 40 cm distance with a metric ruler immediately adjacent to the wound for scale (Figure 19), and the area of the unhealed wound (Figure 20) at each time point was calculated using Image J software (imagej.nih.gov/ij/). WSA was calculated as percentage of the original wound size on

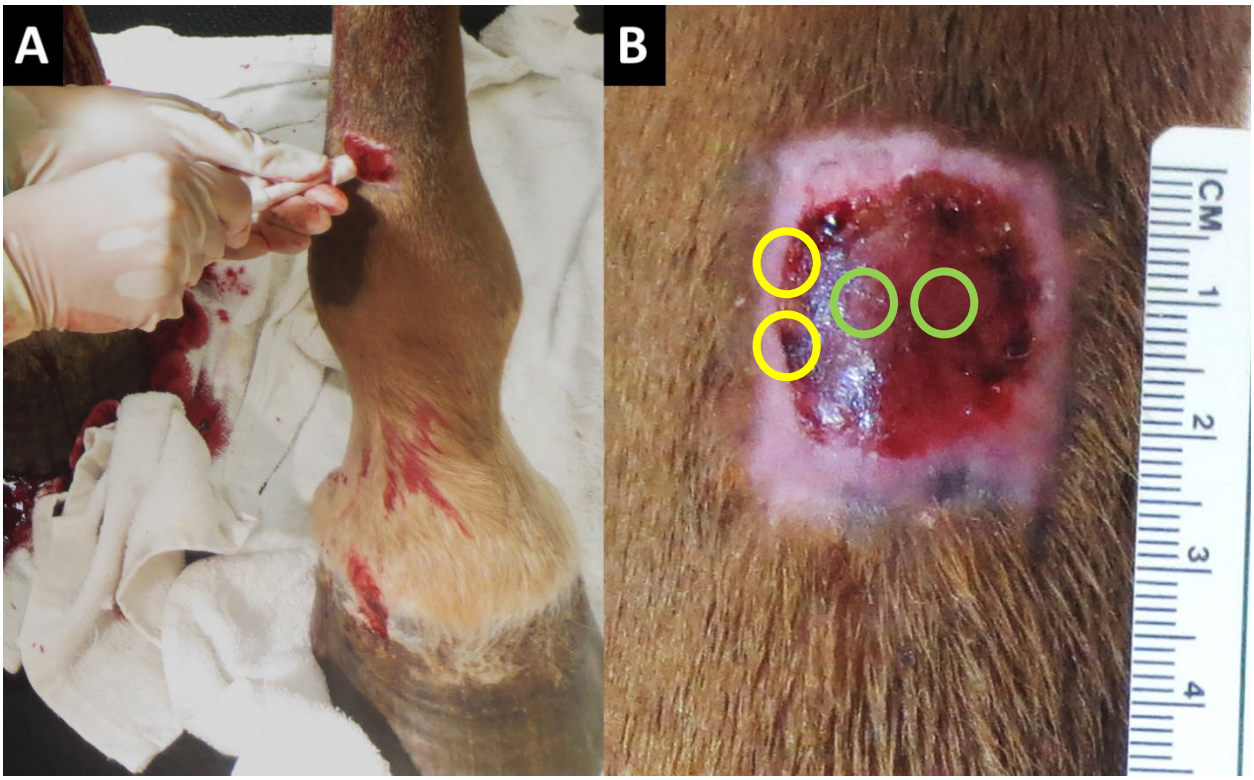

Figure 18. Location of biopsies. A) Photograph showing the process of obtaining punch biopsies. B) Photograph illustrating the representative locations of biopsy positions for the leading edge of wound healing (yellow circles) and the wound center (green circles).

Figure 19. Wound assessment with digital photography. Representative image demonstrating the digital photography technique for wound size measurement. The ruler was placed at the same location next to the wound for every image.

Figure 20. Measurement of wound surface area. Representative image demonstrating the use of Image J to trace the margins of the non-healed wound in order to calculate a wound surface area for each wound.

day 0 for non-biopsied wounds. Granulation tissue formation was scored weekly by two investigators (AAW, FJC) blinded to treatment assignment and experienced in equine distal limb wound assessment. Each observer scored all wounds independently based on 3 clinically-relevant parameters: protrusion of granulation tissue (0 = none; 1 = mild; 2 = marked); character of granulation tissue (0 = smooth; 1 = rough); and color of granulation tissue (0 = pink; 1 = yellow or dark red) (Ducharme-Desjarlais et al., 2005). Each category was weighted, with protuberance weighted 50% and quality and color of the granulation tissue weighted 25%. The average score of these was recorded, with the total weighted granulation score (GS) maximum being 1.5 for each wound.

Prior to the study, 24 hr after wound creation, and each week for the duration of the study, thermographic images were obtained with a hand-held infrared imaging radiometer placed at a distance of 45 cm from the distal limb, perpendicular to the wound surface. Infrared imaging emissivity was set at 0.98. Thermographic images were obtained for all horses prior to the initiation of the study to ensure no vascular or blood flow abnormalities existed in these horses' distal limbs. During the study, horses were moved into a temperature controlled, indoor treatment area and allowed to acclimate to the temperature for at least 15 min prior to digital thermography. Digital thermal images were collected for each wound at each time point, and the operator was blinded to the treatment assignments. Specific temperature readings were obtained from each edge of the wound (medial, lateral, proximal, distal), the wound center, and 1 cm above and 1 cm below the wound (FLIR B360, Optics Planet, Northbrook, IL, USA). For edge measurements (medial, lateral, proximal, distal), three distinct values were measured and then averaged for analysis as one value (Figure 21). All other anatomic

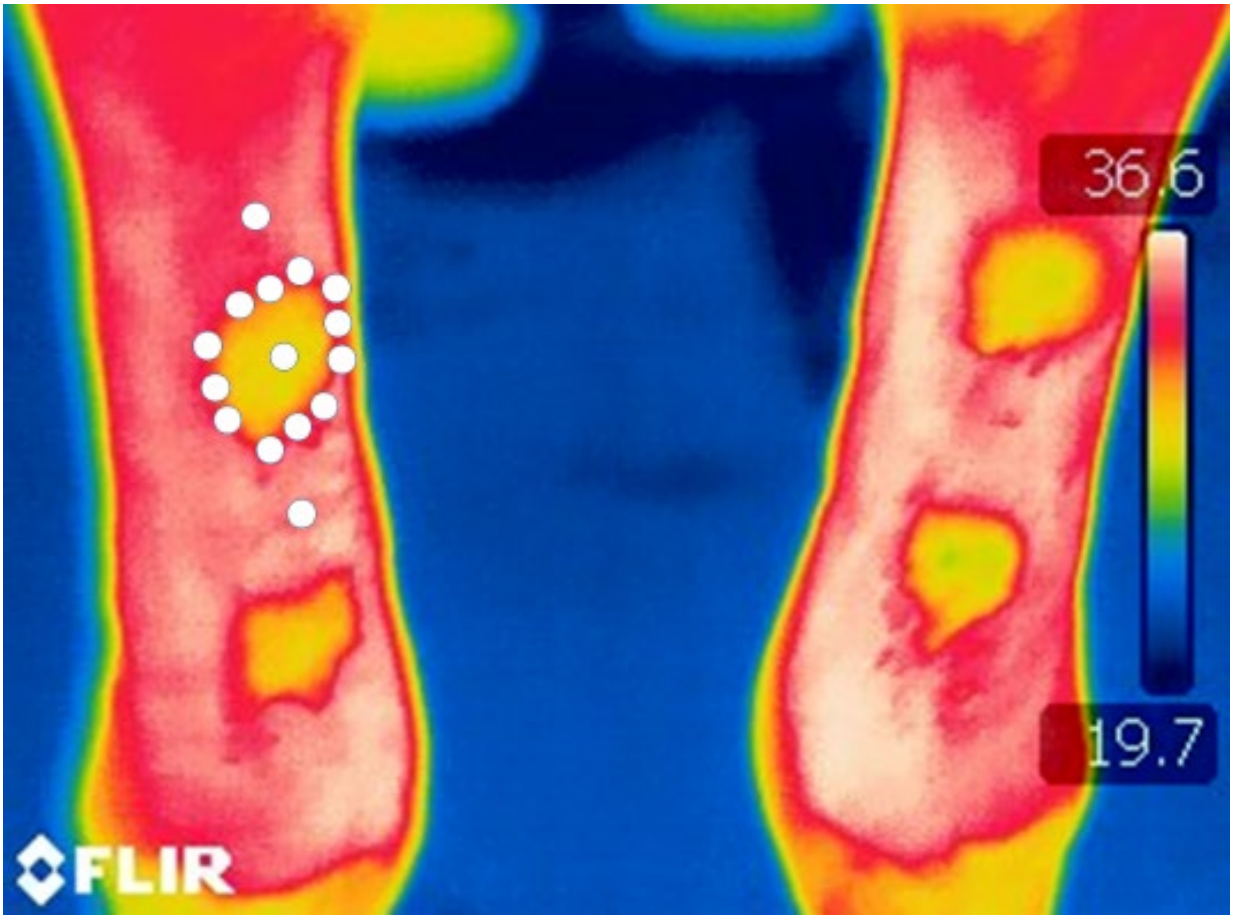

Figure 21. Assessment of wound temperature with thermography. Representative image showing thermographic imaging and the points at which discrete temperature measurements were taken (white circles). Note that the 3 measurements for each edge of the wound were averaged to give one value. These are the forelimbs of a horse as viewed in a cranial to caudal direction.

areas were measured once. Mean temperature for each specified anatomic area was calculated using the recorded ambient temperature and humidity to ensure accurate measurements. Temperature at all time points was compared to wound temperature at baseline (24 hr after initial surgery) and a percent change (% change) value calculated. The timing of this study was chosen to be performed during summer months, as this would best ensure that no cold temperature-related distal limb vasoconstriction would occur.

4.2.9 Tissue staining and Immunohistochemistry

The FFPE samples were cut to a thickness of 4 microns for all staining and immunohistochemistry. Initial review and assessment of adequate tissue quantity, quality, and orientation was performed using standard light microscopy on hematoxylin and eosin stained sections. Tissue sections were stained with Masson's trichrome (Polysciences, Warrington, PA, USA) to quantify collagen formation. The IHC staining was performed on FFPE tissue with the following: elastase to quantify activated neutrophil density (de la Rebiere de Pouyade et al., 2010; Munoz Caro et al., 2014); ionized calcium-binding adapter molecule 1 (IBA1) to quantify macrophage density (Kohler, 2007); von Willebrand factor (vWF) to quantify vascularization (Dejana et al., 1989); CD3 to quantify T-cell density (Murphy and Weaver, 2017); and paired box 5 (Pax5) to quantify B-cell density (Fuxa and Busslinger, 2007). Immunohistochemistry was performed at room temperature with primary antibodies diluted in 3% PBS as follows: polyclonal rabbit anti-human neutrophil elastase antibody diluted at 1:1000 for 30 min (Abcam 68672, Cambridge, MA, USA); polyclonal rabbit anti-mouse IBA1 diluted

1:750 for 30 min (CP290, Biocare Medical, Pacheco, CA, USA); polyclonal rabbit anti-human vWF manufacturer-diluted for 15 min (A0082, Dako, Santa Clara, CA, USA); polyclonal rabbit anti-human CD3 manufacturer-diluted for 15 min (GA503, Dako, Santa Clara, CA, USA); and monoclonal mouse anti-human Pax5 manufacturer-diluted for 20 min (M7307, Dako, Santa Clara, CA, USA). Immunodetection was achieved with a horse radish peroxidase (HRP) enzyme labeled polymer (Dako, Santa Clara, CA, USA) followed by conjugated rabbit secondary antibody applied for 30 min. This was followed by a 5 min PBS wash and visualization of antibody binding by reacting with 3,3'-diaminobenzidine solution for 3 min. Counterstaining of tissue sections was performed using hematoxylin for 4 min, followed by progressive alcoholic dehydration and cover-slipping. A representative image of the vWF immunohistochemical staining from one biopsy is presented in Figure 22.

Stained slides were digitally scanned (Appendix B) at a high resolution (Aperio, Leica Biosystems, Buffalo Grove, IL, USA). Each stain was quantified using custom-designed algorithms in a commercially available software program designed for histologic image analysis (Visiopharm®, Horsholm, Denmark). Within each tissue section, specific regions were designated "Inner Wound" (non-healed wound within advancing line of epithelialization), "Wound Periphery" (skin with epithelial cell cover, just on the periphery of the advancing line of epithelialization), and "Wound Center" (area at the center of the non-healed wound); the staining in these regions was quantified separately (Appendix C). Inner Wound and Wound Periphery regions were found in biopsies from the leading edge (analyzed at weeks 1 and 4), and the Wound

Figure 22. Immunohistochemical staining of blood vessels. Representative photomicrograph of von Willebrand factor immunohistochemical staining from a biopsy taken from the Wound Center at Week 4. Blood vessels are observed as a brown color. Scale bar is 2 mm.

Center region was from the biopsy taken from the center of the wound only at week 4. Within each tissue section, specific regions of interest (ROI) were analyzed as appropriate (Figures 23 and 24), and the software program quantified positively staining pixels / area and expressed as density: positive stain quantity / (positive stain quantity + non-stained quantity). Density values were then normalized to the individual baseline values for that wound as: [(density value – baseline density value) / baseline density value] x 100.

4.2.10 Indirect immunofluorescent staining and confocal microscopy

Samples frozen in OCT were kept at -30° C during sectioning, and all samples were sectioned at 20 micron thickness. There were 10 slides created per wound, with 2 tissue sections per slide for all wounds. Tissue sections were fixed in 4% paraformaldehyde in PBS for 20 min, rinsed twice in PBS, and then blocked with 3% fetal bovine serum (FBS) in PBS for 30 min at room temperature. In order to detect the intracellular protein vWF, tissues were permeabilized with 0.3% Triton in PBS for 10 min and rinsed with PBS 3 times. A polyclonal rabbit anti-human vWF antibody (A0082, Dako, Santa Clara, CA, USA) was added at a 1:200 dilution with 3% FBS and incubated overnight at 4° C. The tissue sections were washed with PBS and incubated with goat anti-rabbit Alexa Fluor 488 (A11008, Life Technologies, Grand Island, NY, USA) at a dilution of 1:400 in dark conditions for 60 min. Tissue sections were incubated with 4', 6-diamidino-2-phenylindole (DAPI) solution and then mounted with Fluoromount (Sigma-Aldrich, St. Louis, MO, USA). Glass slides were stored in the dark at -4° C and imaged within ~2 weeks.

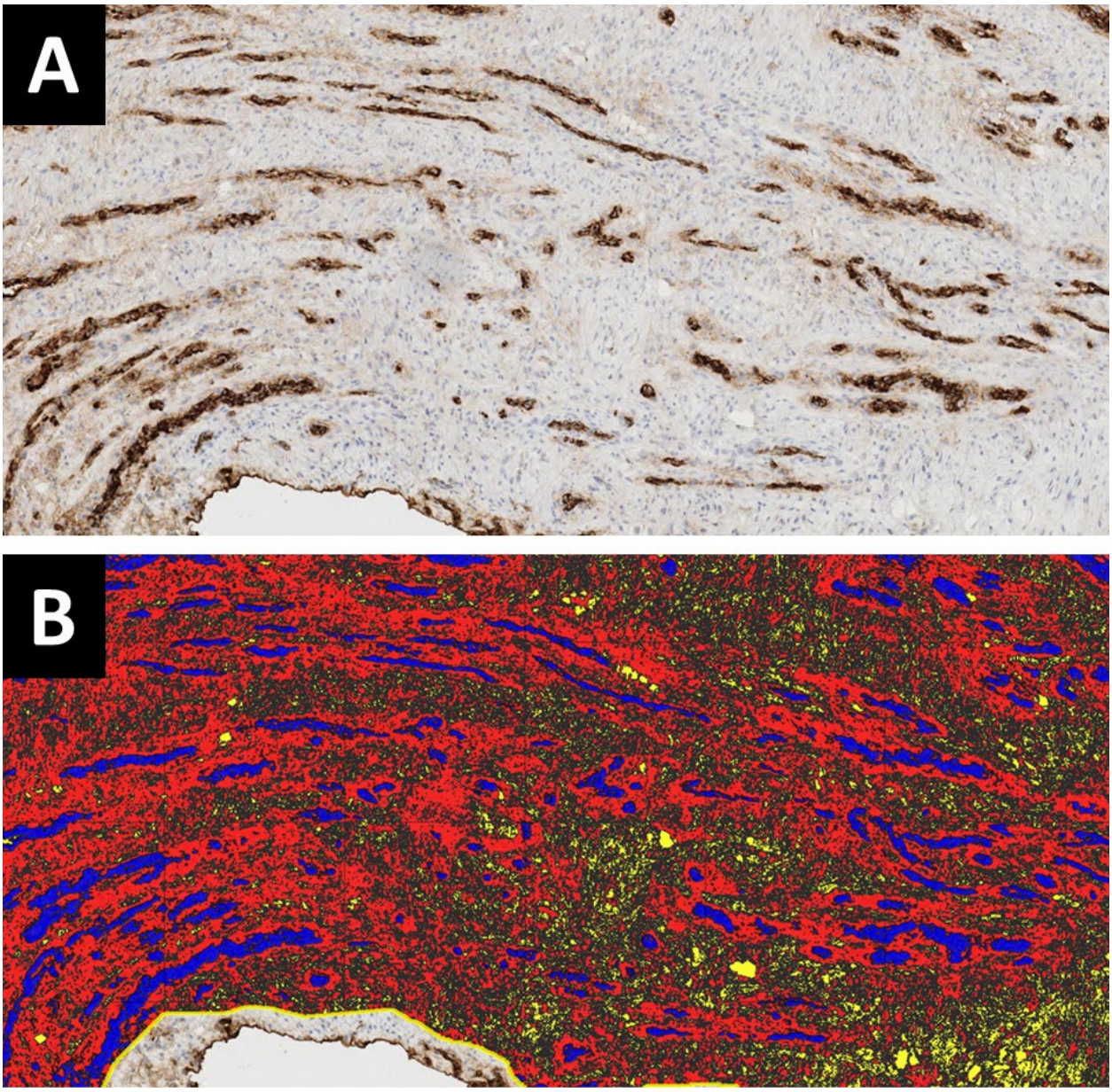

Figure 23. Quantification of IHC stain. Representative color-coded image demonstrating the ability of the Visiopharm® software program to identify different aspects of an immunohistochemical stain. A) Scanned image of a von Willebrand factor (vWF) stained skin biopsy (vWF positive blood vessels were brown). B) The Visiopharm® program has color coded all structures it recognizes as vWF positive in a blue color.

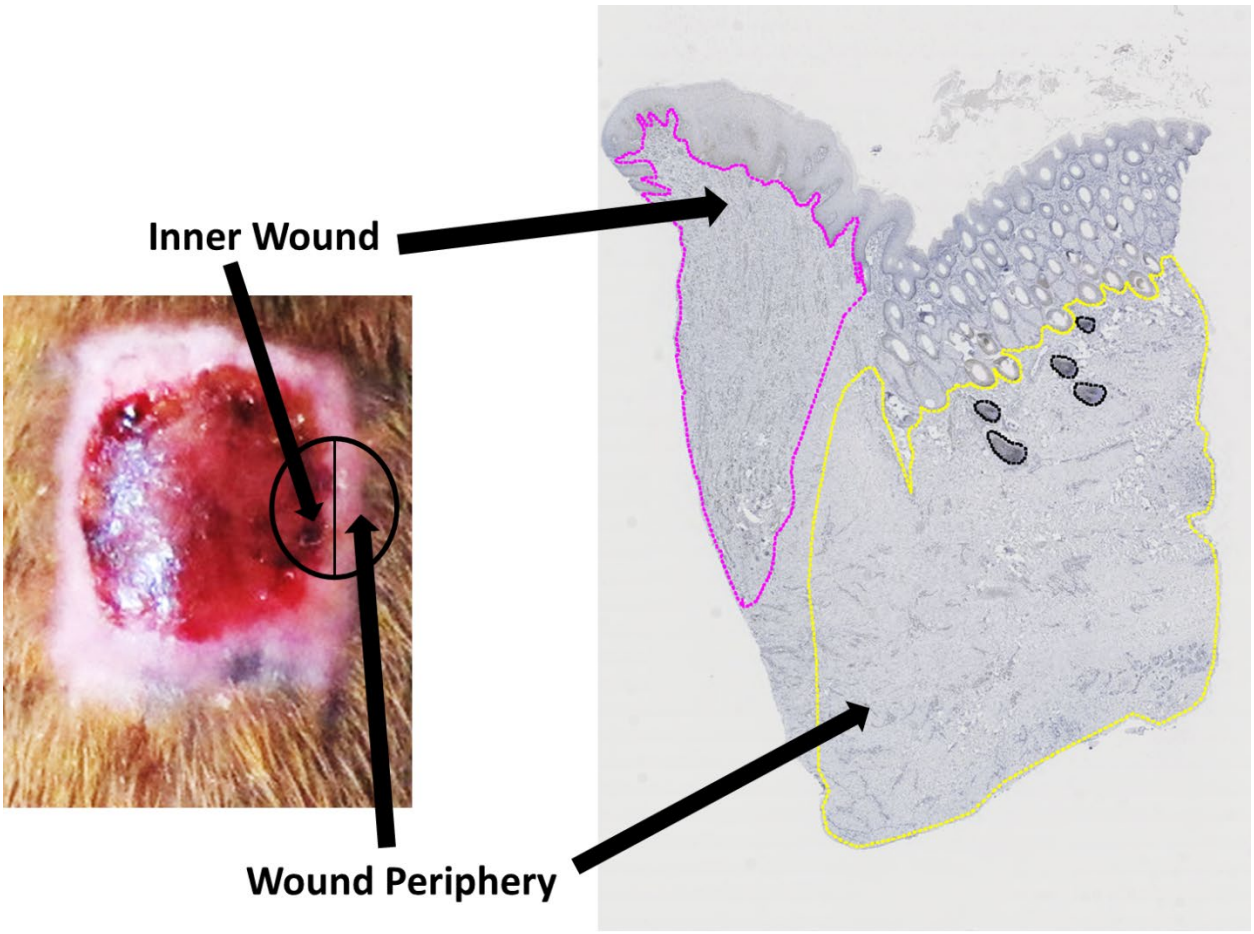

Figure 24. Regions of interest for analysis within a biopsy. The pink region of interest (ROI) indicates the Inner Wound and the yellow ROI indicates the Wound Periphery. Hair follicles encircled with a black ROI and excluded from analysis.

Endothelial cells stained with vWF and presence of QD-labeled ECFCs in cryosections were imaged using fluorescent and confocal microscopy. vWF staining was detected using the FITC filter (488 nm emission) at 20X magnification. Tissue sections from wounds treated with ECFC suspension or ECFC/MS were evaluated for the presence of red QD fluorescence. Confocal microscopy (2 μm slice thickness) was then used to co-localize QD positive cells, the DAPI stained nuclei, and the vWF positive blood vessels. The number of QD-labeled ECFCs in each image was counted and totaled for each cryosection. Preliminary studies were performed prior to the study to assess the impacts of tissue fixation and freezing in OCT had on detection of QD-labeled ECFCs, differentiation of QD fluorescence from tissue auto-fluorescent artifacts, and detection of vWF+ blood vessels within tissue sections (Figures 25, 26, 27).

4.2.11 Statistical analysis

Data were analyzed using commercially available software (JMP Pro 13.0 and SAS 9.4). Descriptive data were analyzed for normality using a Shapiro Wilk test or Q-Q plot and expressed as mean +/- SD or median (range) as appropriate. Thermographic data, WSA, granulation tissue scoring, and IHC stain quantification were assessed with a General Linear Model or a mixed model with repeated measures to assess the effect of individual horse as a random factor, and treatment groups, time point, wound location (forelimb vs hind limb), and effect of biopsy as fixed factors. Analysis of WSA was performed using a mixed model with repeated measures on wounds that were only biopsied at 4 weeks, so the statistical model for this variable

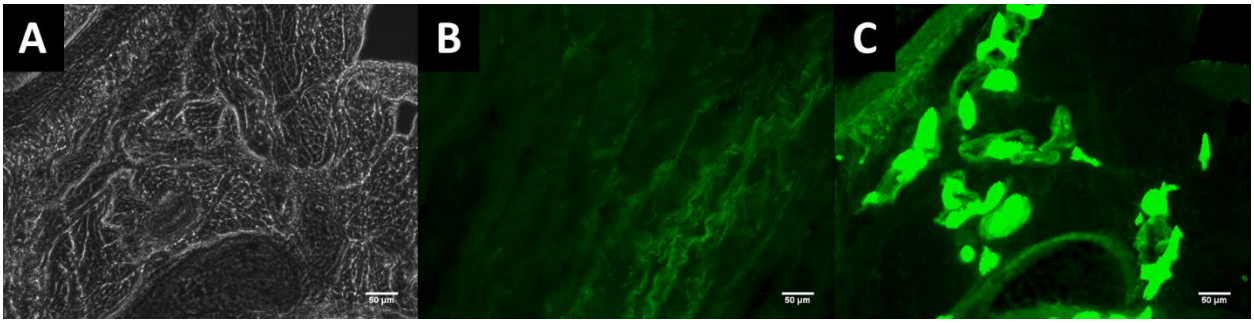

Figure 25. Influence of tissue fixation on blood vessel immunostaining. Tissue biopsies were fixed in formalin and then embedded in paraffin prior to sectioning for analysis. Representative photomicrographs of one field of a tissue section prior to immunostaining (A), after incubation with the anti-rabbit Alexa Fluor 488 secondary antibody (B), and after incubation with the polyclonal rabbit anti-human vWF primary antibody goat and the anti-rabbit Alexa Fluor 488 secondary antibody (C). Note the appearance of positively stained blood vessels in (C). Scale bars are 50 μm.

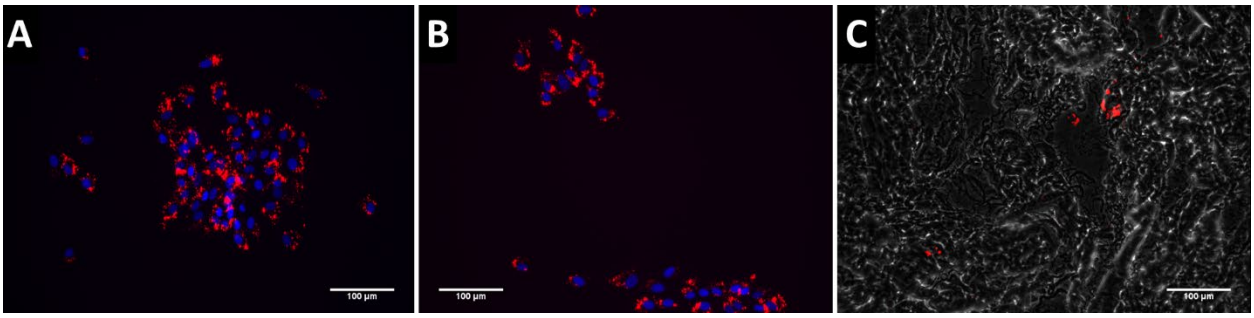

Figure 26. Observation of QD-labeled ECFC fluorescence after fixation. Representative photomicrography of ECFCs labeled with QD (red) and nuclei labeled with DAPI (blue) after 4% paraformaldehyde (A) or formalin (B). C) Representative photomicrograph of QD-labeled ECFCs (red) after injection into a skin biopsy just prior to embedding in OCT and freezing in liquid nitrogen. Scale bars are 100 µm.

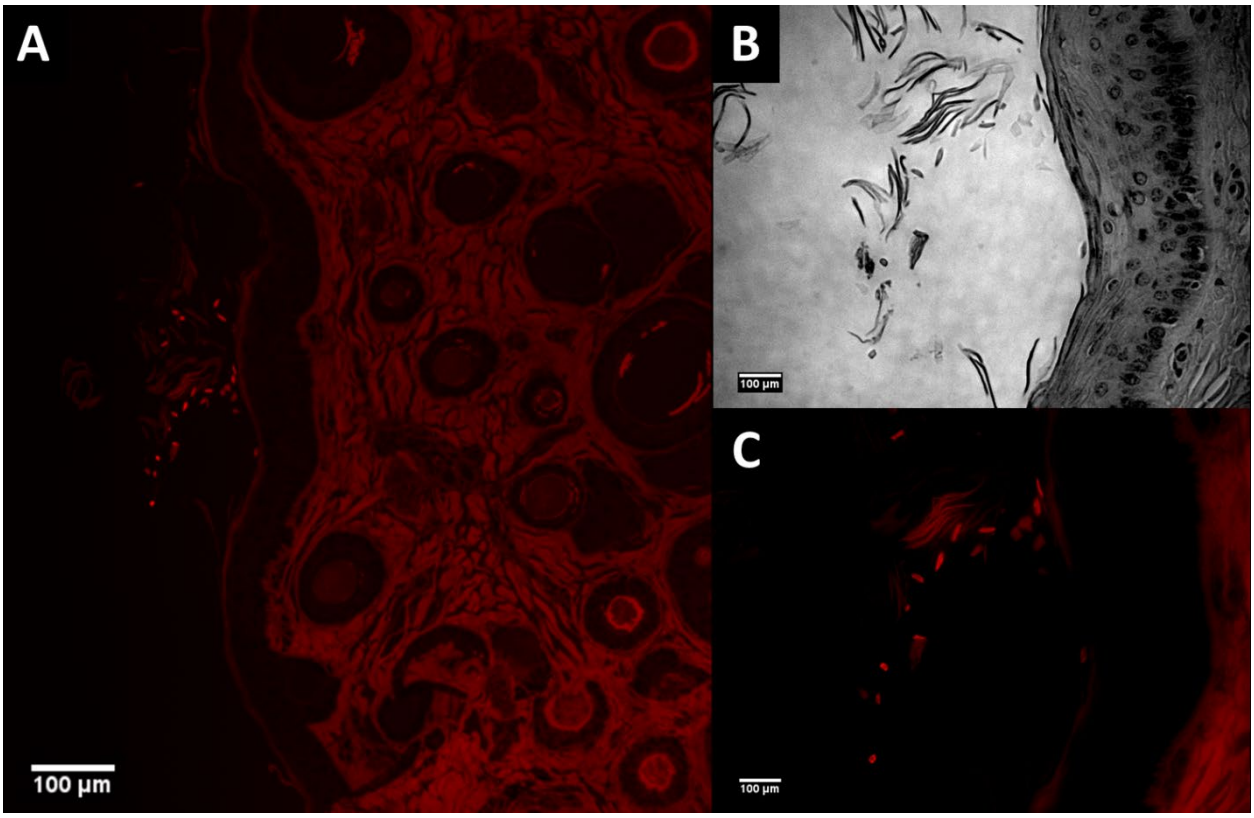

Figure 27. Equine skin auto-fluorescent tissue artifacts. A) Representative photomicrograph demonstrating the auto-fluorescence observed in one tissue section. B & C) Representative photomicrographs demonstrating auto-fluorescence of keratin as viewed with phase contrast imaging (B) and fluorescent microscopy (C). Scale bars are 100 µm.

assessed the effects of time point, wound location, and treatment. Analyses for thermographic data and granulation tissue scoring utilized a generalized linear model that included data from all wounds on all horses, so the effects of the time point, wound location, biopsy, and treatment (including ECFC injection dose and frequency) were included in the statistical model. Quantification of IHC stains was only performed on wounds biopsied once at either week 1 or week 4, so the statistical model for IHC stain quantification was a generalized linear model that included treatment and wound location and not time point since the same wound was not biopsied at each time point. Cell tracking descriptive data was obtained by week, and the number of QD-labeled cells was analyzed for influence of presence or absence of PEG-Fb MS encapsulation and dose of ECFCs injected. Tukey-Kramer tests were used to analyze differences between levels. Pearson correlation coefficients were used for associations between continuous variables. Associations between categorical variables were analyzed with a Fischer's exact test. $P<0.05$ was considered significant.

4.3 Results

4.3.1 ECFC function after encapsulation

Encapsulation of ECFCs produced highly uniform microspheres, and this uniform shape persisted after injection (Figure 28), and the cells that were encapsulated in the hydrogel microspheres had a viability of 96.8% +/- 1.4% as quantified using Live/Dead staining (Figure 29) (Seeto et al., 2017). ECFCs encapsulated into PEG-Fb microspheres not only survived but proliferated and migrated out from the

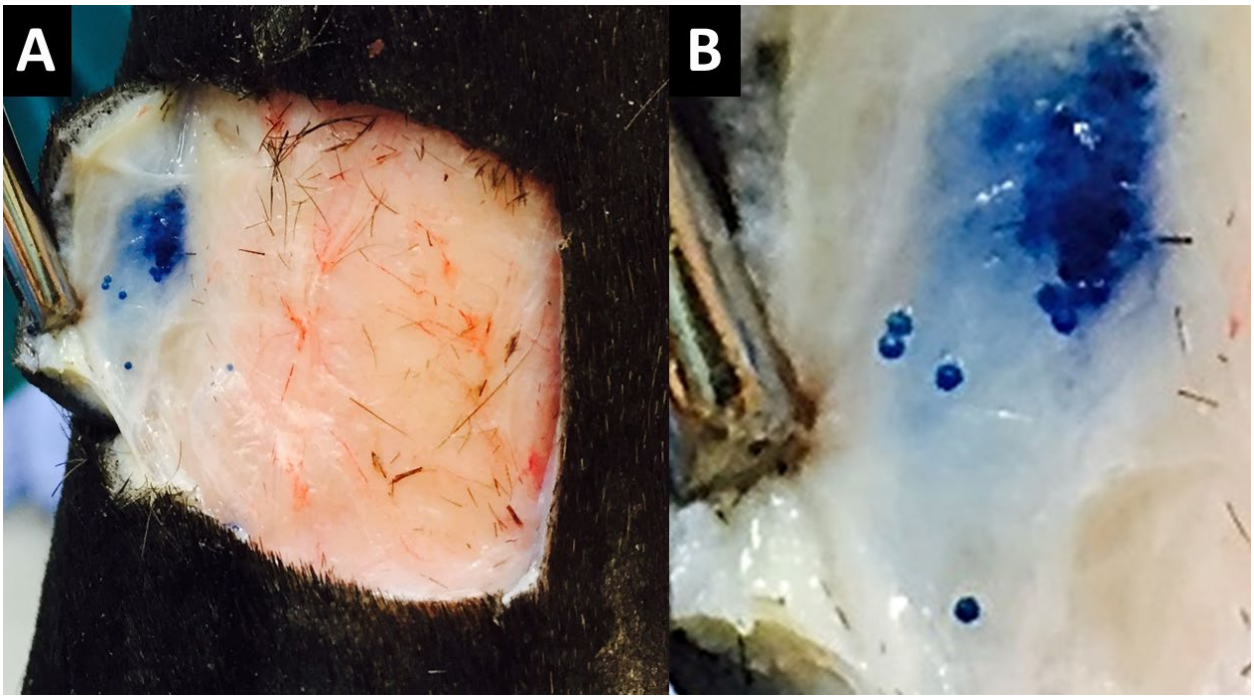

Figure 28. Injected microspheres maintain their shape and location after injection. A) Microspheres created with PEGDA and stained with trypan blue maintain their uniform spherical shape and wound location after subcutaneous injection in the distal limb of a cadaver horse. B) Enlarged portion of image (A).

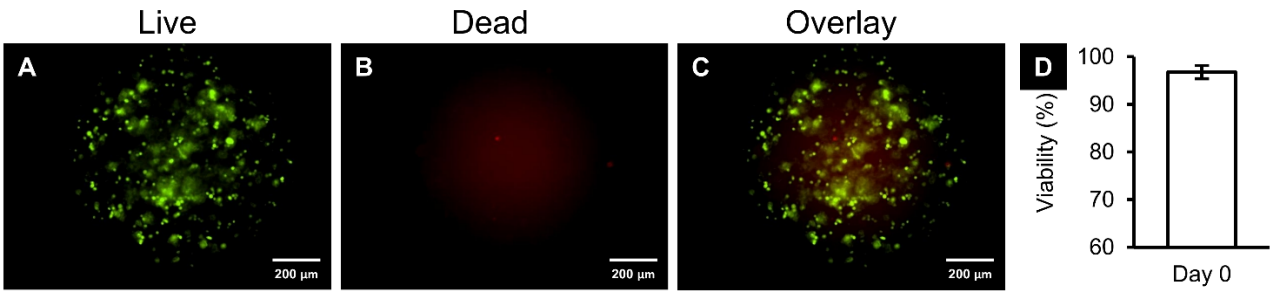

Figure 29. High microsphere uniformity and cell viability post-encapsulation. (A-D) ECFC viability was 96.8% immediately post-encapsulation (Day 0) as quantified using Live (green)/Dead (red) staining (n=3 separate encapsulations) (Seeto et al., 2017). Scale bars are 200 µm.

microspheres (Figure 30) (Seeto et al., 2017). Cell surface marker expression of ECFCs was unaffected by encapsulation and consisted of high levels (all above 95%) of vWF, CD105, and CD14 expression (Figure 31) (Seeto et al., 2017). Functional assays of ECFC function also revealed that encapsulation had no adverse effect on ECFCs' ability for DiI-Ac-LDL uptake and tubule formation (Figure 31) (Seeto et al., 2017).

4.3.2 Clinical findings

The surgical wound model and treatments were generally well tolerated. One horse developed a fever after the surgery and initial treatments, but this was responsive to a single dose of flunixin meglumine (1 mg/kg IV). The same horse became febrile and developed swelling and stiffness in all 4 limbs after the first biopsy and was treated with one dose of flunixin meglumine (1 mg/kg IV) and a 10-day course of Trimethoprim/Sulfa (24 mg/kg PO). The swelling was not specific to any wound or treatment and completely resolved. Wound healing was significantly affected by individual horse (Appendices D - F) and whether the wound was on a forelimb or a hind limb. These sources of variation were accounted for in subsequent analyses, so that any significant differences found due to treatment group occurred despite these sources of variation.

4.3.3 Changes in wound size over time

Comparisons in WSA between treatments was only performed for wounds that were injected at 1 time point (LOW) and only biopsied at 4 weeks (24 wounds from 6 horses, 6 wounds per treatment). Treatment group did not significantly impact WSA

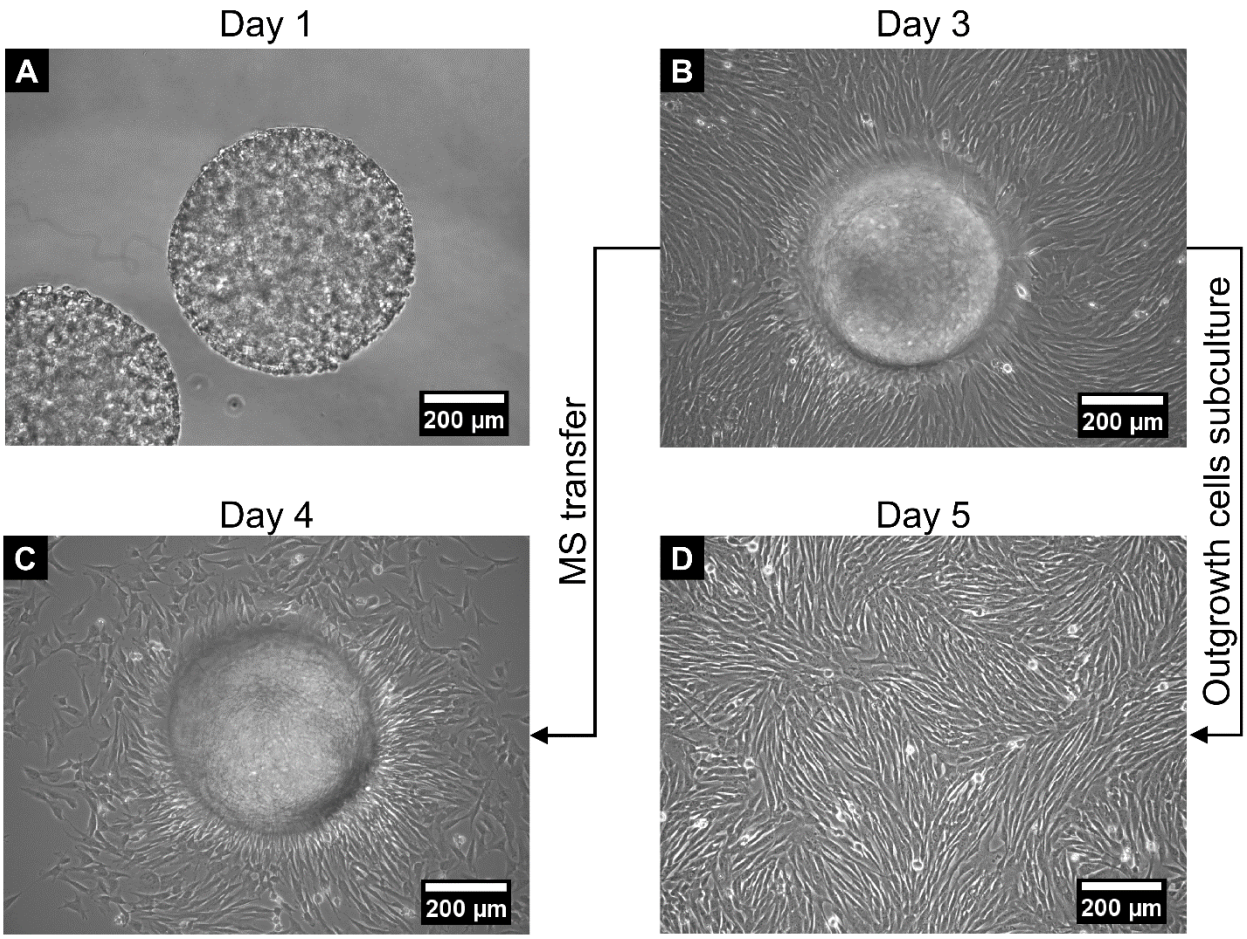

Figure 30. Phase contrast images showing ECFC migration and proliferation phenotypes were maintained post-encapsulation. A) ECFCs encapsulated in PEG-Fb microspheres; B) Proliferation and outgrowth from the PEG-Fb microspheres 2 days after encapsulation; C) After transfer of PEG-Fb microspheres to a new cell culture flask, continued proliferation and outgrowth is observed; D) Characteristic cell morphology and high proliferation observed in cells originating from PEG-Fb (Seeto et al., 2017). Scale bars are 200 µm.

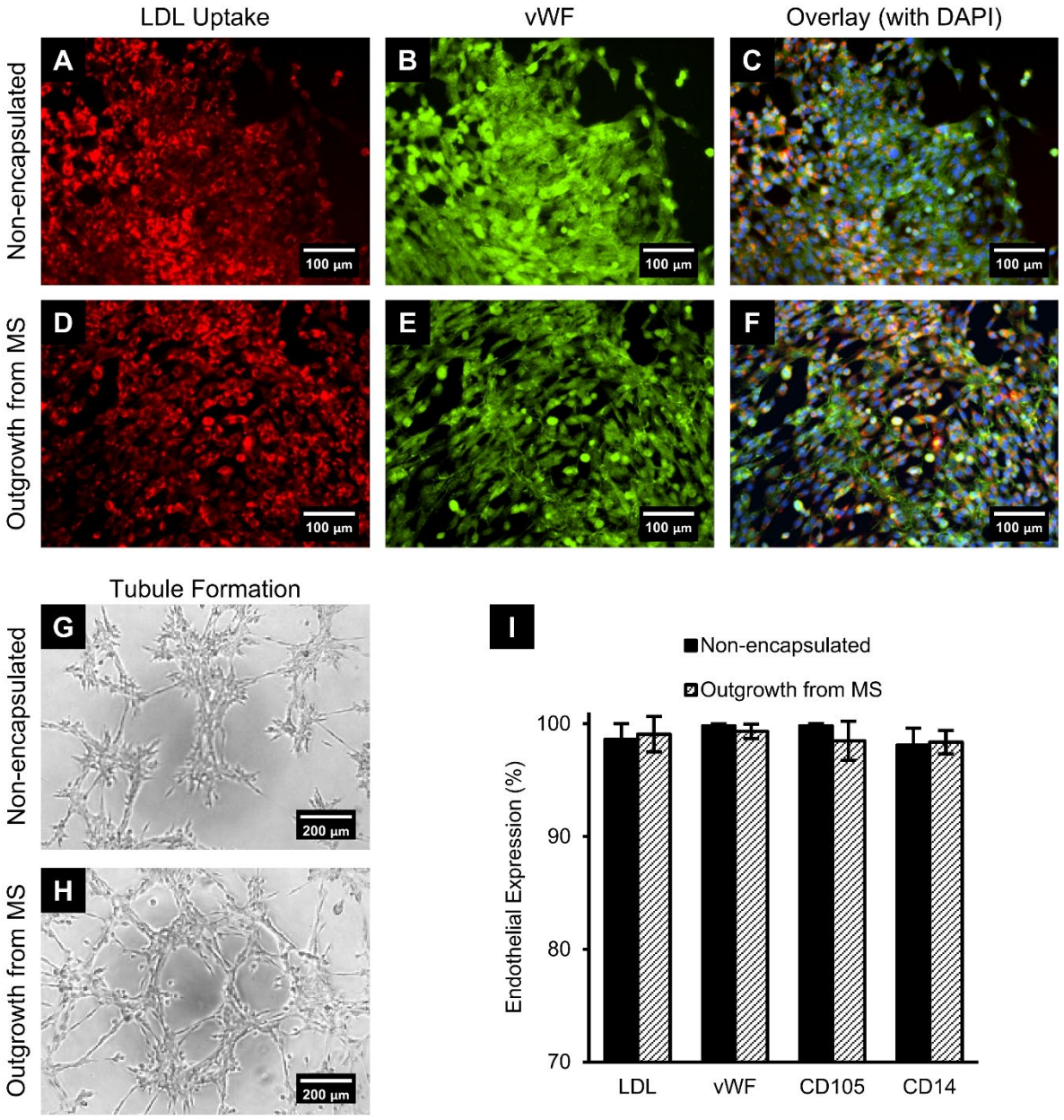

Figure 31. ECFCs maintained an endothelial phenotype after encapsulation and culture. ECFCs from microspheres showed similar endothelial phenotypes compared to non-encapsulated ECFCs in terms of DiI-Ac-LDL uptake, vWF expression (A-F), and tubule formation (G and H). I) No difference was found in cell surface marker expression (vWF, CD105, and CD14) between the outgrowth ECFCs from microspheres and non-encapsulated ECFCs by flow cytometry (n=3 separate encapsulations) (Seeto et al., 2017).

change over time (Figure 32). The WSA initially increased and then decreased over the course of the study in all wounds, and all horses were observed until all wounds were completely epithelialized (approximately 8 weeks). Wounds treated with ECFCs and ECFC/MS had the smallest WSA at week 3 (Figure 32), but this was not significant (P=0.767). All wounds decreased in WSA by 4 weeks, and the effect of time point was significant (P≤0.001).

4.3.4 Granulation tissue assessment

Comparisons in GS between treatments were performed for all wounds over time points of weeks 1, 2, 3 and 4 (48 wounds from 6 horses, 12 per treatment). The effects of ECFC dose (HIGH vs LOW cell numbers) and injection frequency (1 time vs 2 times during the study) were not significant, and therefore only treatment group was included in the analysis. There was no effect of treatment on GS at any time point (P=0.31). The GS were highest at week 3 (0.875, range 0.125 – 1.5) and lowest at week 1 (0.25, 0.0 – 1.0, P≤0.001). Hind limbs had higher GS than forelimbs (P≤0.001) (Figure 33), a finding most prominent at week 4 (Figure 34). Hind limbs had an OR of 3.61 (95% CI 1.87 – 7.00) of having a weighted GS greater than 0.75 (Figure 35). Wounds which were biopsied weekly also had higher scores than wounds biopsied only at week 4 (P=0.023), with weekly biopsied wounds having an OR of 2.11 (95% CI 1.12 – 3.96) of having a weighted GS greater than 0.75 (Figure 35).

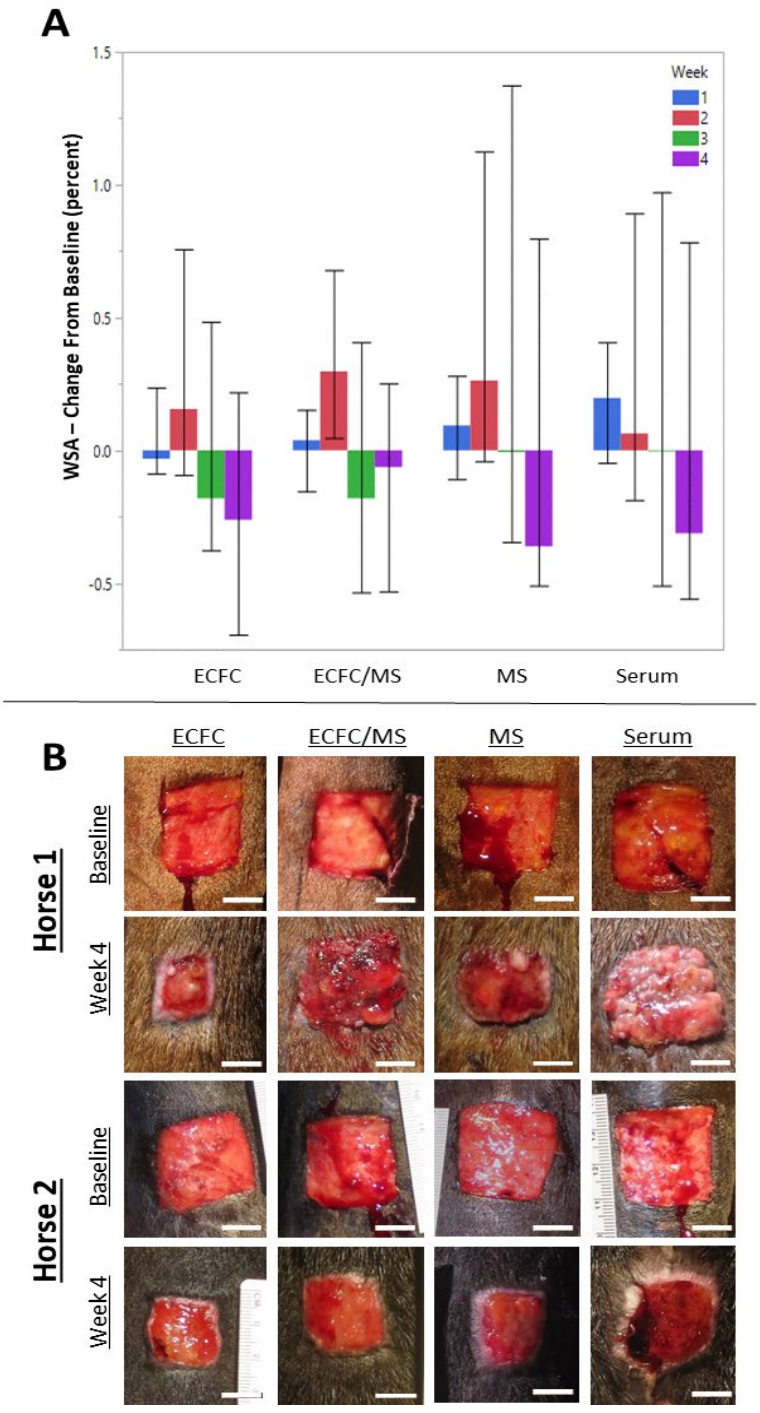

Figure 32. Change in wound size by treatment. (A) Wound surface area (WSA) displayed as median and range for percent change from baseline wound for all treatment groups by week. (B) Photographs from 2 horses of wounds at baseline (24 hours after wound creation) and at 4 weeks for all treatment groups. The variation between horses and different responses to treatments are apparent. ECFC and ECFC/MS treatment groups had 8 mil cells/wound injected at baseline. Scale bars are 1 cm.

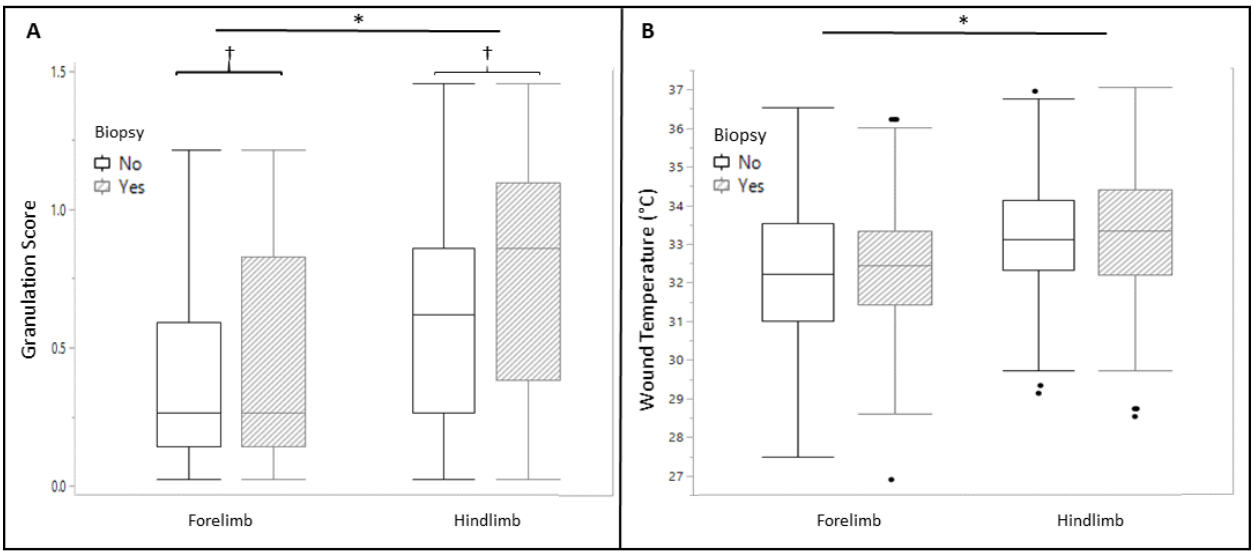

Figure 33. Influence of limb and biopsy on granulation scores and wound temperature. (A) Weighted granulation score for all wounds by whether the wound was on a forelimb or hind limb and whether the wound was biopsied. Data are presented as box-and-whisker plots, with median values represented by the horizontal lines and the interquartile range represented by the box. Black dots are values that are 1.5 times the box length above the 75th percentile. The ends of the whiskers represent the smallest and largest values not classified as outliers. (B) Wound temperature in °C for all wounds by whether the wound was on a forelimb or hind limb and whether the wound was biopsied. * signifies a significant difference in wound temperature and weighted granulation score between forelimbs and hind limbs (P<0.05). † signifies a significant difference in weighted granulation score based on whether the wound was biopsied (P<0.05). Note that wounds on hind limbs had higher temperatures and more granulation tissue compared to wounds on forelimb wounds, but taking biopsies only affected the severity of granulation tissue.

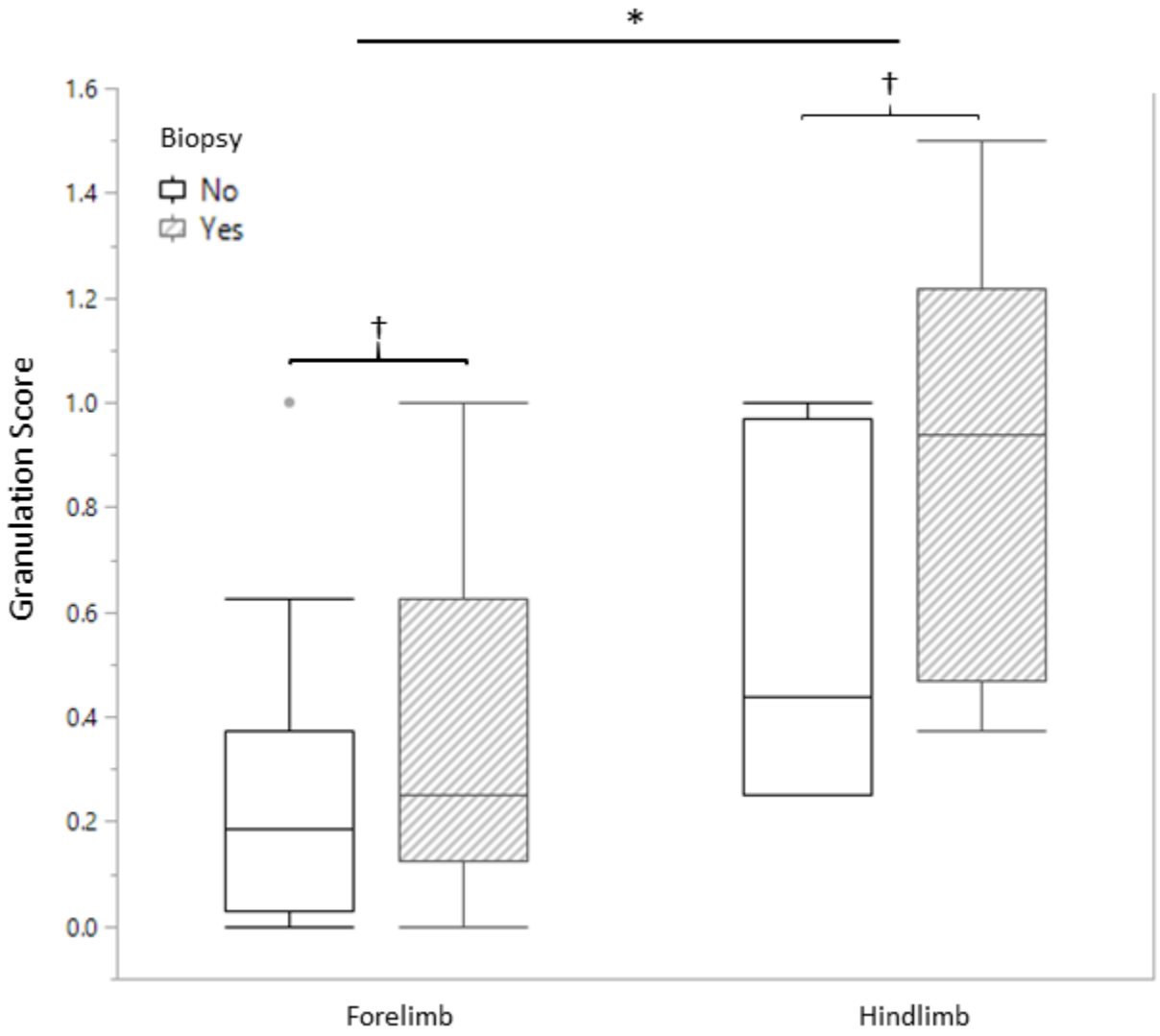

Figure 34. Influence of limb and biopsy on granulation scores at week 4. Weighted granulation score for all wounds at week 4 by whether the wound was on a forelimb or hind limb and whether the wound was biopsied. Data are presented as box-and-whisker plots, with median values represented by the horizontal lines and the interquartile range represented by the box. Grey dots are values that are 1.5 times the box length above the 75th percentile. The ends of the whiskers represent the smallest and largest values not classified as outliers. * signifies a significant difference in weighted granulation score between forelimbs and hind limbs (P<0.05). † signifies a significant difference in weighted granulation score based on whether the wound was biopsied (P<0.05).

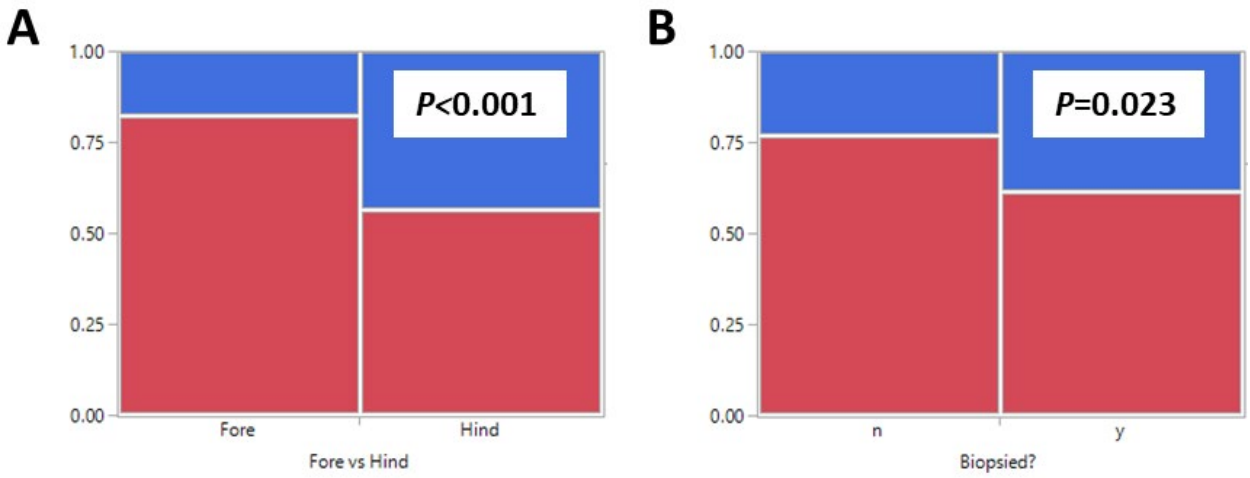

Figure 35. Relative frequency of wounds with weighted granulation scores above 0.75. A) Mosaic plot showing relative frequency of wounds with weighted granulation scores (GS) above 0.75 separated by forelimb versus hind limb (A) or whether or not wounds were biopsied (B). The area in blue represents wounds with GS above 0.75, and the area in red represents wounds with GS below or equal to 0.75. Note that a significantly higher proportion of wounds that are on the hind limb or have been biopsied have GS above 0.75.

4.3.4 Thermographic assessment of wounds

Comparisons of thermography data between treatments were performed for all wounds over time points of weeks 1, 2, 3 and 4 (48 wounds from 6 horses, 12 per treatment). The effects of ECFC dose (HIGH vs LOW cell numbers) and injection frequency (1 time vs 2 times during the study) were not significant. There was no effect on the %change in temperature due to treatment. Wound temperature %change at week 1 was greatest for ECFC (+2.4%, -7.19 to +47.29%) and ECFC/MS (+3.23%, -19.2 to +12.03%) compared to MS alone (+2.14%, -12.25 to +15.11%) and serum (-2.11%, -9.76 to +13.64%), but the effect of treatment group was not significant (P=0.416). The effect of treatment group on wound temperature %change at week 4 was also not significant (P=0.061). Factors that significantly affected wound temperature were time post injection (greatest temperature at week 1 and lowest at week 4, $P \leq 0.001$), location of measurement (measurements either 1 cm above or 1 cm below the wound were lower in temperature; $P \leq 0.001$ and P=0.004, respectfully) (Figure 36), and limb (forelimbs were lower than hind limb wound temperatures, P=0.01). Wounds that were biopsied did not have differences in wound temperature compared to wounds that were not biopsied (P=0.368) (Fig 33).

4.3.5 Evaluation of collagen density

Comparisons of collagen density (quantified by Masson's trichrome staining of wound biopsies) between treatments for individual regions (Inner Wound, Wound Periphery, Wound Center) were performed on all wounds biopsied at week 1 and week

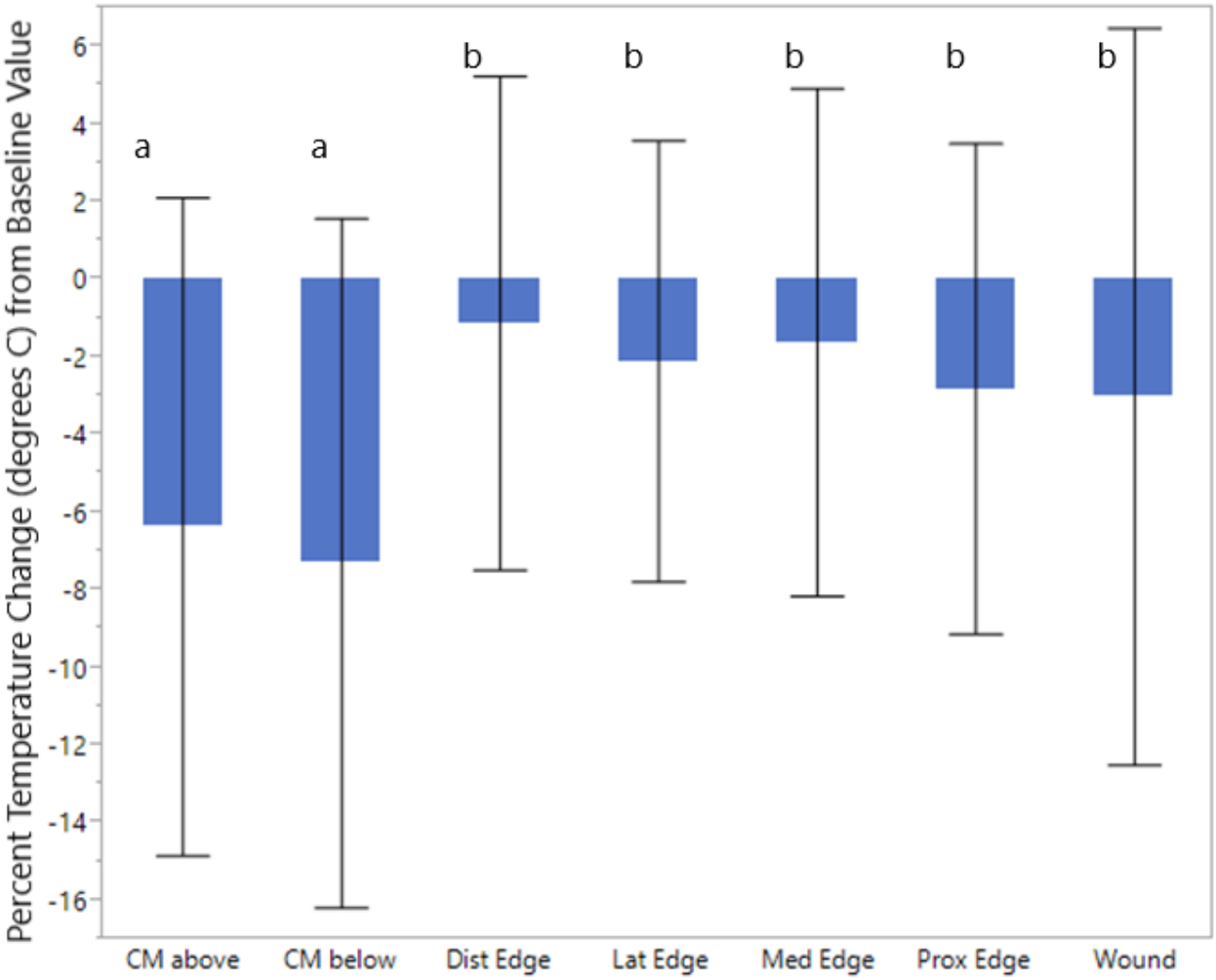

Figure 36. Temperature change by location of infrared thermographic measurement location. Change in wound temperature (° C) by infrared thermographic measurement location, presented as a percent change in wound temperature compared to baseline values, at week 4. Locations of thermographic measurement were: 1 cm above the wound (CM above), 1 cm below the wound (CM below), the distal edge of the wound (Dist Edge), the lateral edge of the wound (Lat Edge), the medial edge of the wound (Med Edge), the proximal edge of the wound (Prox Edge), and the center of the wound (Wound). Data are presented as mean and SD. All locations noted with an 'a' had a significantly (P<0.05) greater decrease in wound temperature compared to locations noted with a 'b'.

4 (48 wounds from 6 horses, 12 per treatment) with different wound regions analyzed separately. Wounds injected with serum had a significantly higher collagen density (i.e. closer to baseline skin collagen density) in the Inner Wound at week 1 (P=0.026); whereas wounds injected with MS alone had a significantly lower collagen density in the Wound Periphery at week 1 (P=0.037) (Figure 37). At week 4, there were no differences in collagen density in the Wound Center (P=0.20), Wound Periphery (P=0.146), or Inner Wound (P=0.623) regions due to treatment.

4.3.6 Assessment of vascularization

Comparisons of blood vessel density (quantified by vWF staining of wound biopsies) between treatments were performed on all wounds biopsied at week 1 and week 4 (48 wounds from 6 horses, 12 wounds per treatment), and each region of the biopsy (Inner Wound, Wound Periphery, or Wound Center) was analyzed separately. Blood vessel density was greatest at week 1 (Figure 38) in wounds treated with ECFCs and ECFC/MS. The Inner Wound region at week 1 had the greatest density of blood vessels in wounds treated with ECFC and ECFC/MS, but was not significant (P=0.173). The Wound Periphery regions at week 1 had overall differences in vascularization (P=0.009); wounds treated with ECFCs and ECFC/MS also had the greatest density of blood vessels in the Wound Periphery, with wounds treated with ECFCs having a significantly greater density of blood vessels compared to wounds treated with MS alone ($P \leq 0.001$) (Figure 38). No significant differences in vascularization were observed in Wound Center regions (P=0.157) or in the Inner Wound regions (P=0.157)

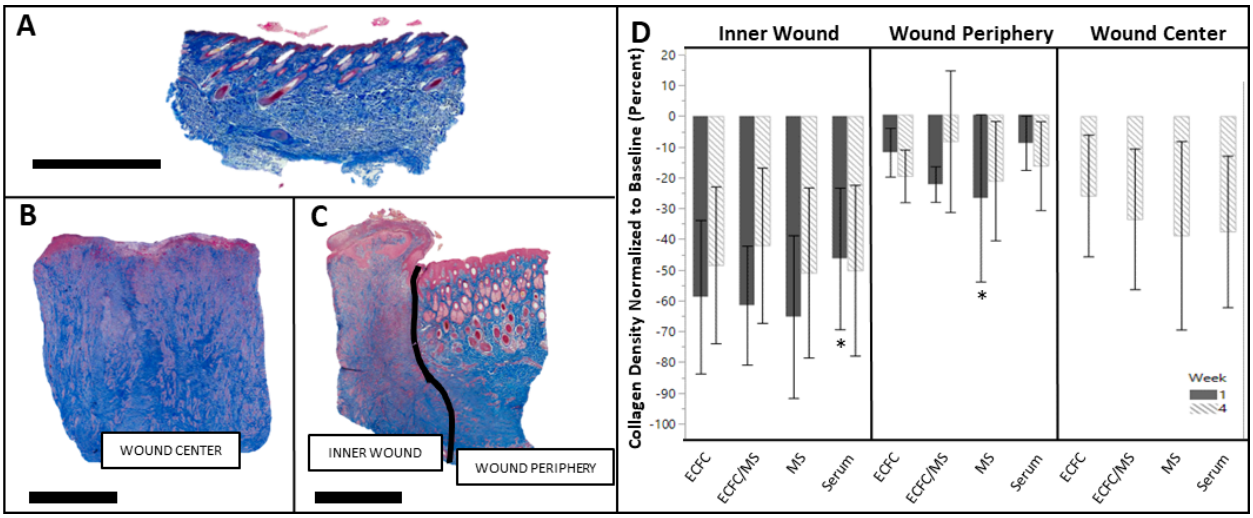

Figure 37. Changes in collagen density by treatment and wound region. (A) Representative image of collagen density (blue) as identified by Masson's trichrome staining of baseline tissue removed during the wound creation. (B) Representative image of collagen density at week 4 in a biopsy from the center of the wound. (C) Representative image of collagen density at week 4 in a biopsy from the leading edge of the wound. Note the demarcation between the Inner Wound and Wound Periphery regions. (D) Collagen density normalized to baseline values at weeks 1 and 4 by treatment group in the Inner Wound, Wound Periphery, and Wound Center regions. Data are presented as mean and standard deviation. The Wound Center was only biopsied at week 4. Note that at week 1 in the Inner Wound region, wounds treated with serum had a collagen density closest to baseline values and significantly greater than the other treatments, and at the week 1 Wound Periphery region, wounds treated with microspheres (MS) had collagen densities least like the baseline collagen density and significantly lower than other treatments. * indicates a significant difference between the Serum treatment group and the rest of the treatments at week 1 in the Inner Wound and between the MS treatment group and the rest of the treatments at week 1 in the Wound Periphery region. (P<0.05). Scale bars are 2 mm.

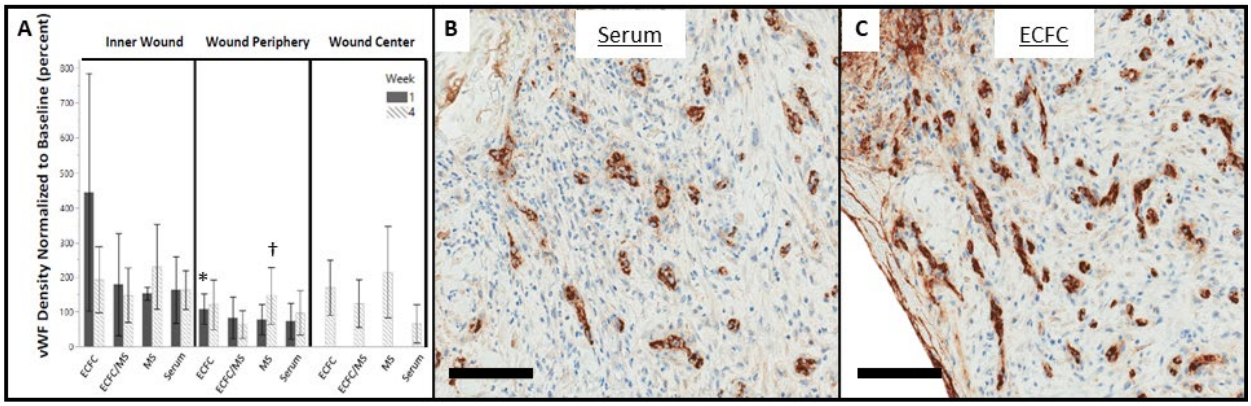

Figure 38**.** Blood vessel quantified with von Willebrand factor immunohistochemistry. (A) Density of von Willebrand factor (vWF) staining (vascularization) normalized to baseline values at weeks 1 and 4 by treatment group in the Inner Wound, Wound Periphery, and Wound Center regions. Data are presented as means and standard deviation. The Wound Center region was only biopsied at week 4. (B) Representative photomicrograph of blood vessel density (brown stain) in the serum treatment group at the Inner Wound region at week 1. (C) Representative photomicrograph of blood vessel density in the ECFC treatment group at the Inner Wound region at week 1. Note the relative increase in blood vessel density in the ECFC treatment group compared to the Serum treatment group in (B) and (C). * indicates a significant difference in vascularization in the Wound Periphery region at week 1, with wounds treated with ECFC having greater blood vessel density compared to wounds treated with MS alone (P=<0.05). † indicates a significant difference in vascularization in the Wound Periphery region at week 4, with wounds treated with MS alone having greater blood vessel density compared to all other treatment groups (P<0.05). Scale bars are 100 μm.

at week 4. In the Wound Periphery regions at week 4, there were significant differences in vascularization due to treatment group (P=0.042), with the MS-alone group having the greatest density of blood vessels.

4.3.7 Assessment of inflammation

Comparisons of the inflammatory response between treatments were performed on all wounds biopsied at week 1 and week 4 (n=48 wounds from 6 horses, 12 wounds per treatment), and each region of the biopsy (Inner Wound, Wound Periphery, or Wound Center) was analyzed separately. Overall, the acute inflammatory response assessed at week 1 was not different between treatments, but macrophagic and neutrophilic inflammation were decreased in week 4 in ECFC and ECFC/MS treated wounds suggesting ECFCs had some effects on chronic inflammation. The Wound Periphery region in wounds treated with ECFCs and ECFC/MS had significantly less macrophagic (quantified by IBA1 staining) inflammation at week 4 (Figure 39), with wounds treated with ECFC/MS having significantly less macrophagic inflammation compared to wounds treated with MS alone (P=0.008) There were no differences in macrophage density in the Wound Center and Inner Wound regions (P=0.078 and P=0.064, respectively) at week 4. The effect of treatment group was not significant in the Inner Wound and Wound Periphery regions at week 1 (P=0.232 and P=0.363, respectively).

Activated neutrophil density, as assessed by elastase positive staining, was not different at week 1 but was at week 4 based on treatment group. In the Wound Center regions of wounds at week 4, there were significant differences in neutrophil densities

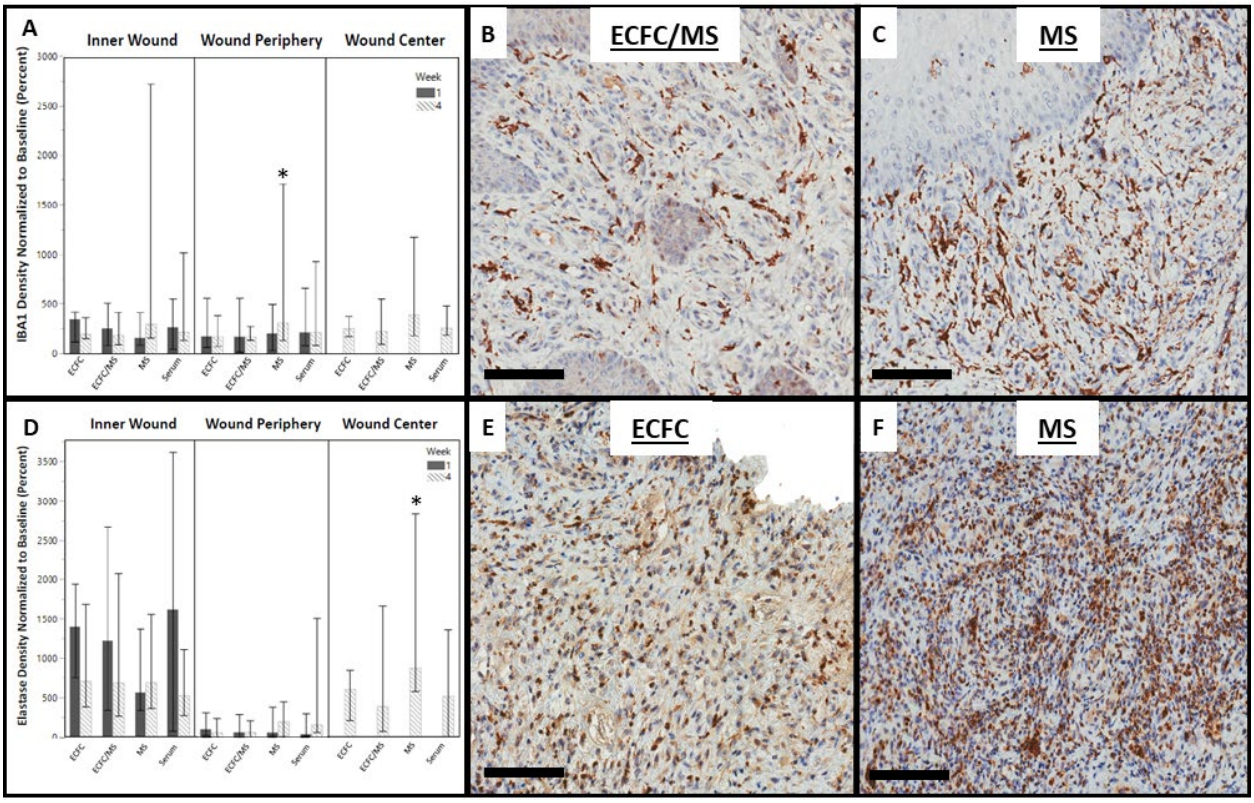

Figure 39. Influence of treatment on wound inflammation. (A) Density of IBA1 staining (macrophages) normalized to baseline values at weeks 1 and 4 by treatment group in the Inner Wound, Wound Periphery, and Wound Center regions. Data are presented as median and range. (B) Representative photomicrograph of macrophages in tissue at week 4 in the Wound Periphery region of wounds treated with ECFC/MS.
(C) Representative photomicrograph of macrophages in tissue at week 4 in the Wound Periphery region of wounds treated with MS. (D) Density of elastase staining (activated neutrophils) normalized to baseline values at weeks 1 and 4 by treatment group in the Inner Wound, Wound Periphery, and Wound Center regions. (E) Representative photomicrograph of neutrophils in tissue at week 4 in the Wound Center region of wounds treated with ECFC (F) Representative photomicrograph of neutrophils in tissue at week 4 in the Wound Center region of wounds treated with MS. Note that there is a subjectively greater density of macrophages in the Wound Periphery region of wounds at week 4 treated with MS (C) compared to wounds treated with ECFC/MS (B); there is also a subjectively greater density of neutrophils in the Wound Center region of wounds at week 4 treated with MS (F) compared to wounds treated with ECFCs (E). * indicates a significant difference between treatment groups, with MS alone wounds having the highest density of macrophages and neutrophils at week 4 ($P<0.05$). Scale bars are 100 μm.

between wounds ($P \leq 0.001$) (Figure 39); the lowest neutrophil densities were found in wounds treated with ECFCs and ECFC/MS. Wounds treated with ECFCs had significantly less neutrophil density as compared to wounds treated with MS alone ($P \leq 0.001$). The Wound Periphery regions of wounds at week 4 had no difference in neutrophil density between wounds ($P=0.114$).

There was not a significant influence of treatment, horse, limb, or week on density of T-cells, as assessed by CD3 positive staining, or B-cells, as assessed by Pax5 positive staining, in this wound model. Densities of T-cells and B-cells were measured and compared to baseline densities. No increase in T-cell or B-cell density was observed compared to baseline for week 1 and week 4 wounds (Figure 40).

4.3.8 Tracking labeled ECFCs

Labeled ECFCs were found up to 3 weeks after injection near blood vessels and also incorporated into blood vessels. In biopsies from horses in Phase 1 with a LOW number of ECFCs and weekly biopsies, labeled ECFCs were found up to three weeks after injection in wounds treated with just ECFCs and up to two weeks in wounds treated with ECFC/MS (Figures 41 and 42). For Phase 2 horses with HIGH number of ECFCs injected that were biopsied at week 1 and week 4, labeled cells were found in wounds treated with both ECFCs and ECFC/MS at week 1 (Figure 43). At week 4, no labeled ECFCs were observed in any tissue sample for either dosage (LOW vs. HIGH), treatment type (ECFCs vs. ECFC/MS), or injection frequency (Figure 44). Overall, labeled ECFCs were found at week 1 in 6/6 horses with wounds that were treated with

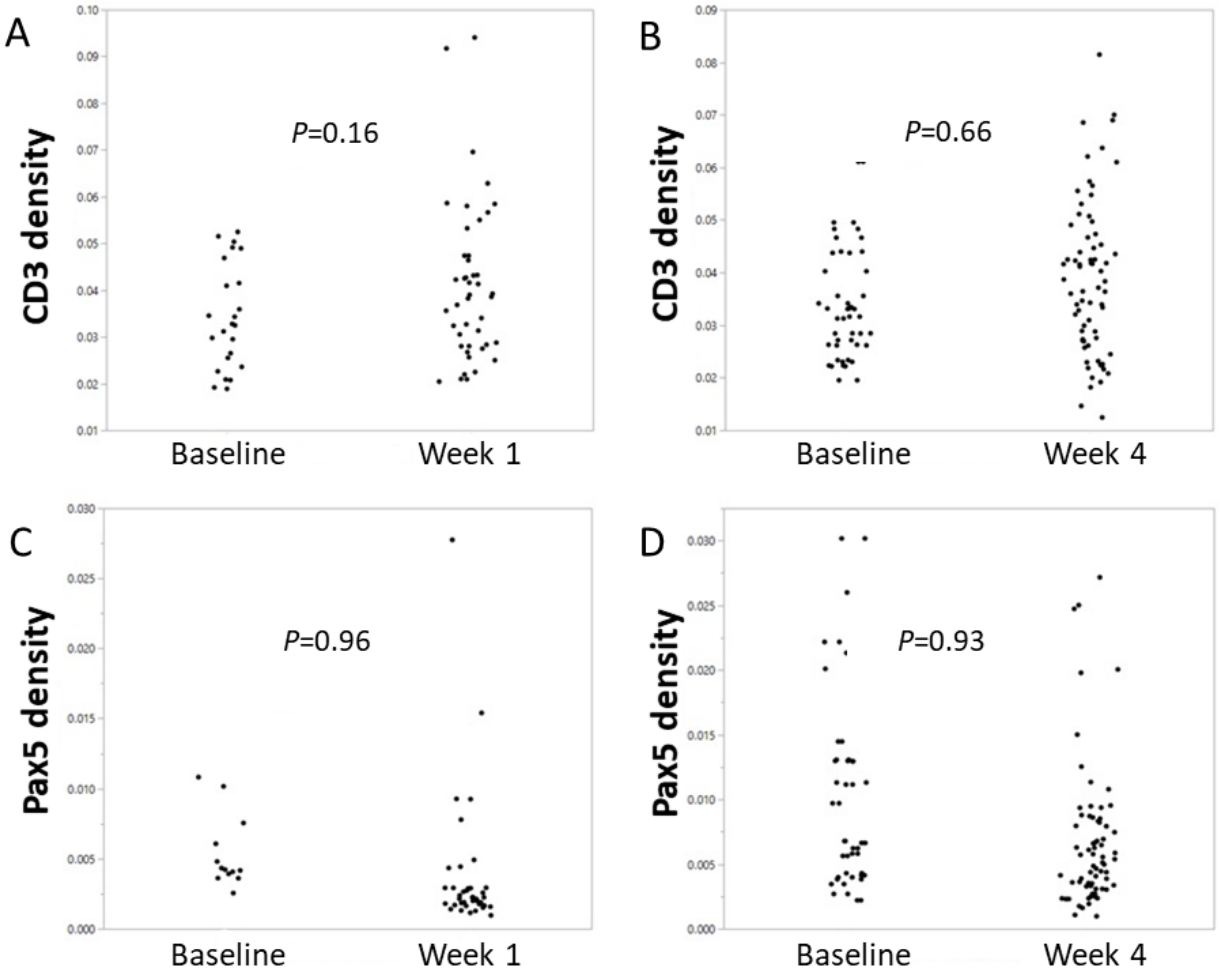

Figure 40**.** B-cell and T-cell density in horses at baseline and at weeks 1 and 4. Density of B-cells and T-cells assessed by Pax5 and CD3 immunohistochemical staining, respectively, in baseline tissue and in wounds at weeks one and four. CD3 (A) and Pax5 (C) densities of wounds biopsied at week 1, at the time of wound creation (Baseline) and at the first biopsy (Week 1). CD3 (B) and Pax5 (D) densities of wounds biopsied only at week 4, at the time of wound creation (Baseline) and at the time of biopsy (Week 4).

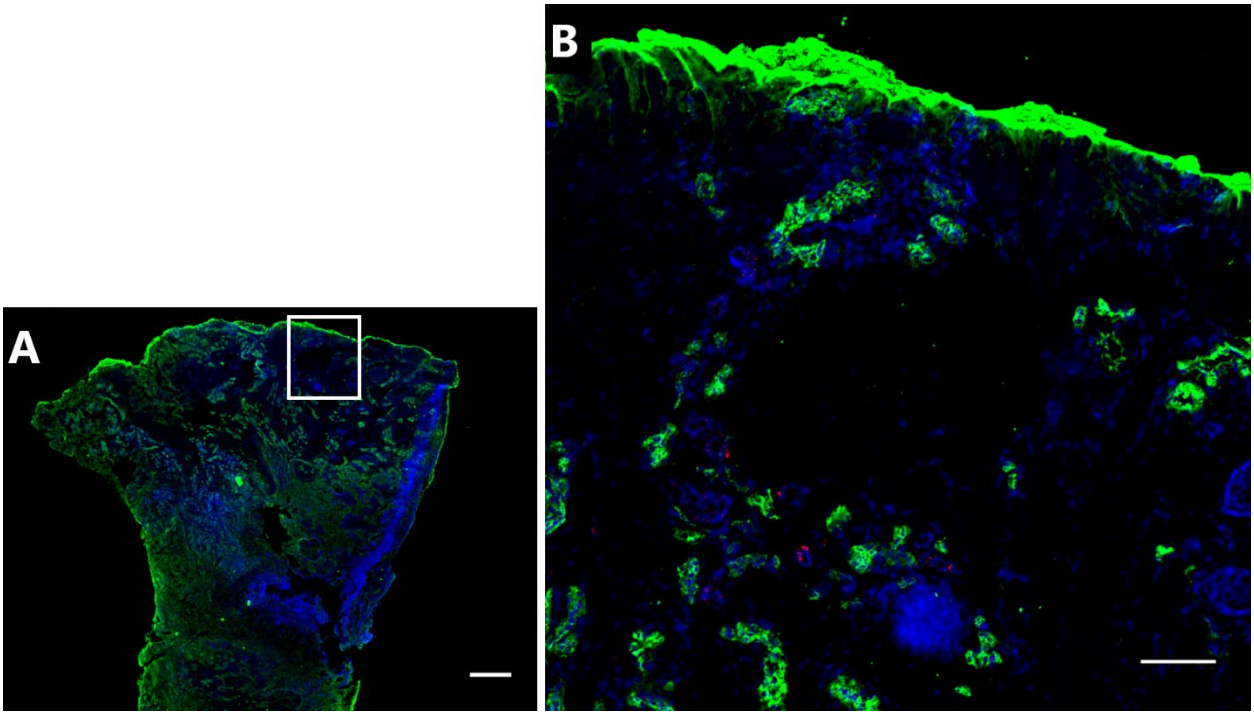

Figure 41. Identification of cell nuclei, blood vessels, and QD-labeled ECFCs within one biopsy. A) Representative fluorescent micrograph demonstrating the cellularity and distribution of blood vessels within one entire biopsy. Scale bar is 500 μm. B) Magnified field of view from the image in (A) showing QD-labeled ECFCs in close association to blood vessels. Scale bar is 100 μm. The area outlined with a white square in (A) is the area represented in (B). Cell nuclei are stained with DAPI (blue), and blood vessels are stained with vWF (green).

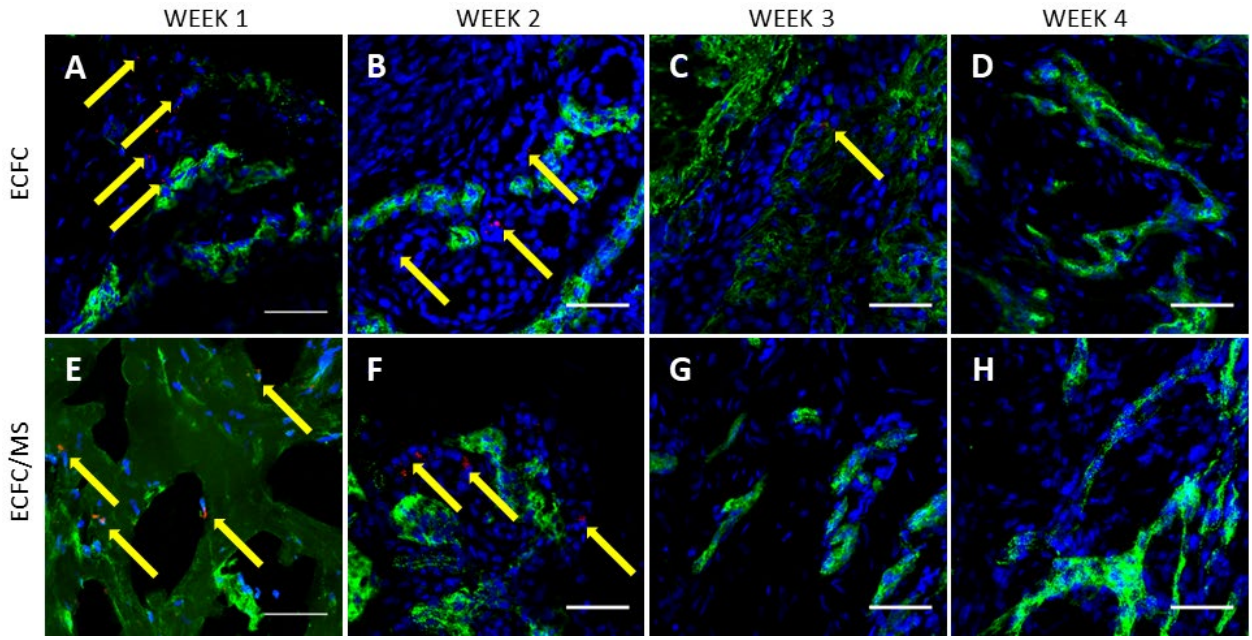

Figure 42**.** Co-localization of blood vessels and ECFCs in Phase I horses. Representative fluorescent photomicrographs of weekly biopsies from wounds treated with ECFCs (A-D) and with ECFC/MS (E-H) from Phase I horses. The yellow arrow points to QD labeled ECFCs. In (E), PEG-Fb is identified as dark green color with few nuclei. vWF labeled blood vessels are light green. DAPI labeled nuclei are blue. QD are red. Scale bars are 50 μm.

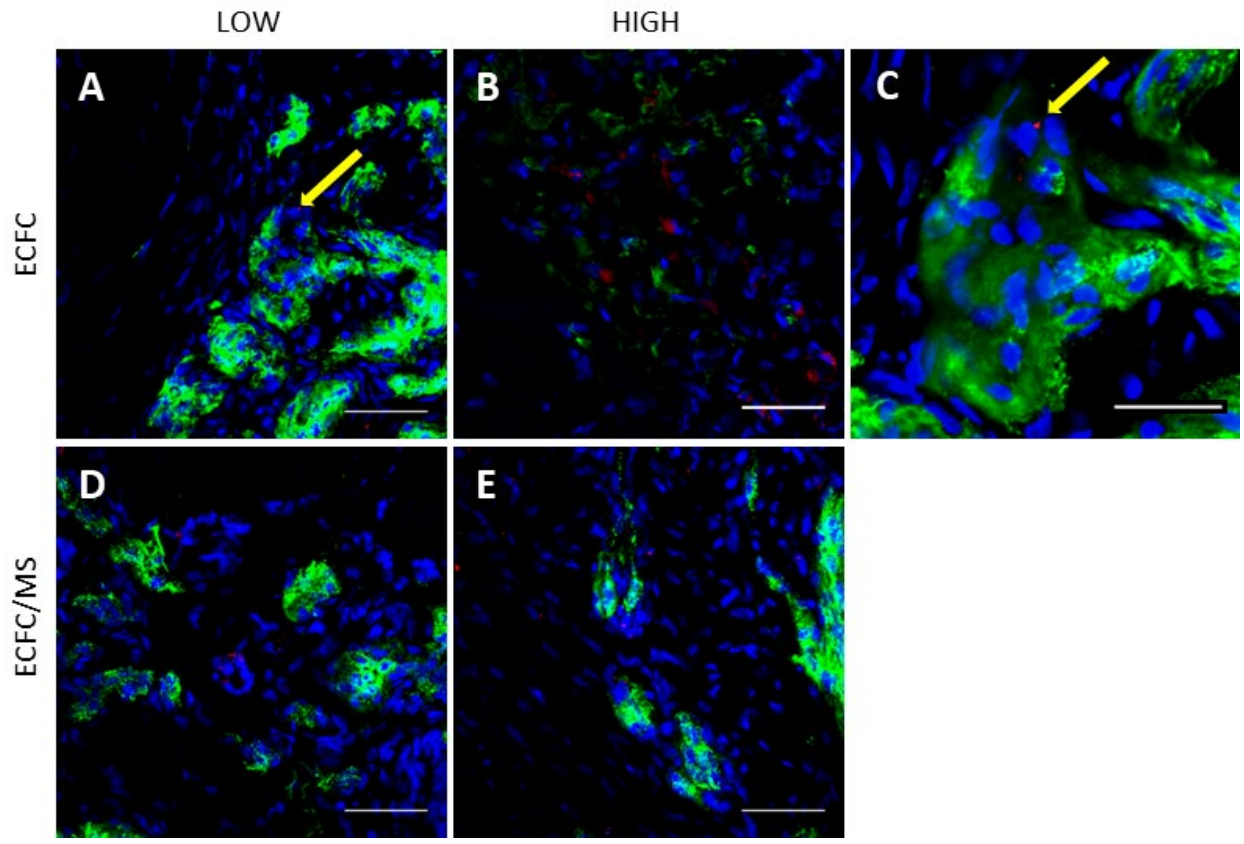

Figure 43**.** Co-localization of blood vessels and ECFCs at week 1 in Phase 1 and Phase 2 horses. Representative fluorescent photomicrographs of week 1 biopsies from wounds treated with (A) 8 million ECFCs per wound (LOW); (B) 16 million ECFCs per wound (HIGH); (C) Higher magnification of the image in A; (D) LOW ECFC/MS and (E) HIGH ECFC/MS. Note that QD labeled ECFCs are present in all images, and the yellow arrow in (A) and (C) indicates a QD labeled ECFC incorporated into a blood vessel based on its location within the blood vessel wall. vWF labeled blood vessels are light green. DAPI labeled nuclei are blue. QD are red. Scale bars are 25 μm (C) or 50 μm (A, B, D, E).

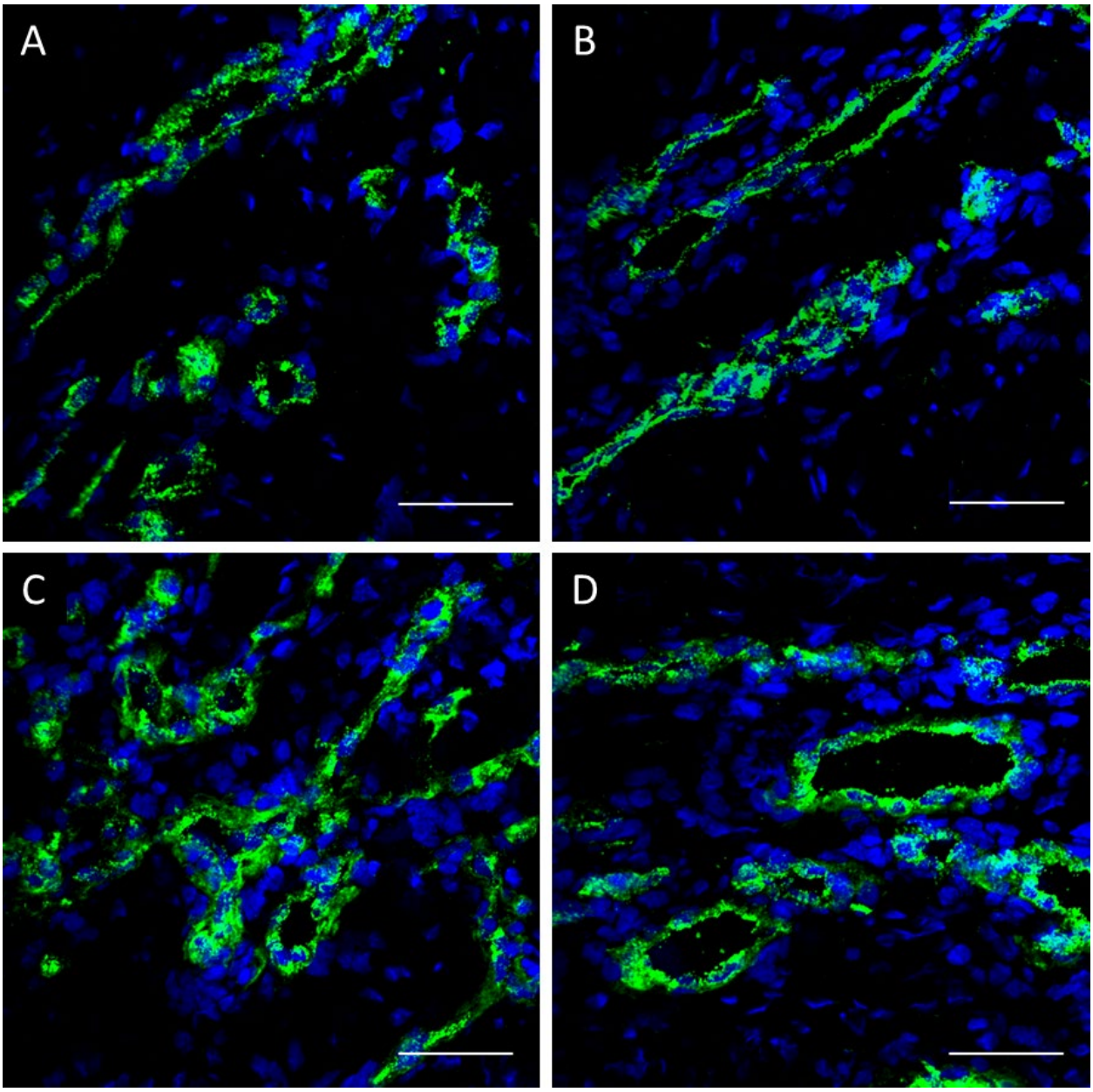

Figure 44. Photomicrographs of biopsy samples at week 4. Representative photomicrographs of biopsies obtained at week 4 showing an absence of labeled ECFCs. A) Biopsy taken from a wound injected one time with ECFCs (Phase 1); B) Biopsy taken from a wound injected two times with ECFCs (Phase 2); C) Biopsy taken from a wound injected one time with ECFC/MS (Phase 1); Biopsy taken from a wound injected two times with ECFC/MS (Phase 2). Cell nuclei are stained with DAPI (blue), and blood vessels are stained with vWF (green). Scale bars are 50 μm.

ECFC/MS and in 3/6 horses with wounds treated with just ECFCs, but the Fisher's exact test was not significant (p=0.27). The number of labeled ECFCs identified in week 1 biopsies was greatest in ECFC/MS treated wounds with a LOW dose (*P*=0.02), but was not different with the HIGH dose (*P*=0.38, Table 2). Labeled ECFCs were commonly found near blood vessels, regardless of whether the wounds were treated with ECFC or ECFC/MS. Rarely, labeled ECFCs could be observed to be incorporated into a newly formed blood vessel (Figure 43). In wounds treated with ECFC/MS, the PEG-Fb biomaterial was observed in some samples 1 week after injection (Figure 42). Labeled ECFCs were observed within the PEG-Fb biomaterial in these samples (Figure 42). The PEG-Fb biomaterial was not observed in any samples after week 1.

4.4 Discussion

Our group has demonstrated a safe and effective method of cell delivery using injectable, cell-laden hydrogel microspheres, and we have shown increased vascularization and reduced inflammation in a research model of equine distal limb wounds treated with ECFCs. Statistical analysis showed sources of variation to be the individual horse, the location of the wound (fore versus hind limb), and whether or not the wound was biopsied, but even given the variability, PEG-Fb MS encapsulated ECFC and non-encapsulated ECFC treated wounds had increased vascularization at week 1 in some regions and a decreased inflammatory response in cell-treated wounds at week 4. The effects were modest, but autologous cells from 6 non-athletic horses of various ages and breed were used for this study, and variability of the source cells is an important issue when evaluating clinical efficacy in stem and progenitor cell therapy.

	ECFC	ECFC/MS	*P* value
Horses with labeled cells at week 1	3/6	6/6	0.27
Labeled cells per cryosection ALL (Median [IQR])	11 [3-24]	21 [9-42]	0.14
Labeled cells per cryosection LOW (Median [IQR])	5.5 [3-20.25]	27 [11.75-44.5]	***0.02***
Labeled cells per cryosection HIGH (Median [IQR])	19 [15.75-35.75]	10 [1-21]	0.38

Table 2. Quantifying QD-labeled ECFCs found in week 1 biopsies. Comparison of number of horses and tissue sections in which QD labeled ECFCs were found at week 1. 10 slides with 2 sections per slide per biopsy were used for cell count analysis. Data are presented as median and IQR. ALL = all cell-treated wounds from week 1 biopsies from both Phases of study. LOW= wounds from Phase 1 of the study where 8 mil cells/wound were injected and a week 1 biopsy was performed. HIGH = wounds from Phase 2 of the study where 12-16 mil cells/wound were injected and a week 1 biopsy was performed.

Studies involving EPCs/ECFCs in horses are few (Salter et al., 2015; Seeto et al., 2017; Sharpe et al., 2016; Winter et al., 2018), and this is the first study looking at any clinical effects of ECFCs in the horse. Wound healing on distal limb wounds in the horse is notoriously problematic, and tissue hypoxia from vascular disruption and formation of abnormal vessels and inflammation are primary reasons for delayed healing (Bertone, 1989). Formation of EGT is common, and this is caused in part by excessive and prolonged inflammation, local hypoxia and excessive apoptotic signals (Bertone, 1989; Celeste et al., 2011; Lepault et al., 2005; Theoret and Wilmink, 2013). Protracted inflammation and poor wound oxygenation promote persistence of fibroblasts and fibroproliferative cytokines, and these persistent fibroblasts continually synthesize extracellular matrix which ultimately lead to production of EGT (Bertone, 1989; Theoret and Wilmink, 2013).

Wounds with EGT are extremely vascular, but microvessels formed within these wounds can be occluded, thus maintaining low wound oxygenation and promoting angiogenesis and fibroproliferation (Lepault et al., 2005). ECFCs have been studied in small animal models extensively for repair of ischemic tissue. Their vasculogenic effects can be due to direct incorporation of injected ECFCs into damaged blood vessels, formation of *de novo* blood vessels, or paracrine support (Asahara et al., 1997; Garbuzova-Davis et al., 2017). Incorporation of human bone marrow-derived ECFCs into brain capillaries proved beneficial for vascular damage repair in rats with ischemic stroke, and similar benefits after vascular incorporation of injected ECFCs have also been demonstrated in people with intracerebral hemorrhage, acute kidney injuries and myocardial infarctions (Garbuzova-Davis et al., 2017; Kim et al., 2016; Patschan et al.,

2016; Pias-Peleteiro et al., 2017). In a mouse model of hind limb ischemia after femoral artery ligation, labeled ECFCs injected into the tail vein were observed integrated within capillary vessel walls of the ischemic leg by histologic examination 1 to 6 weeks after ligation, and labeled cells were arranged into *de novo* capillaries within muscle at 6 weeks (Asahara et al., 1997). ECFCs were also observed in a perivascular location within infarcted myocardium after direct injection, and mRNA analysis revealed that these injected ECFCs upregulated angiogenic and cardiac protective factors (Kim et al., 2016). We hypothesized that treatment of wounds with ECFCs would enhance vascularization and reduce inflammation resulting in more rapid wound healing and less EGT formation. Significant effects on inflammation and vascularization were observed despite the large amount of variability in the model; however wound temperature and EGT formation were not different with treatment. The infrared imaging technique utilized in this study can detect inflammatory responses and changes in circulatory flow. However, the scabs of some wounds present during healing may have interfered with the emittance of radiant heat, and this may have been a limitation to this imaging modality in this model. Wound size was smaller at week 4 in wounds treated with ECFCs, but these effects were not significant.

Based on the relative frequency of ECFCs found near newly formed blood vessels and relative rarity of ECFCs found within the vessel wall, it is possible that ECFCs function in a more paracrine role in neovascularization. The reduced macrophagic and neutrophilic inflammation we observed in cell treated wounds at week 4 could also support a paracrine effect. However further work is required to make this distinction. It is important to note that some vascular tumors such as infantile

hemangiomas in humans have been speculated to possibly be caused by endothelial progenitor cells (Greenberger and Bischoff, 2013). Although the blood vessel density was greater at week 1 in wounds treated with ECFC or ECFC/MS, this effect was not present at the end of the study, and no excessive vascularization or vascular masses were observed.

Cell therapy is very common in equine practice, but using biomaterials to deliver cells in equine cell therapy is still in its infancy. The use of PEG-Fb in horses has only been reported by our group (Seeto et al., 2017), and this is the first study looking at a clinical effect of a PEG-Fb hydrogel in a horse. This is also the first study evaluating a cellular therapy for wound healing that utilizes PEG-Fb microspheres, a biomaterial cell-delivery vehicle designed as an injectable format. We chose to inject 2 – 4 million ECFCs per injection (8 – 16 million per wound) based on several factors. Reports of therapeutic MSC injections used in equine tendon injuries describe around 10 million cells used per lesion (Ortved and Nixon, 2016). Additionally, each microsphere could safely contain a finite number of cells, and the number of microspheres injected determined what volume of liquid was introduced into the subcutaneous tissue around these wounds. Biomaterial support of cells during delivery is very attractive in order to protect cells during or after injection and increase cell retention after injection (Rufaihah et al., 2017; Sandker et al., 2017; Seliktar, 2012). Combining mesenchymal stem cells (MSCs) with an alginate scaffold biomaterial helped to successfully regenerate articular cartilage in a rabbit model (Mata et al., 2017). Enhanced early chondrogenesis has been observed when equine MSCs were injected within a fibrin gel biomaterial into an equine model of cartilage defect (Wilke et al., 2007). Using the PEG-Fb biomaterial to

carry therapeutic agents including cells has been investigated in other species and models (Rufaihah et al., 2017; Seeto et al., 2017). Sustained local release of vascular endothelial growth factor and angiopoietin-1 after injection within PEG-Fb microspheres has been demonstrated in a rat myocardial infarction model with intramyocardial injection (Rufaihah et al., 2017). We showed that we can consistently create uniform, cell-laden microspheres for *in vivo* injection, the equine ECFCs survive encapsulation and injection, and PEG-Fb MS encapsulated labeled ECFCs were detected in tissues up to 3 weeks after injection. The PEG-Fb material was observed only up to 1 week after injection, and this is consistent with the ease of hydrogel breakdown *in vivo* (Rufaihah et al., 2017; Sandker et al., 2017). The fibrinogen backbone of the PEG-Fb biomaterial provides cell adhesion / integrin binding sites found naturally in extracellular matrix proteins, which may have aided cell retention at the point of injection (Almany and Seliktar, 2005; Rufaihah et al., 2017). When we were able to directly visualize the PEG-Fb within tissue sections, we observed no abnormal pattern of vascularization or inflammation associated with this biomaterial. Although the healing rate, vascularization, and number of labeled cells were not different between ECFC treatment and MS-encapsulated ECFC treatment, we were able to detect labeled cells in some biopsies from every horse if they were delivered in microspheres; that was not the case for non-encapsulated ECFCs. No clinically significant adverse effects related specifically to cell therapy or microsphere injection were detected in the 6 treated horses. Other than a single fever and mild generalized limb swelling in one horse, no complications from the injections were encountered, and all wounds were completely epithelialized by 2 months.

Equine wound models are frequently used to study wound healing (Celeste et al., 2011; Jorgensen et al., 2017; Lepault et al., 2005; Tracey et al., 2014; Tsang et al., 2017). Important differences in wound healing based on anatomic location have been noted in some equine wound model studies. When equine wound healing is evaluated using full thickness dermal wounds on both forelimbs and the horse body, wounds on the body have better healing (Celeste et al., 2011; Lepault et al., 2005). Wounds on the forelimbs have lower oxygen saturation, protracted inflammation, slowed epithelialization, and a greater quantity of microvascular occlusion compared to body wounds (Celeste et al., 2011; Lepault et al., 2005). One study that evaluated the effects of topical oxygen therapy on equine distal limb wounds found that forelimbs had significantly greater wound contraction over the course of the study compared to hind limbs (Tracey et al., 2014). Another study evaluating the healing of surgically induced core lesions in the superficial digital flexor tendon of horses found that lesions in the forelimbs had significantly greater vascularization scores than hind limbs (Estrada et al., 2014). In order to parse out cell effects versus biomaterial effects, multiple control conditions were used in the same horse for our study, and autologous cells were utilized leading to variation in the model due to biopsies, different limbs, and function of the autologous cells. We did not choose smaller or more numerous wounds just on the forelimbs for this study because of the concern of treatments on one wound affecting another wound that was in close proximity. Future studies may not require as many control conditions.

In this study, we utilized a histomorphometric software program (Visiopharm, Horsholm, Denmark) to quantitatively evaluate immunohistochemical stain densities in a

semi-automated, unbiased manner (Fiehn et al., 2016; Zhang et al., 2016). The combination of whole slide imaging (Aperio, Leica Biosystems Buffalo Grove, IL) and the histomorphometric software program provided a comprehensive color recognition that allowed an analysis algorithm for the relevant elements specific to each immunohistochemical stain (Fiehn et al., 2016; Zhang et al., 2016). This approach has been used to evaluate collagen density, cancer diagnosis, and inflammatory cell quantification in humans (Fiehn et al., 2016; Roxanis et al., 2018; Sideras et al., 2018). This histomorphometric algorithm-based analysis has also been used to quantify degree of angiogenesis in equine large airways (Herteman et al., 2016), however a common approach for wound healing assessment in the equine involves a semi-subjective scoring system (Jorgensen et al., 2017; Lepault et al., 2005; Tracey et al., 2014). One study of human patients diagnosed with breast cancer found that the histomorphometric software program outperformed traditional pathologist-based analysis of prognostic histologic biomarkers (Stalhammar et al., 2016). An automated, algorithm-based approach for immunohistochemical stain analysis is advantageous for quantitative, non-biased results.

Cell labeling and subsequent tracking of injected cells was performed with QD in this study to identify the location of ECFCs at different time points. We have performed *in vitro* studies with QD in equine ECFCs demonstrating that QD concentrations up to 20 nM do not negatively affect ECFC growth, proliferation, or function (Winter et al., 2018) . Adding QD label to ECFCs is also very easy, as QD nanocrystals are internalized into the cell cytoplasm via an enzyme-independent mechanism (Pi et al., 2010), explaining why QD readily label equine MSCs and ECFCs (Carvalho et al., 2014;

Falomo et al., 2015; Winter et al., 2018). There is also some concern over the possibility of replication-competent lentivirus with transduction and with *ex vivo* identification of iron oxide containing cells (Burk et al., 2016; Peterson GF, 2014). ECFCs labeled with QD were observed up to 3 weeks after injection, and this was independent of whether a low or high number of ECFCs were injected or the number of injections. It is possible that the QD label diminished to an undetectable level with *in vivo* replication, and this may be due to the relatively low concentration of 4 nM QD label used. It is also possible that the QD labeled ECFCs were near and in the wound, but they were not in the specific slices of tissue analyzed.

4.5 Conclusions

This study highlights that equine ECFCs with or without encapsulation in PEG-Fb microspheres can be administered locally to distal limb wounds without adverse effect. This is the first report of clinical effects of ECFCs and of PEG-Fb hydrogel microspheres in the horse. Wounds that were treated with ECFCs with or without PEG-Fb encapsulation had increased vascularization acutely and decreased neutrophilic and macrophagic inflammation chronically, which may be an advantageous to wound healing. No clinically relevant changes were observed in GS or wound size due to treatment, but the observations and cell tracking pave the way for future studies using ECFCs or other cell types combined with the injectable PEG-Fb microspheres.

Chapter 5: Influence of the inflammatory cytokine TNF-α on ECFC function

5.1 Introduction

Endothelial colony forming cells (ECFCs) are a subset of the endothelial progenitor cell (EPC). EPCs have been described as having an ability to heal ischemic tissue by directly incorporating into damaged blood vessels and forming *de novo* blood vessels in ischemic tissue, and indirectly by decreasing perivascular inflammation in wounded tissue. The ECFC is typically thought to play a more prominent role in these actions than the early-outgrowth EPC subset. Therefore, using ECFCs as a therapeutic intervention in ischemic wounds to heal damaged blood vessels or form new blood vessels has been evaluated in multiple species. In a mouse model of traumatic brain injury characterized by direct vascular injury and secondary ischemic damage, groups with ECFCs injected at the site of injury had improved microvessel density and clinical outcomes compared to control groups (Zhang et al., 2013). In humans with diabetic foot wounds, ECFCs have been found to migrate to sites of vascular injury (Seo et al., 2013) and also contribute to improved local blood flow and healing times (Dubsky et al., 2013). In a distal limb wound model in the horse, ECFCs have been shown to associate near newly formed blood vessels in wounds as well as incorporate into new blood vessels (Chapter 4). Additionally, equine ECFCs decrease inflammation within wounded tissue in this model (Chapter 4).

Distal limb wounds in the horse are well studied. Common findings in this wound location are exaggerated and prolonged inflammatory responses, which delay wound healing and in some cases leads to an excessive and detrimental formation of

granulation tissue, called exuberant granulation tissue (EGT). Acute changes in the dermis include moderate to severe neutrophilic and eosinophilic infiltration, with neutrophilic and macrophagic inflammation dominating over time (Theoret et al., 2013; Wilmink et al., 1999). Activated neutrophils and macrophages have been found to persist in these wounds over a period of at least 5 weeks (Wilmink et al., 1999). The persistence of inflammatory cells in equine distal limb wounds may be driven by local hypoxia, local pro-inflammatory cytokine inflammation, or both (Deschene et al., 2011; Wilmink et al., 1999). One consequence of the prolonged presence of activated inflammatory cells is the constitutive expression of pro-inflammatory cytokines such as interleukin (IL) 1 beta, IL-6, and TNF-α. These and other pro-inflammatory cytokines are elevated in as early as 1.5 hr after the initiation of an inflammatory stimulus (Loftus et al., 2007). Macrophages are present in equine limb wounds starting several days after the wound initiation (Theoret et al., 2002) and persist chronically in wounds with EGT, and these cells are a known source of local TNF-α production (Carswell et al., 1975).

Human ECFCs are negatively affected by TNF-α *in vitro*, and this is observed as a reduction in proliferation, tubule formation on basement membrane matrix, and migration (Mena et al., 2018). Human ECFCs also demonstrate significant apoptosis in the presence of TNF-α, and this effect is dependent on both the TNF-α dose and the time of contact with ECFCs (Bian et al., 2017). Exposure to TNF-α compromises the *in vitro* and *in vivo* function of ECFCs. After exposure to TNF-α *in vitro*, human ECFCs had a significant reduction in their ability to incorporate into vascular structures (Hong et al., 2015). Additionally, ECFCs have a reduced ability to incorporate into vascular

structures after isolation from human patients with systemic vasculitis (Hong et al., 2015), a condition known to have elevated levels of TNF-α in the circulation (Edwards et al., 1993). The number of circulating EPCs is also decreased in human patients with systemic lupus erythematosus, a condition associated with elevated levels of TNF-α in the circulation as well as elevated expression of TNF-α mRNA in the bone marrow (Moonen et al., 2007). Despite the wealth of knowledge on the effects of TNF-α on human ECFCs, the effect on equine ECFCs is unknown.

Equine ECFCs have been evaluated in a distal limb wound model and may be considered a therapeutic option for clinical patients with distal limb wounds in the future. As has been well-established, distal limb wounds in the horse have pro-inflammatory microenvironments. However, the effect of pro-inflammatory cytokines such as TNF-α on the equine ECFC has not been evaluated. The hypothesis of this preliminary study was that TNF-α would have negative effects on equine ECFC function *in vitro*. The aims of this study were to: 1) determine the ideal concentration and time of contact for TNF-α to use with equine ECFCs; 2) to evaluate cell viability, cell migration, cell adherence, and cell function via low density lipoprotein uptake and tubule formation assays with and without TNF-α exposure *in vitro*.

5.2 Methods

5.2.1 Isolation, storage, and classification of ECFCs

All protocols that involved animals were approved by the Auburn University Animal Care and Use Committee. Whole blood was collected from a healthy, adult

horse aged 15 from either the cephalic vein or the jugular vein for ECFC isolation using either a whole blood isolation or density gradient centrifugation isolation method as previously described (Salter et al., 2015; Sharpe et al., 2016). The ECFCs were cryopreserved at a concentration of 300,000 cells / mL in a freezing medium containing 95% equine serum and 5% dimethyl sulfoxide and then stored in liquid nitrogen as P3 cells. ECFCs were thawed and used for all experiments at P4 or P5. ECFCs were cultured in either 25 cm^2 or 75 cm^2 tissue culture polystyrene flasks in endothelial cell growth medium with manufacturer-supplied growth factors and anti-microbials (EGM-2 with Bullet Kit, Lonza, Visp, Switzerland) with equine serum at a final concentration of 10% (HyClone Laboratories Inc, Logan, UT, USA) at standard cell culture conditions (37° C, 5% CO_2, 95% humidity). ECFCs were defined as late-outgrowth EPCs based on characteristic cobblestone morphology and rapid *in vitro* cell division (Salter et al., 2015). The ECFCs used in this study expressed CD34, CD105, VEGFR-2, vWF, and CD14, formed vascular tubules on basement membrane and also had receptor-mediated uptake of fluorescently-labeled acetylated low-density lipoprotein (DiO-Ac-LDL) (Biomedical Technologies Inc, Stoughton, MA, USA), consistent with our group's previous work (Salter et al., 2015).

5.2.2 Exposure of equine ECFCs to TNF-α - data to determine dose and contact time

The effects of TNF-α exposure to human EPCs has been studied, and researchers have utilized protocols with varying concentrations and contact time of TNF-α with the cells. Concentrations that elicited responses *in vitro* range widely from 1 ng/mL to 50 ng/mL, with the TNF-α exposure time also varying from 1 – 48 hr. Since

there are no published reports of the contact times and concentrations of TNF-α needed to elicit a response *in vitro* in equine ECFCs, a pilot study was performed using P5 equine ECFCs.

Recombinant equine TNF-α was obtained as a 25 µg powder (Kingfisher Biotech Inc, Saint Paul, MN, USA). Based on manufacturer's recommendations, this was diluted in 500 µL of 0.4% BSA. The 0.4% BSA solution was filtered through a 0.22 micron sterile membrane filter prior to addition to the TNF-α powder to ensure sterility. After adequate mixing by vortex, the 500 µL stock solution was partitioned into 25 aliquots of 20 µL. This working solution had a concentration of 50 ng / µL and was then frozen at -20° C. All aliquots used for the study underwent only one freeze – thaw cycle prior to use.

Equine ECFCs were assessed for cell viability, cell adherence, and cell migration under the following conditions:

1) 0 ng/mL TNF-α (control group)

2) 10 ng/mL TNF-α, with 6 hr contact time

3) 10 ng/mL TNF-α, with 24hr contact time

4) 25 ng/mL TNF-α, with 6 hr contact time

5) 25 ng/mL TNF-α, with 24 hr contact time

6) 50 ng/mL TNF-α, with 6 hr contact time

7) 50 ng/mL TNF-α, with 24 hr contact time

A dose-dependent decline in cell function was observed with exposure to TNF-α, with exposure to 50 ng/mL TNF-α showing the greatest decline in cell function (further detailed below). No significant differences were observed in cell function between 6 hr and 24 hr exposure times to TNF-α for any given concentration (further detailed below). Based on these data, a TNF-α concentration of 50 ng/mL was used for the remainder of the study with a contact time of 6 hr with the cells which is described in detail below.

5.2.3 Assessment of TNF-α effect on ECFC viability

Equine ECFCs of P4 were seeded into a collagen-coated (50 µg/mL) 75 cm^2 cell culture flask with 225,000 cells (3,000 cells/cm^2) in standard cell culture conditions (37° C, 5% CO_2, 95% humidity). When cells reached ~80% confluency, cells were subcultured by adding trypsin-EDTA at 0.25 mg/mL (Lonza, Visp, Switzerland) and incubating at 37° C for 1 min. Trypsin was neutralized with an equal volume of fresh ECFC culture medium, followed by centrifugation at 200 x g for 5 min. These cells were then reseeded onto collagen-coated wells of 12-well plates at 50,000 cells / well. Cells were cultured in triplicate (3 wells used per condition) until ~50% confluent. A marker was used on the outside bottom of each well to mark a specific field of view. The purpose of the marked field of view was to allow serial photomicrographs to be obtained for the same region in the wells over time.

Photomicrographs were obtained for each well immediately prior to addition of TNF-α. All culture medium was removed from the wells, and these wells were then rinsed once with PBS. New culture medium was then added to each well, with either 0

ng/mL or 50 ng/mL of TNF-α added to the medium. The 12-well flasks were incubated in standard cell culture conditions for 6 hr. Photomicrographs were then obtained for each well at the previously specified marked field of view (i.e. the same field of view as the previous photomicrograph obtained prior to the addition of TNF-α). The subjective appearance of the adherent cells and the number of dead cells floating in the medium was quantified before and after exposure to TNF-α.

5.2.4 Assessment of TNF-α effect on ECFC adherence

Equine ECFCs of P3 were seeded into a collagen-coated (50 µg/mL) 75 cm^2 cell culture flask with 225,000 cells (3,000 cells/cm^2) in standard cell culture conditions. When cells reached ~80% confluency, they were subcultured by adding trypsin-EDTA at 0.25 mg/mL (Lonza, Visp, Switzerland) and incubating at 37° C for 1 min. Trypsin was neutralized with an equal volume of fresh ECFC culture medium, followed by centrifugation at 200 x g for 5 min. These cells were then reseeded onto collagen-coated 25 cm^2 cell culture flasks with 75,000 cells (3,000 cells/cm^2) and cultured in standard cell culture conditions. Once cells were ~66% confluent, cell culture medium was removed from each flask. Each cell culture flask was then rinsed once with PBS, and fresh cell culture medium was added which contained either 0 ng/mL or 50 ng/mL of TNF-α.

After 6 hr of incubation in standard cell culture conditions, cell culture medium was removed from each cell culture flask. Each of these flasks was then rinsed once with PBS. Cells were subcultured by adding trypsin-EDTA at 0.25 mg/mL (Lonza, Visp,

Switzerland) and incubating at 37° C for 1 min. Trypsin was neutralized with an equal volume of fresh ECFC culture medium, followed by centrifugation at 200 x g for 5 min. These cells were then reseeded onto collagen-coated wells of a 12-well plate with 30,000 cells per well. Each TNF-α concentration (0 ng/mL and 50 ng/mL) was represented in triplicate (3 wells per concentration). After 60 min incubation at standard cell culture conditions, photomicrographs were obtained of each well. Photomicrographs of 5 random fields of view were obtained at 20X magnification for each well. A total cell count was obtained, which included all cells that were completely within the field of view. Distinction was made between cells which were not adhered and floating in the medium, and those cells which were adhered to the surface of the well. The number of cells adhered to the bottom of the well was averaged over the 5 random fields of view within one well, so that one value for cells adhered / high powered field was used for statistical analysis.

5.2.5 Assessment of TNF-α effect on ECFC migration

Equine ECFCs of P4 were seeded into a collagen-coated (50 µg/mL) 75 cm^2 cell culture flask with 225,000 cells (3,000 cells/cm^2) in standard cell culture conditions. When cells reached ~80% confluency, they were subcultured by adding trypsin-EDTA at 0.25 mg/mL (Lonza, Visp, Switzerland) and incubating at 37° C for 1 min. Trypsin was neutralized with an equal volume of fresh ECFC culture medium, followed by centrifugation at 200 x g for 5 min. These cells were then reseeded onto collagen-coated wells of 12-well plates at 50,000 cells / well. Each condition was represented in triplicate (3 wells for each condition). Cells were cultured until ~80% confluent. A

marker was used on the outside bottom of each well to mark a specific field of view. The purpose of the marked field of view was to allow repeat photomicrographs to be obtained for the same region in the wells over time. Each well had cell culture medium removed, was then rinsed once with PBS, and then had fresh cell culture medium added which contained either 0 ng/mL or 50 ng/mL of TNF-α.

After 6 hr of incubation at standard cell culture conditions, a sterile 200 μm micropipette tip was used to create a wound defect in the ECFC monolayer in each well. Working in a sterile environment, the narrow end of this micropipette tip was firmly dragged across the cell monolayer surface in proximity to the marked portion of the well. Detached cells were removed by gently removing cell culture medium. All wells were then rinsed once with PBS, before the addition of fresh cell culture medium with or without TNF-α. The 12-well plates were then cultured in standard cell culture conditions. Photomicrographs were taken immediately after addition of fresh cell culture medium, at 3 hr, and at 6 hr after addition of fresh culture medium. The marked area on the outside of the well bottom was used to image the same field of view at each time. Migration rate (μm / hr) was then calculated for all wells using Image J software (imagej.nih.gov/ij). Migration distance at 3 hr post-wounding and 6 hr post-wounding was used to calculate a migration rate for each well.

5.2.6 Assessment of TNF-α effect on ECFC *in vitro* tubule formation

Equine ECFCs of P3 were seeded at 75,000 cells per flask into a collagen-coated 25 cm^2 cell culture flask, and cultured until ~80% confluent. When cells reached

~80% confluency, they were subcultured by adding trypsin-EDTA at 0.25 mg/mL (Lonza, Visp, Switzerland) and incubating at 37° C for 1 min. Trypsin was neutralized with an equal volume of fresh ECFC culture medium, followed by centrifugation at 200 x g for 5 min. These cells were then reseeded into 25 cm^2 cell culture flasks (1 per condition) with 75,000 cells (3,000 cells/cm^2). Once ~66% confluent, cell culture media was removed from each flask. Flasks were rinsed once with PBS, and fresh cell culture medium with either 0 ng/mL or 50 ng/mL TNF-α was added. After 6 hr incubation at standard cell culture conditions, cells were subcultured as described above. These cells were then reseeded into wells of a 96-well cell culture disk which were prepared with 75 µL/well of solubilized basement membrane (BD Matrigel Basement Membrane Matrix, BD Biosciences, Bedford, MA, USA) and incubated for 30 min at 37° C prior to cell seeding. Each well was seeded with 12,000 cells and then incubated at 37° C. Vascular tubule formation was assessed at 24 hr post seeding. The presence or absence of tubule formation was noted using light microscopy. Tubule quality score was subjectively scored as previously described (Salter et al., 2015) (1 = no tubule formation, 2 = tubules projecting from cells but no connections between cells, 3 = vascular tubule formation with connecting tubules in $\leq$ 50% of the field, and 4 = vascular tubule formation with connecting tubules in > 50% of the field).

5.2.7 Assessment of TNF-α effect on uptake of low density lipoprotein

Equine ECFCs of P3 were seeded at 75,000 cells per flask into a collagen-coated 25 cm^2 cell culture flask, and cultured until ~80% confluent. When cells reached ~80% confluency, they were subcultured by adding trypsin-EDTA at 0.25 mg/mL

(Lonza, Visp, Switzerland) and incubating at 37° C for 1 min. Trypsin was neutralized with an equal volume of fresh ECFC culture medium, followed by centrifugation at 200 x g for 5 min. These cells were then reseeded into collagen-coated wells of a 12-well plate (3 wells per condition) with cell culture media and 50,000 cells per well in standard cell culture conditions. Once cells were ~50% confluent, cell culture medium was removed from all wells. Wells were rinsed with PBS once, and fresh cell culture medium with either 0 ng/mL or 50 ng/mL TNF-α was added.

After 6 hr of incubation in standard cell culture conditions, cell culture medium was removed from all wells. Wells were rinsed once with PBS, and DiO-Ac-LDL diluted in pre-warmed supplemented medium (50 μg/mL concentration) was added to all wells. Cells were incubated with DiO-Ac-LDL for 4 hr at standard cell culture conditions. After incubation, ECFCs were then washed with fresh cell culture medium 3 times. Cells were harvested by adding trypsin-EDTA at 0.25 mg/mL (Lonza, Visp, Switzerland) and incubated at 37° C for 1 min. Trypsin was neutralized with an equal volume of fresh ECFC culture medium, followed by centrifugation at 200 x g for 5 min. Cells were washed with PBS solution, and then 1 mL of 4% paraformaldehyde solution was added. Cells were then incubated at room temperature (25° C) for 20 min, after which they were centrifuged at 200 x g for 5 min and then washed with PBS solution twice. Cells were then re-suspended in 1% bovine serum albumin solution (OmniPur, Gibbstown, NJ, USA), covered to protect from light, and kept at 4° C.

Cells were filtered through a 35 μm mesh filter and then immediately underwent flow cytometric analysis (BD Accuri C6 software, BD Biosciences, Brea, CA, USA). Using a FLH-1 flow cytometry gate, analysis was performed to quantify the percentage

of ECFCs that had DiO-Ac-LDL uptake. A total of 15,000 events were collected for each duplicate sample, and forward scatter versus side scatter plots were used for imaging. Gates were set in order to both select for live cultured cells and eliminate doubled cells, dead cells, and debris.

5.2.8 Statistical analysis

Statistical analyses were performed with commercially available statistical software (JMP®, Version 13.0.0 SAS Institute Inc., Cary, NC, USA). Normality of data was assessed using a Shapiro-Wilk test and expressed as mean +/- SD or median (range) as appropriate. Data with a normal distribution were compared using either a Student's t-test or ANOVA. Data with a nonparametric distribution were expressed as median (interquartile range) and compared using a Wilcoxon rank sums or Kruskal Wallis test. Significance was assessed as a *P* value <0.05.

5.3 Results

5.3.1 Dose-dependent effect of TNF-α on ECFC function – results of pilot study

Cell viability was not adversely affected by either 6 hr or 24 hr of contact with TNF-α at doses of 10 ng/mL, 25 ng/mL, or 50 ng/mL. Photomicrographs of equine ECFCs from 1 horse cell line immediately prior to addition of TNF-α and after 6 hr or 24 hr of contact with TNF-α were obtained (Figures 45 and 46). Subjective comparisons of cell morphology revealed no changes with the addition of TNF-α. In the 24 hr contact

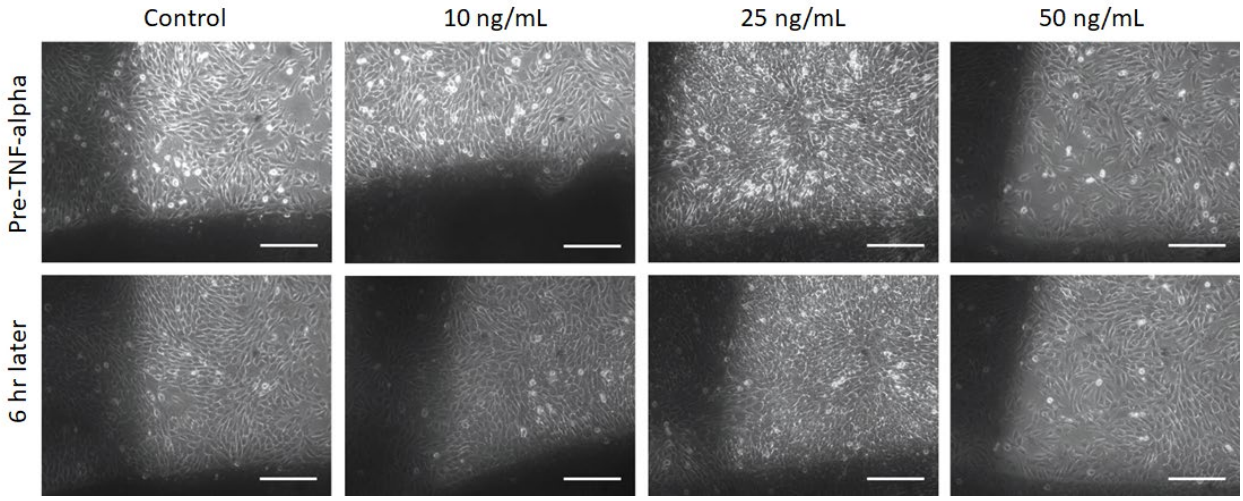

Figure 45. ECFC viability after 6 hr contact with TNF-α. Photomicrographs of equine ECFCs taken immediately prior to and after 6 hr of contact with TNF-α at concentrations of 0 ng/mL (Control), 10 ng/mL, 25 ng/mL, and 50 ng/mL. The marks on the outside of the well bottoms are evident as thick, black lines. Scale bars are 250 μm.

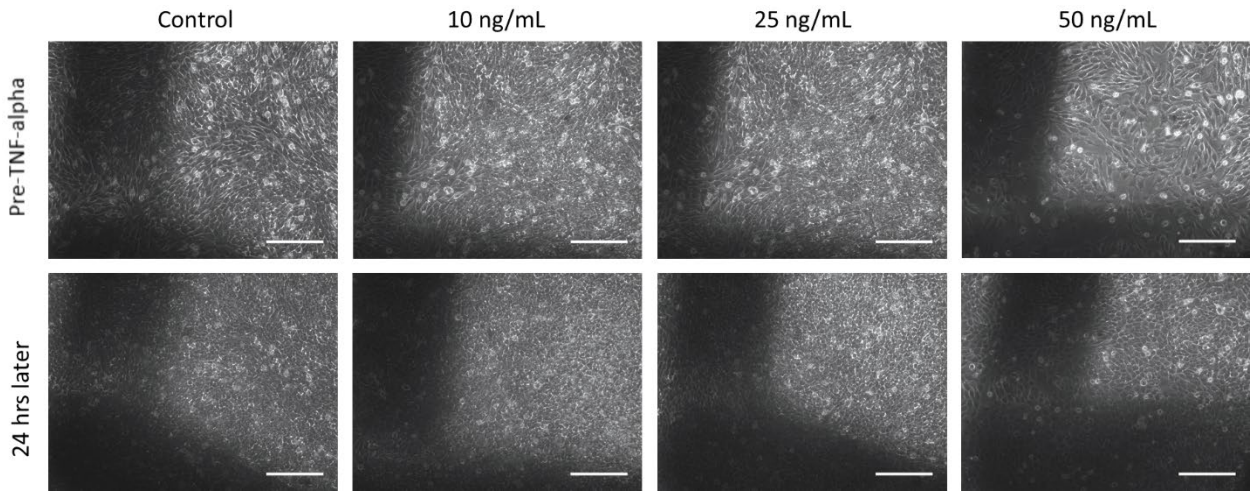

Figure 46. ECFC viability after 24 hr contact with TNF-α. Photomicrographs of equine ECFCs taken immediately prior to and after 24 hr of contact with TNF-α at concentrations of 0 ng/mL (Control), 10 ng/mL, 25 ng/mL, and 50 ng/mL. The marks on the outside of the well bottoms are evident as thick, black lines. Scale bars are 250 μm.

groups, cells became smaller and more crowded (Figure 46). However this was noted in the control group (0 ng/mL TNF-α added) and the groups that had TNF-α added to the cell culture medium and was therefore attributed to normal cell proliferation over 24 hr. There was no evidence of an increase in the number of cells floating in the cell culture medium (subjective evidence of cell death) with the addition of TNF-α.

Adherence of equine ECFCs from 1 horse cell line to collagen-coated wells of cell culture plates was negatively affected by the addition of TNF-α. The number of cells adhered to wells of a 12-well plate was significantly decreased compared to control cells (0 ng/mL TNF-α), but there was not an obvious dose-dependent change (Figure 47). Control cells which did not contact TNF-α had a significantly greater number of cells adhered to the collagen-coated well bottom at 60 min after addition of cells compared to all concentrations of TNF-α after 6 hr contact (P=0.035). This effect was observed with the TNF-α 6 hr contact groups and also with the 24 hr contact groups. However, there was not a significant difference in cell adherence after contact with TNF-α between the 6 hr contact and 24 hr contact groups (P = 0.626) (Figure 48).

Migration rates of equine ECFCs from 1 horse cell line were negatively affected by addition of TNF-α. The migration rate (μm / hr) of equine ECFCs after wounding, based on measurements obtained at 3 hr post-wounding and 6 hr post-wounding, had a dose-dependent response to TNF-α concentrations (Figure 49). Cells exposed to 50 ng/mL TNF-α had the slowest migration rate (Figure 50). A similar trend was observed in migration rate for cells exposed to TNF-α for 24 hr. There was not a significant

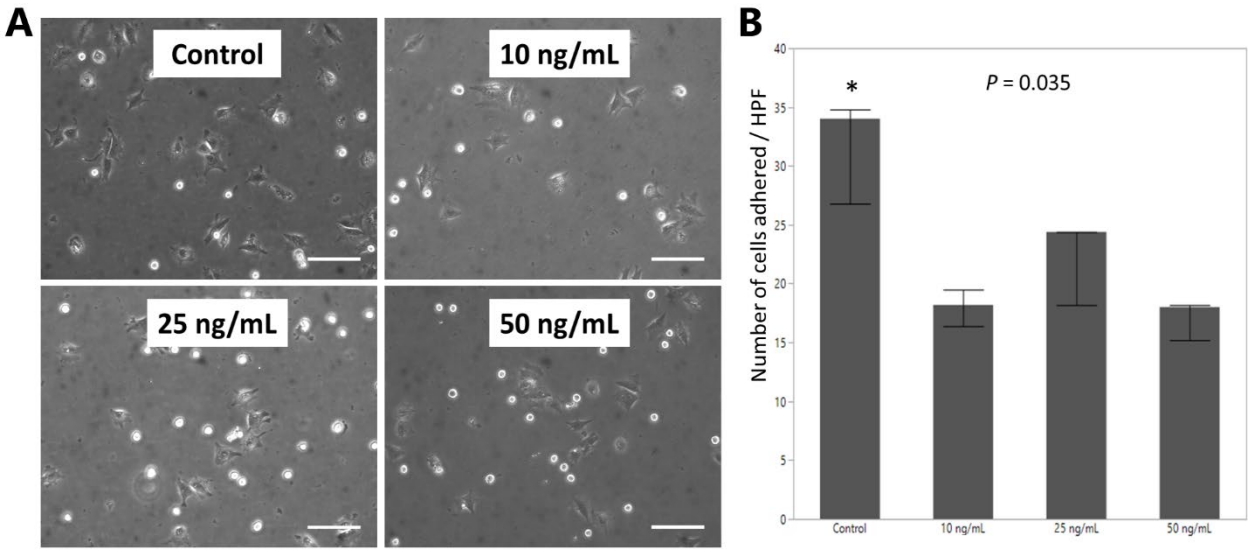

Figure 47. ECFC adherence to collagen-coated cell culture wells after exposure to TNF-α. A) Representative photomicrographs 60 min after seeding of equine ECFCs exposed to varying concentrations of TNF-α (Control = 0 ng/mL) for 6 hr. Scale bars are 250 μm. B) Number of cells adhered per high powered microscopy field (HPF) 60 min after seeding of equine ECFCs with 6 hr contact with various TNF-α concentrations (Control = 0 ng/mL). Data are represented as median and range. * denotes that control cells have significantly greater adherence than all other groups (P<0.05).

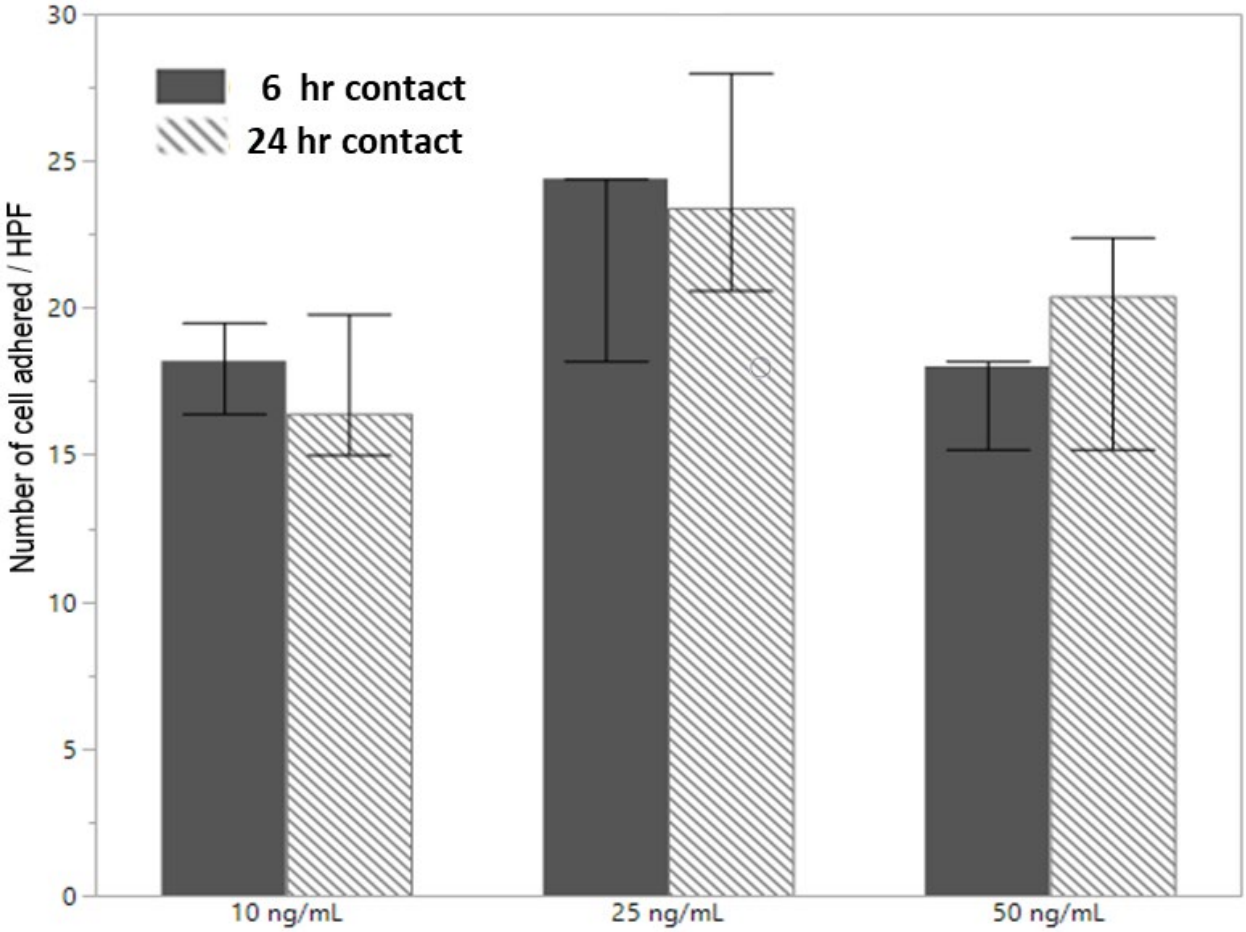

Figure 48. ECFC adherence with 6 hr and 24 hr contact with TNF-α. Number of equine ECFCs adhered to collagen-coated cell culture flasks 60 min after seeding in cells exposed to various TNF-α concentrations for either 6 hr or 24 hr. Data is presented as median and range.

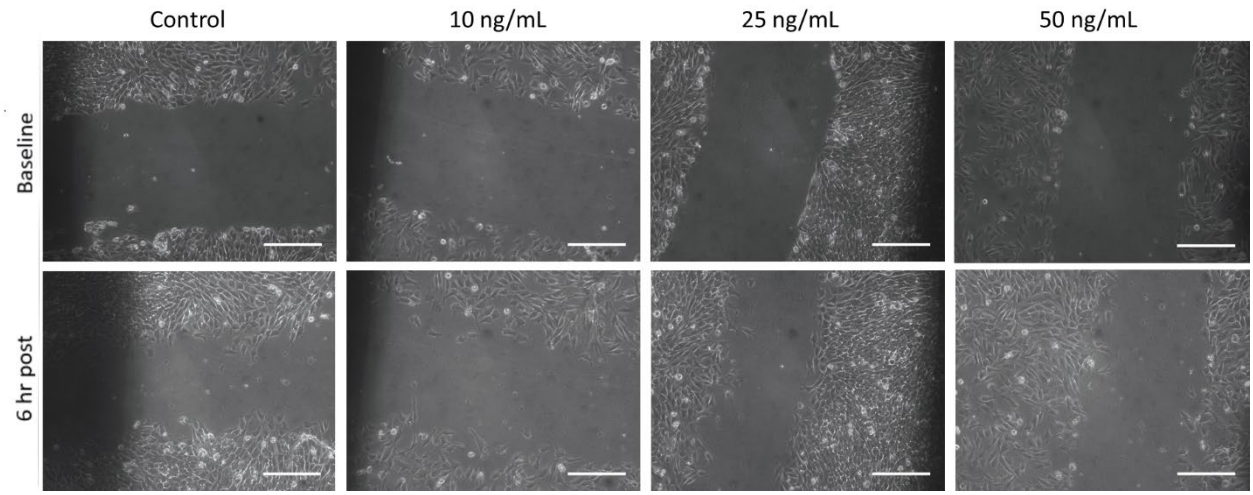

Figure 49. Migration of ECFCs after wounding. Representative photomicrographs immediately after wounding (top row) and 6 hr later (bottom row) for Control cells (0 ng/mL TNF-α) and cells exposed to TNF-α for 6 hr. Scale bars are 250 μm.

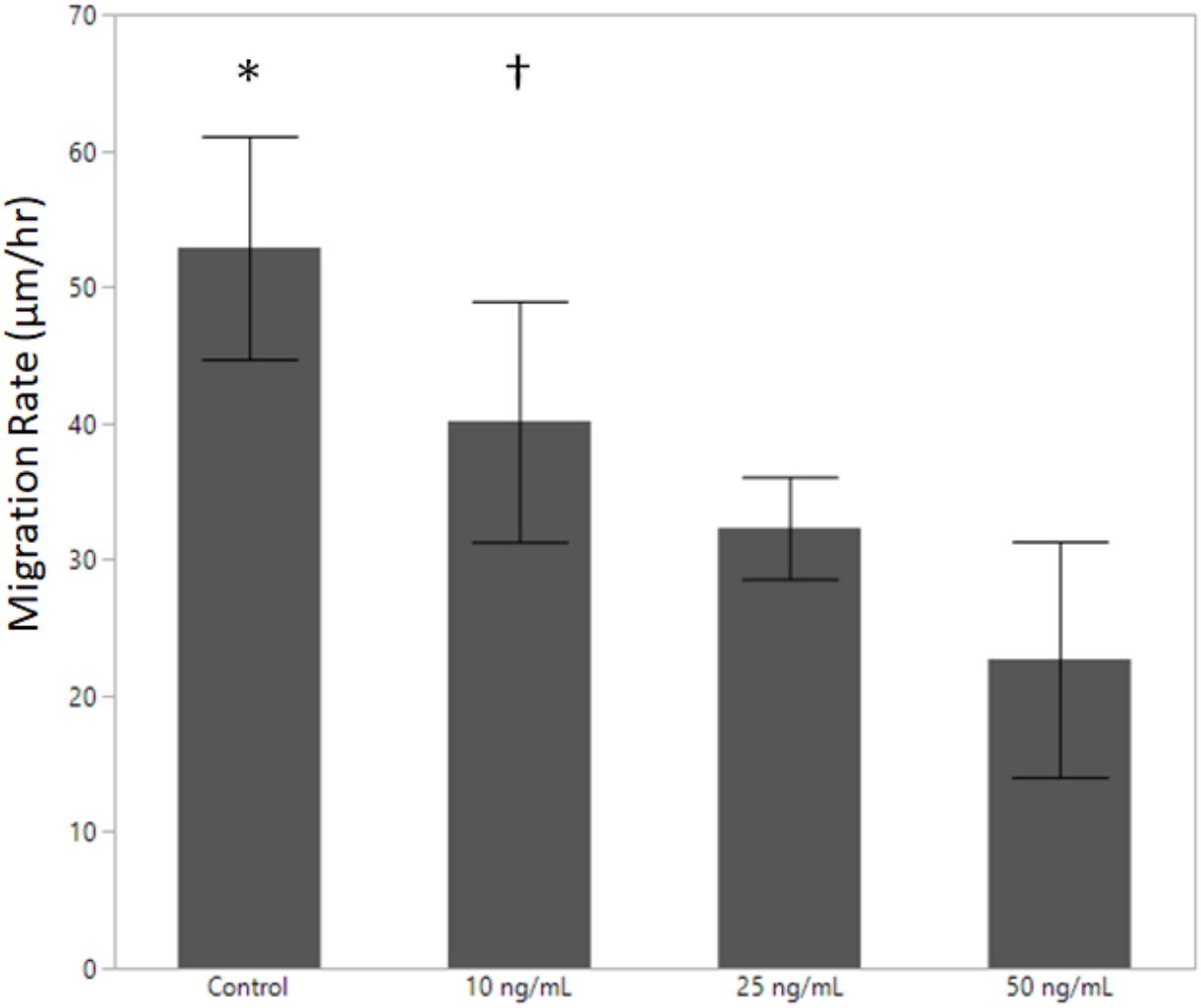

Figure 50. Migration rates for ECFCs exposed to varying concentrations of TNF-α. Migration rate (µm/hr) after cell monolayer wounding for Control cells (0 ng/mL) and varying concentrations of TNF-α with a 6 hr exposure are presented as mean and SD. * indicates that control cells had a significantly higher migration rate (µm/hr) than all other groups (P<0.05). † indicates that cells exposed to 10 ng/mL TNF-α for 6 hr had a significantly greater migration rate (µm/hr) than cells exposed to 50 ng/mL TNF-α for 6 hr (P<0.05).

difference in migration rate of cells exposed to TNF-α for 6 hr contact compared to 24 hr contact for all concentrations (P = 0.73) (Figure 51).

5.3.2 Tubule formation in cells exposed to TNF-α

Equine ECFCs maintained their ability to form *in vitro* tubules after exposure to TNF-α. *In vitro* tubule formation of equine ECFCs from 1 horse cell line seeded onto basement membrane matrix as described above was assessed in cells exposed to either 0 ng/mL TNF-α (control cells) or 50 ng/mL TNF-α for 6 hr. Three replicates of each condition were performed, and representative photomicrographs were analyzed 24 hr after seeding. Both control cells and cells exposed to 50 ng/mL TNF-α for 6 hr had tubule scores of 4, demonstrating no notable difference in the ability of ECFCs to form tubules after exposure to TNF-α (Figure 52).

5.3.3 Cell uptake of DiO-Ac-LDL after exposure to TNF-α

The ability of equine ECFCs from 1 horse cell line to uptake DiO-Ac-LDL was negatively affected by exposure to TNF-α. Flow cytometry was used to assess the percentage of the ECFCs that did and did not uptake DiO-Ac-LDL based on 15,000 events. This was performed for cells exposed to 0 ng/mL TNF-α (Control cells) and those exposed to 50 ng/mL TNF-α for 6 hr. Control cells had 93.63% uptake

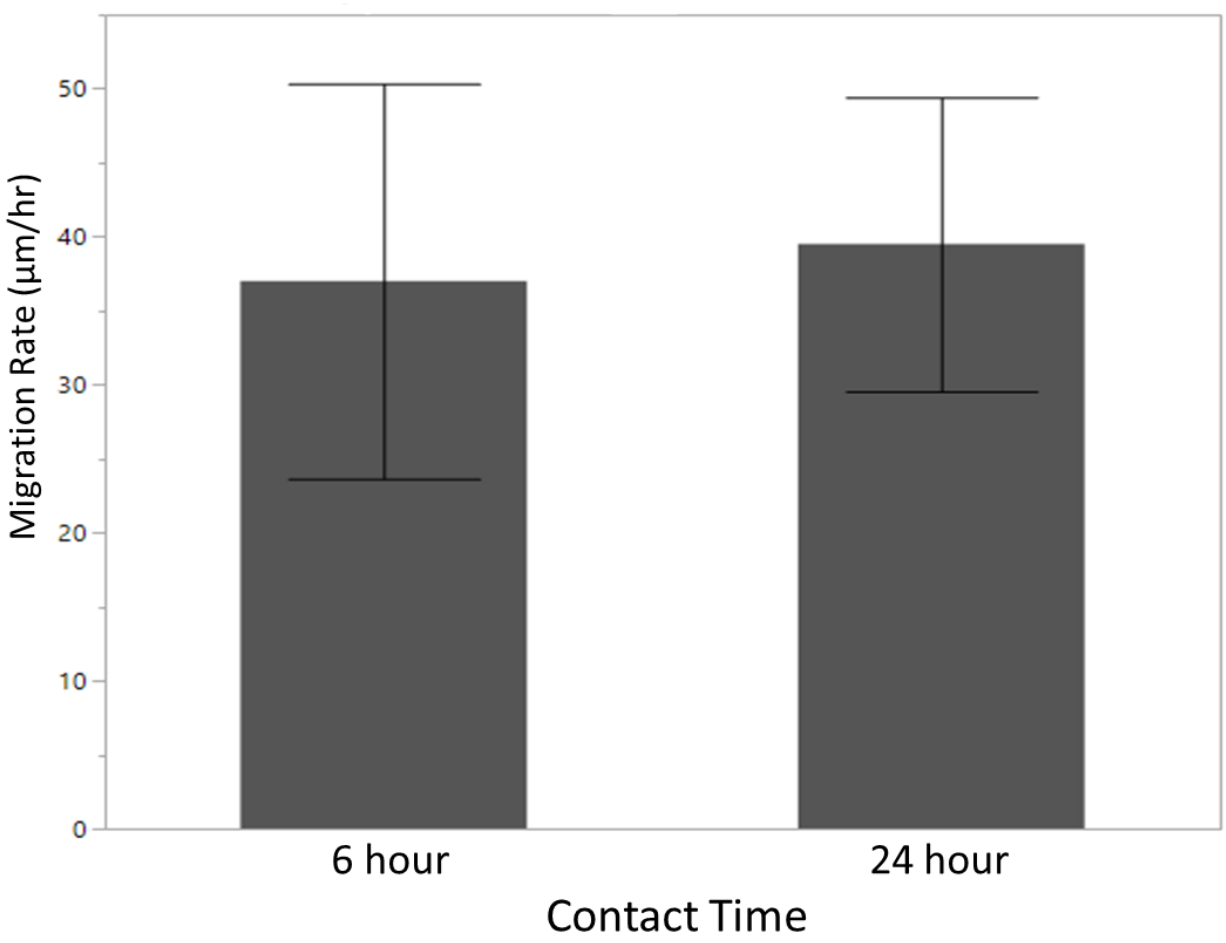

Figure 51. Migration rate of equine ECFCs exposed to TNF-α for 6 hr or 24 hr. Migration rates (µm/hr) after cell monolayer wounding of equine ECFCs exposed to 10 ng/mL, 25 ng/mL, and 50 ng/mL TNF-α for either 6 hr or 24 hr. Data are represented as mean and SD.

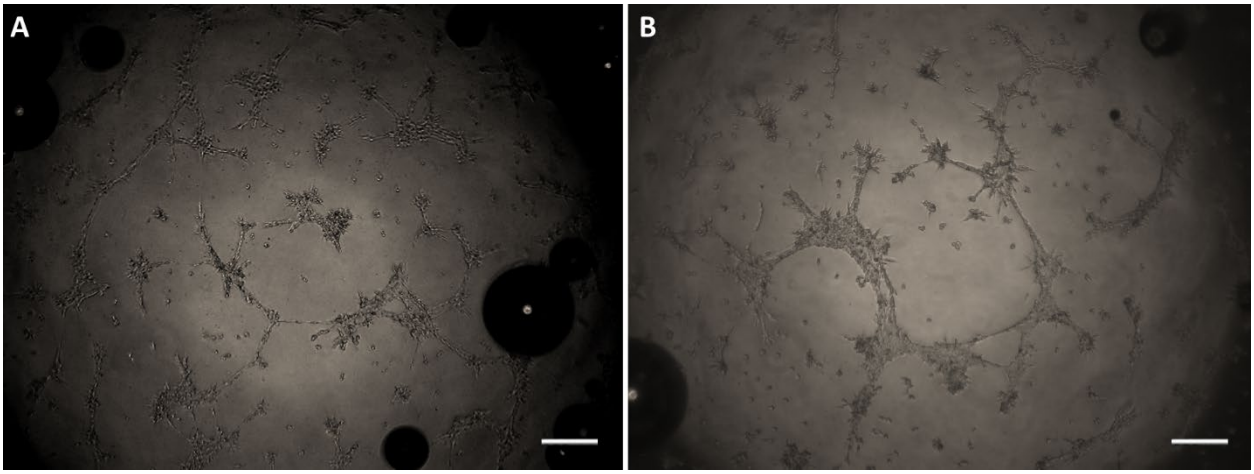

Figure 52. *In vitro* tubule formation of ECFCs exposed to TNF-α. Representative photomicrographs of *in vitro* tubule formation after 24 hr on basement membrane matrix in control cells (0 ng/mL TNF-α) (A) and in cells exposed to 50 ng/mL TNF-α for 6 hr prior to seeding (B). Scale bars are 250 μm.

DiO-Ac-LDL, whereas only 66.70% of cells exposed to TNF-α had uptake of DiO-Ac-LDL (Figure 53).

5.4 Discussion

Results of this study demonstrate that the pro-inflammatory cytokine TNF-α negatively affects equine ECFC function. ECFC function was decreased in multiple *in vitro* assays after TNF-α exposure such as adherence to cell culture wells and also decreased migration rate which may affect vasculogenesis *in vivo*. Cell migration and cellular uptake of DiO-Ac-LDL were decreased after exposure to TNF-α, and this may indicate that other cell functions may be impacted by exposure to TNF-α. The ability to form *in vitro* tubules on basement membrane matrix was not affected by 50 ng/mL TNF-α after a 6 hr cell contact time, and this warrants further investigation.

The cytokine TNF-α was chosen to study, because it is commonly present in many different types of inflammatory conditions. EPCs and their subset ECFCs have been administered as a therapy both in experimental and clinical diseases, many of which have local or systemic inflammation. As such, TNF-α is present in many of these diseases. Human EPCs demonstrate a reduced expression of VEGFR-1 and stromal cell-derived factor-1 mRNA in response to TNF-α exposure, both of which are critical for angiogenesis and cell homing with subsequent differentiation (Chen et al., 2011). Equine ECFCs have been found to remain within and near newly formed blood vessels in a wound model, which was observed up to 3 weeks after ECFC injection (Chapter 4). Since the injection of the ECFCs occurred at the periphery of the wounds, and wound size decreased over that 3-week time period, this may indicate a preserved homing

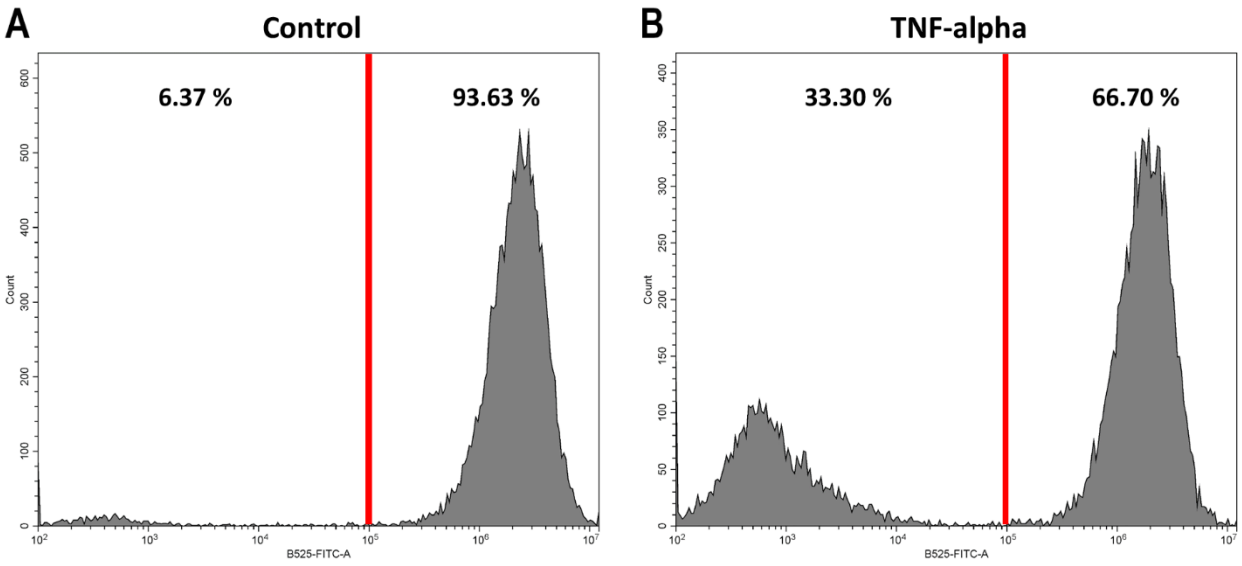

Figure 53. Uptake of DiO-Ac-LDL after exposure to TNF-α. Equine ECFCs were exposed to DiO-Ac-LDL and then analyzed for percentage of cells with uptake. A) Control cells (0 ng/mL) have 93% cells positive for DiO-Ac-LDL, indicating cellular uptake. B) Cells exposed to 50 ng/mL TNF-α for 6 hr had 66% cells positive for DiO-Ac-LDL, indicating cellular uptake. The red line marks the demarcation between cells that have (right of line) and have not (left of line) had cellular uptake of DiO-Ac-LDL based on fluorescent signal.

capability for equine ECFCs in an overtly inflammatory wound environment. Concentrations of TNF-α were not measured in that study, but macrophagic inflammation was a prominent component of the wound which suggests the local presence of TNF-α (Carswell et al., 1975; Loftus et al., 2007) (Chapter 4). The presence of TNF-α in a variety of wounds that have prominent macrophagic inflammation has been demonstrated in multiple species (Ahn et al., 2016; Dong et al., 2013; Green et al., 2006). Human ECFCs develop apoptosis in response to TNF-α exposure *in vitro*, and this is observed in both a concentration-dependent and time-dependent manner (Bian et al., 2017). Equine ECFCs did not experience obvious decline in viability with the addition of TNF-α, but this was only subjectively assessed. Apoptosis needs to be assessed in equine ECFCs in response to TNF-α. There is some evidence that certain populations of ECFCs may be inherently resistant to apoptosis in response to TNF-α exposure. Apoptosis assessed by caspase 3 activity was significantly higher in ECFCs isolated from healthy human subjects and those with benign breast cancer compared with those isolated from humans with malignant breast cancer (Chou et al., 2016). Since some but not all ECFC populations are negatively affected with exposure to TNF-α, it will be important to assess the response of each specific ECFC population in response to TNF-α prior to the therapeutic use of ECFCs in inflammatory environments.

The effect of TNF-α on cell viability and cell function is an important consideration for the use of cell therapy in wounds and inflammatory diseases. Human ECFCs show a decreased ability to incorporate into existing vascular structures *in vitro* when exposed

to TNF-α (Hong et al., 2015). It is possible that this lack of vascular incorporation may be due to impaired migration, as decreased migration rates after exposure to TNF-α have been observed in human ECFCs (Chen et al., 2011) and also in equine ECFCs. A significant decrease in the number of cells migrating towards VEGF was observed in human EPCs with a 6 hr TNF-α exposure at a concentration of 50 ng/mL (Chen et al., 2011; Wang et al., 2015). In the equine ECFCs of this study, a significant decrease in migration rate was observed with as little as 10 ng/mL TNF-α with a 6 hr contact time, but this was concentration-dependent with the slowest migration rate observed in the group of ECFCs that received 50 ng/mL TNF-α. An impaired ability to uptake acetylated LDL has been observed in human ECFCs after TNF-α exposure (Chen et al., 2011; Chou et al., 2016), and this was observed as a significant decrease in DiI-Ac-LDL uptake in human ECFCs exposed to just 1 pg/mL of TNF-α compared to control ECFCs. A decrease in DiO-Ac-LDL was also observed in the equine ECFCs of this study after TNF-α exposure. Both exposure to TNF-α and cellular senescence has been shown to negatively influence ECFC function. In one study of equine ECFCs, cell function was significantly better with the first 4 passages compared to passages 5 through 10 (Salter et al., 2015). Exposure to TNF-α has been shown to cause premature senescence in human ECFCs via the p38 mitogen-activated protein kinase pathway (Zhang et al., 2009), and it is possible that premature senescence is in part responsible for the decrease in function of equine ECFCs after exposure to TNF-α.

The ability to form tubules on basement membrane matrix medium is reduced in human ECFCs after exposure to TNF-α (Chen et al., 2011; Wang et al., 2015). Dose-dependent decrease in tubule formation was observed in human ECFCs *in vitro* after

TNF-α exposure starting at 10 ng/mL (Chen et al., 2011). Another study demonstrated a significant decrease of *in vitro* tubule length in ECFCs exposed to TNF-α compared to control ECFCs (Wang et al., 2015). However, obvious effects on tubule formation *in vitro* were not observed in equine ECFCs exposed to TNF-α in this study where both the control group and the group exposed to 50 ng/mL TNF-α had a tubule formation score of 4/4. There is some evidence that certain populations of ECFCs are inherently resistant to the negative effects of TNF-α on cell function. This finding was observed in human ECFCs, where those isolated from humans with malignant breast cancer did not have a decreased ability to uptake DiI-Ac-LDL in response to TNF-α exposure as was found with ECFCs isolated from healthy humans or humans with benign breast cancer (Chou et al., 2016). It is possible that exposure to TNF-α may not affect the ability of equine ECFCs to form tubules *in vitro*, which may indicate some degree of resistance to the detrimental effects TNF-α has on ECFC function in the horse. This warrants further study prior to use of ECFCs as a therapy in equine wounds.

5.5 Suggested further investigation

The results from this study demonstrate a detrimental effect of TNF-α exposure on equine ECFC *in vitro* function. However, the results from the pilot study portion were obtained from ECFCs isolated from one horse. Additionally, the cell function assays (DiO-Ac-LDL uptake and *in vitro* tubule formation) were performed on ECFCs isolated from this same horse. Based on the results from the pilot study portion, the use of 50 ng/mL TNF-α with a 6 hr cell contact is an appropriate concentration and duration to use in equine ECFCs. *In vitro* analysis of cell function under various conditions is commonly

performed in cells from 3 subjects. All *in vitro* tests performed thus far (cell adherence, cell migration rate, uptake of DiO-Ac-LDL, and *in vitro* tubule formation on basement membrane matrix medium) should be performed with at least 2 additional horse ECFC cell lines.

The ultimate goal of studying the ECFC in the horse is to determine if this may be an appropriate therapy to use in wounds, particularly distal limb wounds in the horse. As discussed above, there is good reason to believe that TNF-α is present in distal limb wounds in the horse. Prolonged inflammation, which prominently features the macrophage, is a characteristic of the equine distal limb wound. However, there are other aspects of the wound environment which may influence ECFC function. Human keloids and equine EGT from distal limb wounds are similar in disease initiation and propagation (Theoret et al., 2013). Both conditions are considered fibroproliferative disorders that result in excessive fibrosis and delayed wound healing times (Dong et al., 2013; Theoret et al., 2013). In addition to elevated transcription levels of TNF-α, upregulation of interleukin-1 beta (IL-1b) by as much as 15% have been observed in keloid fibroblasts (Dong et al., 2013). The pro-inflammatory cytokine IL-1b, like TNF-α, is present in many different inflammatory conditions across multiple species (Dong et al., 2013; Kamm et al., 2010; Leise et al., 2012; Siemieniuch et al., 2016). In the horse, elevations of IL-1b have been observed in laminar inflammation, endometritis, and osteoarthritis. Equine recombinant IL-1b is readily available (Kingfisher Biotech, St. Paul, MN). The *in vitro* effects of IL-1b should be assessed in 3 horse ECFC cell lines, utilizing the same function tests that were used with exposure to TNF-α.

Although human keloids and equine EGT are similar in many aspects, the presence of myofibroblasts is expected in equine EGT but absent in human keloids (Theoret et al., 2013). In response to TGF-β1, fibroblasts in adult wounds differentiate into myofibroblasts (Wang et al., 2018). Activated fibroblasts and myofibroblasts promote the deposition of extracellular matrix proteins such as collagen I and collagen III (Profyris et al., 2012; Wang et al., 2018). Wounds in humans that heal with excessive scarring typically overexpress proteins that are involved in the activation of TGF-b proteins (Profyris et al., 2012). The cytokine TGF-β1 is secreted by activated macrophages in humans (Profyris et al., 2012), and TGF-β1 expression is persistently elevated in equine limb wounds (Theoret et al., 2001). In a study comparing the TGF-b expression profiles of equine wounds of skin in distal limbs and the thorax, distal limb wounds but not thoracic skin wounds were found to have elevated levels of TGF-β1 expression that persisted over a 14-day period (Theoret et al., 2001). In addition to the pro-fibrotic effects that TGF-β1 may have in equine distal wounds, this cytokine may also affect the ability of ECFCs to assist in wound healing. When exposed to TGF-β1, ECFCs undergo a molecular transition to become mesenchymal cells (Bianchini et al., 2017; Piera-Velazquez and Jimenez, 2012). During this process endothelial specific markers such as vascular endothelial cadherin are lost, and mesenchymal cell products such as alpha-smooth muscle actin and collagen types I and III are produced (Piera-Velazquez and Jimenez, 2012). Understanding the extent that this does or does not happen in equine ECFCs is an important consideration for possible therapeutic use, since a marked endothelial to mesenchymal cell transition of injected ECFCs in the presence of local TGF-β1 may actually promote EGT. Equine recombinant TGF-β1 is

readily available (Kingfisher Biotech, St. Paul, MN). The *in vitro* effects of TGF-β1 should be assessed in 3 horse ECFC cell lines, utilizing the same function tests that were used with exposure to TNF-α. In addition to assessing cell function differences after exposure to TGF-β1, assessing whether an endothelial to mesenchymal cell transition occurs should be performed. If transition to a mesenchymal cell has occurred, then cell expression of alpha smooth muscle actin and vimentin will be demonstrated. This should be evaluated in cells from 3 horse ECFC cell lines after TGF-β1.

At the conclusion of these tests, there will be data describing the *in vitro* activity and function of equine ECFCs from 3 different cell lines after exposure to multiple pro-inflammatory cytokines. Both IL-1b and TNF-α have been found in inflammatory conditions in the horse and in human conditions where wound healing is similar to distal limb wound healing in the horse, so this evaluation is clinically relevant to the potential therapeutic use of equine ECFCs in wound healing. Based on the pro-fibrotic activity of TGF-β1 in wound healing and its association with excessive scarring in humans and EGT in the horse, this evaluation is also clinically relevant to possible therapeutic uses of equine ECFCs.

Understanding how equine ECFCs react to these cytokines is part of the critical understanding of how ECFCs can be used therapeutically as a component of regenerative medicine. These cytokines have either been proven to be in the local wound environment of equine distal limb wounds or they can reasonably be assumed to be present based on research in similar wounds in humans. With the long-term goal of using equine ECFCs therapeutically, another aspect that warrants study involves preventing a decline in cell function once cells encounter exposure to these cytokines.

Human ECFCs experience a decline in proliferation rate and cell function in response to the exposure or high glucose levels, TNF-α, or both (Mena et al., 2018). However when ECFCs were preconditioned with incubation in medium with a pH of 6.6 for 6 hr and then exposed to high glucose and / or TNF-α, no decline in proliferation or function was observed (Mena et al., 2018). Additionally, the endothelial to mesenchymal cell transition in human ECFCs exposed to TGF-β1 *in vitro* was prevented by co-culturing in a triazole-derived Arg-Gly-Asp antagonist (Bianchini et al., 2017). The apoptosis that occurs in ECFCs exposed to TNF-α can be attenuated by treating ECFCs with pituitary adenylate cyclase-activating polypeptide, which is one of the members of the vasoactive intestinal peptide/secretin/growth hormone-releasing hormone/glucagon superfamily (Bian et al., 2017). These studies highlight how the *in vitro* treatment of ECFCs prior to injection into inflammatory environments such as distal limb wounds may be necessary in order to optimize the desired therapeutic effect of these cells in the horse.

Chapter 6: Summary and conclusions

Endothelial colony forming cells (ECFCs) are a subset of the EPC which has been investigated for clinical use to promote healing for wounds characterized by ischemia, infarction, or other vascular compromise. ECFCs can be isolated from peripheral blood and used as autologous cellular therapy. The ease of isolation and possible vascular regenerative capabilities have prompted research in the human field, experimental animal models, and to a limited degree, naturally-occurring veterinary diseases. Exuberant granulation tissue in equine distal limb wounds is commonly encountered by veterinarians, and these and other wounds may benefit from the vascular reparative attributes of ECFC therapy. The research presented here describes the therapeutic use of ECFCs on a distal limb wound model in the horse. We have demonstrated that labeling equine ECFCs with a QD label is effective and allows *ex vivo* tracking of cells injected into a distal limb wound. We have also demonstrated that blood vessel quantity is increased compared to controls in wounds treated with equine ECFCs with or without PEG-Fb encapsulation. Neutrophlic and macrophagic inflammation are decreased compared to controls in wounds treated with equine ECFCs with or without PEG-Fb encapsulation. Distal limb wounds in the horse that develop EGT often have local tissue ischemia, hypoxia, and excessive inflammation, so these results are promising for the therapeutic use of ECFCs in equine distal limb wounds. However, the therapeutic use of ECFCs in equine distal limb wounds has challenges, as local inflammatory cytokines such as TNF-α affect equine ECFC function.

As described above, the therapeutic potential of using equine ECFCs to treat distal limb wounds is intriguing. Prior to undertaking this study in an equine distal limb wound model, we described methods to perform the following: reliably label equine ECFCs to track their location / migration; encapsulate equine ECFCs in a PEG-Fb hydrogel biomaterial to improve their survival during injection; and safeguard cell function during the labeling and encapsulation processes. We have described the first use of equine ECFCs as a therapy in a distal limb wound model. From the present study we identified factors which may be important to consider for future study design. Repeated wound biopsies and wound location on a hind limb worsen granulation tissue in the horse. We also identified that treatment with ECFCs with or without prior encapsulation into PEG-Fb microspheres increased blood vessel density after 1 week and decreased neutrophilic- and macrophagic-associated inflammation after 4 weeks in distal limb wounds. These were considered promising results, as increased blood vessel density and decreased inflammation may both contribute to better wound healing. No significant differences in macroscopic wound healing comparing between treatments were observed, but there was significant inherent variation in wound healing due to the individual horse. Future study design to create more wounds per horse or having more horses in a study may ameliorate this problem.

Accurate identification of cell type is one challenge that exists when using ECFCs as a therapeutic intervention. There is no consensus on what combination of cell surface markers or functional cellular assays constitute an ECFC. Our group has demonstrated that ECFCs may be isolated from peripheral blood samples obtained from the jugular and cephalic veins of horses using whole blood and density centrifugation

methods. These cells manifest in culture flasks from 6 – 14 days after plating, and they express CD14, CD34, CD105, VEGFR-2, and vWF. They are able to uptake low density lipoprotein and form tubules on basement membrane matrix medium *in vitro*. These characteristics are similar to reports of ECFCs in other species including humans. After *in vivo* subcutaneous injection around distal limb wounds in the horse, these cells were found near and within newly formed blood vessels. These attributes suggest that the cells used in these studies were ECFCs. However, the gold standard for identification of the ECFC has not been performed in the horse. This would involve injecting these cells into immunocompromised mice, with subsequent observation of those injected cells forming *de novo*, functional blood vessels which connect to the existing vasculature; this may represent a necessary future study.

The ability to track ECFCs once injected is vital to understand how these cells contribute to wound healing. Although different methods for *in vivo* cell tracking have been investigated in the horse, we have documented a safe and reliable method to track equine ECFCs using fluorescent quantum dot nanocrystals (QD). Labeling equine ECFCs with QD of concentrations up to 20 nM did not negatively affect *in vitro* cell growth or cell function characteristics. By labeling equine ECFCs with QD prior to subcutaneous injection in an equine distal limb wound model, we have also demonstrated that equine ECFCs were detected up to 3 weeks after injection within *ex vivo* biopsy samples. Equine ECFCs labeled with QD were consistently found near and within newly formed blood vessels in our distal limb wound model, even after 3 weeks of wound healing. This suggests that accurate tracking of the cells' *in vivo* movement was achieved using this QD label.

Another important consideration for *in vivo* therapeutic use of ECFCs is cell survival and subsequent retention at the time of injection. Studies have shown that many different types of cells experience significant cell death during the process of injection with a syringe and needle, and cells can migrate away from the site of injection to peripheral blood and other organs in the days to weeks after injection. We have described a method to remedy both of these problems. By encapsulating equine ECFCs in the hydrogel biomaterial PEG-Fb, ECFCs are able to survive the injection without significant cell death. We have proven that equine ECFCs encapsulated in PEG-Fb microspheres demonstrated no decline in cell growth or function characteristics *in vitro*, and cell marker expression was not altered during the encapsulation process. Encapsulating equine ECFCs prior to *in vivo* injection may help cell retention, as injected ECFCs were found after 1 week in all wounds with injections of ECFCs encapsulated in PEG-Fb microspheres; whereas this was not observed for wounds with injections of ECFCs alone. The PEG-Fb microspheres were observed in biopsies up to 1 week after injection which suggests the ECFCs they contained were retained at site of injection for that time period.

Distal limb wounds in the horse are in large part characterized by prolonged, excessive inflammation. Our work with ECFC treatment of distal limb wounds in the horse identified some positive aspects to this novel therapy, namely decreasing inflammation in treated wounds. However, even with the decreased inflammation observed histologically, there were no differences in granulation tissue formation or wound size over time between treatments. Many different cell types have a decline in cell growth, cell function, and even viability in response to inflammatory cytokine

exposure. We initiated a preliminary investigation into the performance of equine ECFCs with exposure to the inflammatory cytokine, TNF-α. We identified a TNF-α concentration and contact time which altered cell function *in vitro* for one equine ECFC cell line. We observed that some but not all functional characteristics were negatively affected by *in vitro* exposure to TNF-α. Additional information is needed for this assessment, including evaluation of additional equine ECFC cell lines as well as evaluation of ECFC function in response to other inflammatory stimuli.

In conclusion, the data presented in this manuscript builds upon the knowledge of equine ECFCs previously reported. Research in this manuscript has added to that collective knowledge by describing in detail: an *in vitro* cell labeling technique; an *in vitro* cell encapsulation method; *in vivo* and *ex vivo* evaluation of equine ECFCs used as therapeutic agents in an equine distal limb wound model; and an *in vitro* evaluation of the influence of TNF-α on equine ECFCs. This manuscript describes novel *in vitro* and *in vivo* analyses of equine ECFCs, which collectively represents a significant advancement in our understanding of these cells. Therapeutic use of ECFCs in equine distal limb wounds is promising, and additional investigation is warranted.

References

Aguado, B.A., Mulyasasmita, W., Su, J., Lampe, K.J., Heilshorn, S.C., 2012. Improving viability of stem cells during syringe needle flow through the design of hydrogel cell carriers. Tissue Eng Part A 18, 806-815.

Ahn, J., Kim, S.G., Kim, M.K., Kim, D.W., Lee, J.H., Seok, H., Choi, J.Y., 2016. Topical delivery of 4-hexylresorcinol promotes wound healing via tumor necrosis factor-alpha suppression. Burns 42, 1534-1541.

Almany, L., Seliktar, D., 2005. Biosynthetic hydrogel scaffolds made from fibrinogen and polyethylene glycol for 3D cell cultures. Biomaterials 26, 2467-2477.

Arici, V., Perotti, C., Fabrizio, C., Del Fante, C., Ragni, F., Alessandrino, F., Viarengo, G., Pagani, M., Moia, A., Tinelli, C., Bozzani, A., 2015. Autologous immuno magnetically selected CD133+ stem cells in the treatment of no-option critical limb ischemia: clinical and contrast enhanced ultrasound assessed results in eight patients. J Transl Med 13, 342.

Asahara, T., Murohara, T., Sullivan, A., Silver, M., van der Zee, R., Li, T., Witzenbichler, B., Schatteman, G., Isner, J.M., 1997. Isolation of putative progenitor endothelial cells for angiogenesis. Science 275, 964-967.

Baldus, S.E., Thiele, J., Charles, A., Hanisch, F.G., Fischer, R., 1994. Carbohydrate antigens of human megakaryocyte and platelet glycoproteins: a comparative study. Histochemistry 102, 205-211.

Bearzi, C., Gargioli, C., Baci, D., Fortunato, O., Shapira-Schweitzer, K., Kossover, O., Latronico, M.V., Seliktar, D., Condorelli, G., Rizzi, R., 2014. PlGF-MMP9-

engineered iPS cells supported on a PEG-fibrinogen hydrogel scaffold possess an enhanced capacity to repair damaged myocardium. Cell Death Dis 5, e1053.

Berkovitch, Y., Seliktar, D., 2017. Semi-synthetic hydrogel composition and stiffness regulate neuronal morphogenesis. Int J Pharm 523, 545-555.

Berner, D., Brehm, W., Gerlach, K., Gittel, C., Offhaus, J., Paebst, F., Scharner, D., Burk, J., 2016. Longitudinal Cell Tracking and Simultaneous Monitoring of Tissue Regeneration after Cell Treatment of Natural Tendon Disease by Low-Field Magnetic Resonance Imaging. Stem Cells Int 2016, 1207190.

Bertone, A.L., 1989. Management of exuberant granulation tissue. Vet Clin North Am Equine Pract 5, 551-562.

Bertone, A.L., Sullins, K.E., Stashak, T.S., Norrdin, R.W., 1985. Effect of wound location and the use of topical collagen gel on exuberant granulation tissue formation and wound healing in the horse and pony. Am J Vet Res 46, 1438-1444.

Bian, N., Du, G., Ip, M.F., Ding, J., Chang, Q., Li, Z., 2017. Pituitary adenylate cyclase-activating polypeptide attenuates tumor necrosis factor-alpha-induced apoptosis in endothelial colony-forming cells. Biomed Rep 7, 11-16.

Bianchini, F., Peppicelli, S., Fabbrizzi, P., Biagioni, A., Mazzanti, B., Menchi, G., Calorini, L., Pupi, A., Trabocchi, A., 2017. Triazole RGD antagonist reverts TGFbeta1-induced endothelial-to-mesenchymal transition in endothelial precursor cells. Mol Cell Biochem 424, 99-110.

Bourzac, C.A., Koenig, J.B., Link, K.A., Nykamp, S.G., Koch, T.G., 2014. Evaluation of ultrasmall superparamagnetic iron oxide contrast agent labeling of equine cord blood and bone marrow mesenchymal stem cells. Am J Vet Res 75, 1010-1017.

Bulte, J.W.M., Daldrup-Link, H.E., 2018. Clinical Tracking of Cell Transfer and Cell Transplantation: Trials and Tribulations. Radiology 289, 604-615.

Burk, J., Berner, D., Brehm, W., Hillmann, A., Horstmeier, C., Josten, C., Paebst, F., Rossi, G., Schubert, S., Ahrberg, A.B., 2016. Long-Term Cell Tracking Following Local Injection of Mesenchymal Stromal Cells in the Equine Model of Induced Tendon Disease. Cell Transplant 25, 2199-2211.

Cahoon, J.M., Rai, R.R., Carroll, L.S., Uehara, H., Zhang, X., O'Neil, C.L., Medina, R.J., Das, S.K., Muddana, S.K., Olson, P.R., Nielson, S., Walker, K., Flood, M.M., Messenger, W.B., Archer, B.J., Barabas, P., Krizaj, D., Gibson, C.C., Li, D.Y., Koh, G.Y., Gao, G., Stitt, A.W., Ambati, B.K., 2015. Intravitreal AAV2.COMP-Ang1 prevents neurovascular degeneration in a murine model of diabetic retinopathy. Diabetes 64, 4247-4259.

Carswell, E.A., Old, L.J., Kassel, R.L., Green, S., Fiore, N., B., W., 1975. An endotoxin-induced serum factor that causes necrosis of tumors. Proc Natl Acad Sci U S A 72, 3666-3670.

Carvalho, A.M., Yamada, A.L., Golim, M.A., Alvarez, L.E., Hussni, C.A., Alves, A.L., 2014. Evaluation of mesenchymal stem cell migration after equine tendonitis therapy. Equine Vet J 46, 635-638.

Case, J., Mead, L.E., Bessler, W.K., Prater, D., White, H.A., Saadatzadeh, M.R., Bhavsar, J.R., Yoder, M.C., Haneline, L.S., Ingram, D.A., 2007. Human CD34+AC133+VEGFR-2+ cells are not endothelial progenitor cells but distinct, primitive hematopoietic progenitors. Exp Hematol 35, 1109-1118.

Celeste, C.J., Deschene, K., Riley, C.B., Theoret, C.L., 2011. Regional differences in wound oxygenation during normal healing in an equine model of cutaneous fibroproliferative disorder. Wound Repair Regen 19, 89-97.

Celeste, C.J., Deschesne, K., Riley, C.B., Theoret, C.L., 2013. Skin temperature during cutaneous wound healing in an equine model of cutaneous fibroproliferative disorder: kinetics and anatomic-site differences. Vet Surg 42, 147-153.

Chatterjee, S., De, A., 2014. Applications of lentiviral vectors in molecular imaging. Front Biosci (Landmark Ed) 19, 835-853.

Chen, G., Zhang, Y., Li, C., Huang, D., Wang, Q., Wang, Q., 2018. Recent Advances in Tracking the Transplanted Stem Cells Using Near-Infrared Fluorescent Nanoprobes: Turning from the First to the Second Near-Infrared Window. Adv Healthc Mater 7, e1800497.

Chen, J., Park, H.C., Addabbo, F., Ni, J., Pelger, E., Li, H., Plotkin, M., Goligorsky, M.S., 2008. Kidney-derived mesenchymal stem cells contribute to vasculogenesis, angiogenesis and endothelial repair. Kidney Int 74, 879-889.

Chen, T.G., Zhong, Z.Y., Sun, G.F., Zhou, Y.X., Zhao, Y., 2011. Effects of tumour necrosis factor-alpha on activity and nitric oxide synthase of endothelial progenitor cells from peripheral blood. Cell Prolif 44, 352-359.

Choi, K., Kennedy, M., Kazarov, A., Papadimitriou, J.C., Keller, G., 1998. A common precursor for hematopoietic and endothelial cells. Development, 725-732.

Chou, C.P., Jiang, S.S., Pan, H.B., Yen, Y.C., Tseng, H.H., Hung, Y.T., Wang, S.H., Chen, Y.L., Chen, Y.W., 2016. Endothelial cell colony forming units derived from

malignant breast diseases are resistant to tumor necrosis factor-alpha-induced apoptosis. Sci Rep 6, 37450.

Cohen, N., Toister, E., Lati, Y., Girshengorn, M., Levin, L., Silberstein, L., Seliktar, D., Epstein, E., 2018. Cell encapsulation utilizing PEG-fibrinogen hydrogel supports viability and enhances productivity under stress conditions. Cytotechnology 70, 1075-1083.

Cui, F., Ji, J., Sun, J., Wang, J., Wang, H., Zhang, Y., Ding, H., Lu, Y., Xu, D., Sun, X., 2019. A novel magnetic fluorescent biosensor based on graphene quantum dots for rapid, efficient, and sensitive separation and detection of circulating tumor cells. Anal Bioanal Chem 411, 985-995.

D'Avola, D., Fernandez-Ruiz, V., Carmona-Torre, F., Mendez, M., Perez-Calvo, J., Prosper, F., Andreu, E., Herrero, J.I., Inarrairaegui, M., Fuertes, C., Bilbao, J.I., Sangro, B., Prieto, J., Quiroga, J., 2017. Phase 1-2 pilot clinical trial in patients with decompensated liver cirrhosis treated with bone marrow-derived endothelial progenitor cells. Transl Res 188, 80-91 e82.

de la Rebiere de Pouyade, G., Riggs, L.M., Moore, J.N., Franck, T., Deby-Dupont, G., Hurley, D.J., Serteyn, D., 2010. Equine neutrophil elastase in plasma, laminar tissue, and skin of horses administered black walnut heartwood extract. Vet Immunol Immunopathol 135, 181-187.

Dejana, E., Lampugnani, M.G., Giorgi, M., Gaboli, M., Federici, A.B., Ruggeri, Z.M., Marchisio, P.C., 1989. Von Willebrand factor promotes endothelial cell adhesion via an Arg-Gly-Asp-dependent mechanism. J Cell Biol 109, 367-375.

Deschene, K., Celeste, C., Boerboom, D., Theoret, C.L., 2011. Constitutive expression of hypoxia-inducible factor-1 alpha in keratinocytes during the repair of skin wounds in horses. Wound Repair Regen 19, 250-259.

Deschene, K., Celeste, C., Boerboom, D., Theoret, C.L., 2012. Hypoxia regulates the expression of extracellular matrix associated proteins in equine dermal fibroblasts via HIF1. J Dermatol Sci 65, 12-18.

Dipietro, L.A., 1995. Wound healing: the role of the macrophage and other immune cells. Shock 4, 233-240.

Dong, X., Mao, S., Wen, H., 2013. Upregulation of proinflammatory genes in skin lesions may be the cause of keloid formation (Review). Biomed Rep 1, 833-836.

Donofrio, G., Capocefalo, A., Franceschi, V., Morini, G., Bue, M.D., Conti, V., Cavirani, S., Grolli, S., 2010. Virally and physically transgenized equine adipose-derived stromal cells as a cargo for paracrine secreted factors. BMC Cell Biology 11, 73.

Dubois, C., Liu, X., Claus, P., Marsboom, G., Pokreisz, P., Vandenwijngaert, S., Depelteau, H., Streb, W., Chaothawee, L., Maes, F., Gheysens, O., Debyser, Z., Gillijns, H., Pellens, M., Vandendriessche, T., Chuah, M., Collen, D., Verbeken, E., Belmans, A., Van de Werf, F., Bogaert, J., Janssens, S., 2010. Differential effects of progenitor cell populations on left ventricular remodeling and myocardial neovascularization after myocardial infarction. J Am Coll Cardiol 55, 2232-2243.

Dubsky, M., Jirkovska, A., Bem, R., Fejfarova, V., Pagacova, L., Sixta, B., Varga, M., Langkramer, S., Sykova, E., Jude, E.B., 2013. Both autologous bone marrow mononuclear cell and peripheral blood progenitor cell therapies similarly improve

ischaemia in patients with diabetic foot in comparison with control treatment. Diabetes Metab Res Rev 29, 369-376.

Dubuc, V., Lepault , E., Theoret, C.L., 2006. Endothelial cell hypertrophy is associated with microvascular occlusion in horse wounds. Can J Vet Res 70, 206-210.

Ducharme-Desjarlais, M., Celeste, C.J., Lepault, E., Theoret, C.L., 2005. Effects of a silicone-containing dressing on exuberant granulation tissue formation and wound repair in horses. Am J Vet Res 66, 1133-1139.

Edwards, M.J., Heniford, B.T., Miller, F.N., 1993. Tumor necrosis factor mediates disseminated intravascular inflammation (DII) in the genesis of of multiorgan edema. J Surg Res 54, 140-144.

Estrada, R.J., van Weeren, P.R., van de Lest, C.H., Boere, J., Reyes, M., Ionita, J.C., Estrada, M., Lischer, C.J., 2014. Comparison of healing in forelimb and hindlimb surgically induced core lesions of the equine superficial digital flexor tendon. Vet Comp Orthop Traumatol 27, 358-365.

Falomo, M.E., Ferroni, L., Tocco, I., Gardin, C., Zavan, B., 2015. Immunomodulatory Role of Adipose-Derived Stem Cells on Equine Endometriosis. Biomed Res Int 2015, 141485.

Fiehn, A.M., Kristensson, M., Engel, U., Munck, L.K., Holck, S., Engel, P.J., 2016. Automated image analysis in the study of collagenous colitis. Clin Exp Gastroenterol 9, 89-95.

Fortier, L.A., Potter, H.G., Rickey, E.J., Schnabel, L.V., Foo, L.F., Chong, L.R., Stokol, T., Cheetham, J., Nixon, A.J., 2010. Concentrated bone marrow aspirate

improves full-thickness cartilage repair compared with microfracture in the equine model. J Bone Joint Surg Am 92, 1927-1937.

Freyman, T., Polin, G., Osman, H., Crary, J., Lu, M., Cheng, L., Palasis, M., Wilensky, R.L., 2006. A quantitative, randomized study evaluating three methods of mesenchymal stem cell delivery following myocardial infarction. Eur Heart J 27, 1114-1122.

Fuoco, C., Salvatori, M.L., Biondo, A., Shapira-Schweitzer, K., Santoleri, S., Antonini, S., Bernardini, S., Tedesco, F.S., Cannata, S., Seliktar, D., Cossu, G., Gargioli, C., 2012. Injectable polyethylene glycol-fibrinogen hydrogel adjuvant improves survival and differentiation of transplanted mesoangioblasts in acute and chronic muscle degeneration. Skelet Muscle, 24.

Fuxa, M., Busslinger, M., 2007. Reporter gene insertions reveal a strictly B lymphoid-specific expression pattern of Pax5 in support of its B cell identity function. The Journal of Immunology 178, 8221-8221.

Garbuzova-Davis, S., Haller, E., Lin, R., Borlongan, C.V., 2017. Intravenously Transplanted Human Bone Marrow Endothelial Progenitor Cells Engraft Within Brain Capillaries, Preserve Mitochondrial Morphology, and Display Pinocytotic Activity Toward Blood-Brain Barrier Repair in Ischemic Stroke Rats. Stem Cells 35, 1246-1258.

Gobin, A.S., West, J.L., 2002. Cell migration through defined, synthetic extracellular matrix analogues. FASEB J 16, 751-753.

Godwin, E.E., Young, N.J., Dudhia, J., Beamish, I.C., Smith, R.K., 2012. Implantation of bone marrow-derived mesenchymal stem cells demonstrates improved outcome

in horses with overstrain injury of the superficial digital flexor tendon. Equine Vet J 44, 25-32.

Green, D.M., Noble, P.C., Bocell Jr, J.R., Ahuero, J.S., Poteet, B.A., Birdsall, H.H., 2006. Effect of early full weight-bearing after joint injury on inflammation and cartilage degradation. J Bone Joint Surg Am 88, 2201-2209.

Greenberger, S., Bischoff, J., 2013. Pathogenesis of infantile haemangioma. Br J Dermatol 169, 12-19.

Guest, D.J., Smith, M.R., Allen, W.R., 2010. Equine embryonic stem-like cells and mesenchymal stromal cells have different survival rates and migration patterns following their injection into damaged superficial digital flexor tendon. Equine Vet J 42, 636-642.

Guo, S., Dipietro, L.A., 2010. Factors affecting wound healing. J Dent Res 89, 219-229.

Hackett, C.H., Flaminio, M.J.B.F., Fortier, L.A., 2011. Analysis of CD14 expression levels in putative mesenchymal progenitor cells isolated from equine bone marrow. Stem Cell Dev 20, 721-735.

Hardman, R., 2006. A toxicologic review of quantum dots: toxicity depends on physiochemical and environmental factors. Environ Health Perspect 114, 165 - 172.

He, M., Gan, A.W., Lim, A.Y., Goh, J.C., Hui, J.H., Chong, A.K., 2015. Bone Marrow Derived Mesenchymal Stem Cell Augmentation of Rabbit Flexor Tendon Healing. Hand Surg 20, 421-429.

Hendrickx, B., Verdonck, K., Van den Berge, S., Dickens, S., Eriksson, E., Vranckx, J.J., Luttun, A., 2010. Integration of blood outgrowth endothelial cells in dermal

fibroblast sheets promotes full thickness wound healing. Stem Cells 28, 1165-1177.

Herrick, S., Blanc-Brude, O., Gray, A., Laurent, G., 1999. Fibrinogen. Int J Biochem Cell Biol 31, 741-746.

Herteman, N., Bullone, M., Lavoie, J.P., 2016. Endoscopic Evaluation of Angiogenesis in the Large Airways of Horses with Heaves Using Narrow Band Imaging. J Vet Intern Med 30, 671-674.

Hong, Y., Eleftheriou, D., Klein, N.J., Brogan, P.A., 2015. Impaired function of endothelial progenitor cells in children with primary systemic vasculitis. Arthritis Res Ther 17, 292.

Huang, X.T., Zhang, Y.Q., Li, S.J., Li, S.H., Tang, Q., Wang, Z.T., Dong, J.F., Zhang, J.N., 2013. Intracerebroventricular transplantation of ex vivo expanded endothelial colony-forming cells restores blood-brain barrier integrity and promotes angiogenesis of mice with traumatic brain injury. J Neurotrauma 30, 2080-2088.

Hubbell, J.A., 2003. Materials as morphogenetic guides in tissue engineering. Current Opinion in Biotechnology 14, 551-558.

Hur, J., Yoon, C.H., Kim, H.S., Choi, J.H., Kang, H.J., Hwang, K.K., Oh, B.H., Lee, M.M., Park, Y.B., 2004. Characterization of two types of endothelial progenitor cells and their different contributions to neovasculogenesis. Arterioscler Thromb Vasc Biol 24, 288-293.

Iacono, E., Merlo, B., Pirrone, A., Antonelli, C., Brunori, L., Romagnoli, N., Castagnetti, C., 2012. Effects of mesenchymal stem cells isolated from amniotic fluid and

platelet-rich plasma gel on severe decubitus ulcers in a septic neonatal foal. Res Vet Sci 93, 1439-1440.

Ishihara, A., Zachos, T.A., Bartlett, J.S., Bertone, A.L., 2006. Evaluation of permissiveness and cytotoxic effects in equine chondrocytes, synovial cells, and stem cells in response to infection with adenovirus 5 vectors for gene delivery. Am J Vet Res 67, 1145-1155.

Jameson, J., Havran, W.L., 2007. Skin gamma delta T-cell functions in homeostasis and wound healing. Immunol Rev 215, 114-122.

Jorgensen, E., Bay, L., Bjarnsholt, T., Bundgaard, L., Sorensen, M.A., Jacobsen, S., 2017. The occurrence of biofilm in an equine experimental wound model of healing by secondary intention. Vet Microbiol 204, 90-95.

Kamm, J.L., Nixon, A.J., Witte, T.H., 2010. Cytokine and catabolic enzyme expression in synovium, synovial fluid and articular cartilage of naturally osteoarthritic equine carpi. Equine Vet J 42, 693-699.

Kawamoto, A., Katayama, M., Handa, N., Kinoshita, M., Takano, H., Horii, M., Sadamoto, K., Yokoyama, A., Yamanaka, T., Onodera, R., Kuroda, A., Morioka, S., Fukushima, M., Asahara, T., 2009. Intramuscular transplantation of G-CSF-mobilized CD34(+) cells in patients with critical limb ischemia: a phase I/IIa, multicenter, single-blinded, dose-escalation clinical trial. Stem Cells 27, 2857-2864.

Keighron, C., Lyons, C.J., Creane, M., O'Brien, T., Liew, A., 2018. Recent Advances in Endothelial Progenitor Cells Toward Their Use in Clinical Translation. Front Med (Lausanne) 5, 354.

Kim, S.W., Jin, H.L., Kang, S.M., Kim, S., Yoo, K.J., Jang, Y., Kim, H.O., Yoon, Y.S., 2016. Therapeutic effects of late outgrowth endothelial progenitor cells or mesenchymal stem cells derived from human umbilical cord blood on infarct repair. Int J Cardiol 203, 498-507.

Kinoshita, M., Fujita, Y., Katayama, M., Baba, R., Shibakawa, M., Yoshikawa, K., Katakami, N., Furukawa, Y., Tsukie, T., Nagano, T., Kurimoto, Y., Yamasaki, K., Handa, N., Okada, Y., Kuronaka, K., Nagata, Y., Matsubara, Y., Fukushima, M., Asahara, T., Kawamoto, A., 2012. Long-term clinical outcome after intramuscular transplantation of granulocyte colony stimulating factor-mobilized CD34 positive cells in patients with critical limb ischemia. Atherosclerosis 224, 440-445.

Kohler, C., 2007. Allograft inflammatory factor-1/Ionized calcium-binding adapter molecule 1 is specifically expressed by most subpopulations of macrophages and spermatids in testis. Cell Tissue Res 330, 291-302.

Kostura, L., Kraitchman, D.L., Mackay, A.M., Pittenger, M.F., Bulte, J.W., 2004. Feridex labeling of mesenchymal stem cells inhibits chondrogenesis but not adipogenesis or osteogenesis. NMR Biomed 17, 513-517.

Kovacic, J.C., Moore, J., Herbert, A., Ma, D., Boehm, M., Graham, R.M., 2008. Endothelial progenitor cells, angioblasts, and angiogenesis--old terms reconsidered from a current perspective. Trends Cardiovasc Med 18, 45-51.

Laflamme, M.A., Chen, K.Y., Naumova, A.V., Muskheli, V., Fugate, J.A., Dupras, S.K., Reinecke, H., Xu, C., Hassanipour, M., Police, S., O'Sullivan, C., Collins, L., Chen, Y., Minami, E., Gill, E.A., Ueno, S., Yuan, C., Gold, J., Murry, C.E., 2007.

Cardiomyocytes derived from human embryonic stem cells in pro-survival factors enhance function of infarcted rat hearts. Nat Biotechnol 25, 1015-1024.

Lee, O., Kim, J., Park, G., Kim, M., Son, S., Ha, S., 2015. Non-invasive assessment of cutaneous wound healing using fluorescent imaging. Skin Res Technol 21, 108 - 113.

Lee, S.H., Lee, J.H., Asahara, T., Kim, Y.S., Jeong, H.C., Ahn, Y., Jung, J.S., Kwon, S.M., 2014. Genistein promotes endothelial colony-forming cell (ECFC) bioactivities and cardiac regeneration in myocardial infarction. PLoS One 9, e96155.

Lee, S.Y., Kwon, B., Lee, K., Son, Y.H., Chung, S.G., 2017. Therapeutic Mechanisms of Human Adipose-Derived Mesenchymal Stem Cells in a Rat Tendon Injury Model. Am J Sports Med 45, 1429-1439.

Leise, B.S., Faleiros, R.R., Watts, M., Johnson, P.J., Black, S.J., Belknap, J.K., 2012. Hindlimb laminar inflammatory response is similar to that present in forelimbs after carbohydrate overload in horses. Equine Vet J 44, 633-639.

Lepault, E., Celeste, C., Dore, M., Martineau, D., Theoret, C.L., 2005. Comparative study on microvascular occlusion and apoptosis in body and limb wounds in the horse. Wound Repair Regen 13, 520-529.

Li, J., Lee, W.Y., Wu, T., Xu, J., Zhang, K., Li, G., Xia, J., Bian, L., 2016. Multifunctional Quantum Dot Nanoparticles for Effective Differentiation and Long-Term Tracking of Human Mesenchymal Stem Cells In Vitro and In Vivo. Adv Healthc Mater 5, 1049-1057.

Lin, S., Xie, X., Patel, M.R., Yang, Y.H., Li, Z., Cao, F., Gheysens, O., Zhang, Y., Gambhir, S.S., Rao, J.H., Wu, J.C., 2007. Quantum dot imaging for embryonic stem cells. BMC Biotechnol 7, 67.

Loftus, J.P., Black, S.J., Pettigrew, A., Abrahamsen, E.J., Belknap, J.K., 2007. Early laminar events involving endothelial activation in horses with black walnut-induced laminitis. Am J Vet Res 68, 1205-1211.

Lopez, M.J., Jarazo, J., 2015. State of the art: stem cells in equine regenerative medicine. Equine Vet J 47, 145-154.

Lu, Q., Pandya, M., Rufaihah, A.J., Rosa, V., Tong, H.J., Seliktar, D., Toh, W.S., 2015. Modulation of Dental Pulp Stem Cell Odontogenesis in a Tunable PEG-Fibrinogen Hydrogel System. Stem Cells Int 2015, 525367.

Lutolf, M.P., Hubbell, J.A., 2003. Synthesis and physiochemical characterization of end-linked poly(ethylene glycol)-co-peptide hydrogels formed by michael-type addition. Biomacromolecules 4, 713-722.

Lutolf, M.P., Hubbell, J.A., 2005. Synthetic biomaterials as instructive extracellular microenvironments for morphogenesis in tissue engineering. Nat Biotechnol 23, 47-55.

Maher, M., Kuebelbeck, L., 2018. Nonhealing Wounds of the Equine Limb. Vet Clin North Am Equine Pract 34, 539-555.

Mannucci, S., Calderan, L., Quaranta, P., Antonini, S., Mosca, F., Longoni, B., Marzola, P., Boschi, F., 2017. Quantum dots labelling allows detection of the homing of mesenchymal stem cells administered as immunomodulatory therapy in an experimental model of pancreatic islets transplantation. J Anat 230, 381-388.

Mata, M., Milian, L., Oliver, M., Zurriaga, J., Sancho-Tello, M., de Llano, J.J.M., Carda, C., 2017. In Vivo Articular Cartilage Regeneration Using Human Dental Pulp Stem Cells Cultured in an Alginate Scaffold: A Preliminary Study. Stem Cells Int 2017, 8309256.

Matea, C.T., Mocan, T., Tabaran, F., Pop, T., Mosteanu, O., Puia, C., Iancu, C., Mocan, L., 2017. Quantum dots in imaging, drug delivery and sensor applications. Int J Nanomedicine 12, 5421-5431.

McDuffee, L.A., Pack, L., Lores, M., Wright, G.M., Esparza-Gonzalez, B., Masaoud, E., 2012. Osteoprogenitor cell therapy in an equine fracture model. Vet Surg 41, 773-783.

Medina, R.J., Barber, C.L., Sabatier, F., Dignat-George, F., Melero-Martin, J.M., Khosrotehrani, K., Ohneda, O., Randi, A.M., Chan, J.K.Y., Yamaguchi, T., Van Hinsbergh, V.W.M., Yoder, M.C., Stitt, A.W., 2017. Endothelial Progenitors: A Consensus Statement on Nomenclature. Stem Cells Transl Med 6, 1316-1320.

Medina, R.J., O'Neil, C.L., Sweeney, M., Guduric-Fuchs, J., Gardiner, T.A., Simpson, D.A., Stitt, A.W., 2010. Molecular analysis of endothelial progenitor cell (EPC) subtypes reveal two distinct cell populations with different identities. BMC Med Genomics 3, 18.

Melero-Martin, J.M., De Obaldia, M.E., Kang, S.Y., Khan, Z.A., Yuan, L., Oettgen, P., Bischoff, J., 2008. Engineering robust and functional vascular networks in vivo with human adult and cord blood-derived progenitor cells. Circ Res 103, 194-202.

Mena, H.A., Zubiry, P.R., Dizier, B., Schattner, M., Boisson-Vidal, C., Negrotto, S., 2018. Acidic preconditioning of endothelial colony-forming cells (ECFC) promote

vasculogenesis under proinflammatory and high glucose conditions in vitro and in vivo. Stem Cell Res Ther 9, 120.

Michler, R.E., 2018. The current status of stem cell therapy in ischemic heart disease. J Card Surg 33, 520-531.

Minami, Y., Nakajima, T., Ikutomi, M., Morita, T., Komuro, I., Sata, M., Sahara, M., 2015. Angiogenic potential of early and late outgrowth endothelial progenitor cells is dependent on the time of emergence. Int J Cardiol 186, 305-314.

Molnar, M., Friberg, P., Fu, Y., Brisslert, M., Adams, M., Chen, Y., 2010. Effects of Quantum Dot Labeling on Endothelial Progenitor Cell Function and Viability. Cell Med 1, 105-112.

Moonen, J.R.A.J., de Leeuw, K., van Seijen, X.J.G.Y., Kallenberg, C.G.M., van Luyn, M.J.A., Bijl, M., Harmsen, M.C., 2007. Reduced number and impaired function of circulating progenitor cells in patients with systemic lupus erythematosus. Arthritis Res Ther 9, R84.

Mukai, N., Akahori, T., Komaki, M., Li, Q., Kanayasu-Toyoda, T., Ishii-Watabe, A., Kobayashi, A., Yamaguchi, T., Abe, M., Amagasa, T., Morita, I., 2008. A comparison of the tube forming potentials of early and late endothelial progenitor cells. Exp Cell Res 314, 430-440.

Munoz Caro, T., Hermosilla, C., Silva, L.M., Cortes, H., Taubert, A., 2014. Neutrophil extracellular traps as innate immune reaction against the emerging apicomplexan parasite Besnoitia besnoiti. PLoS One 9, e91415.

Murphy, K., Weaver, C., 2017. Antigen recognition by B-cell and T-cell receptors. Garland Science, New York.

Mutirangura, P., Ruangsetakit, C., Wongwanit, C., Chinsakchai, K., Porat, Y., Belleli, A., Czeiger, D., 2009. Enhancing limb salvage by non-mobilized peripheral blood angiogenic cell precursors therapy in patients with critical limb ischemia. J Med Assoc Thai 92, 320-327.

NAHMS, 2014. Needs Assessment Survey Results for the Upcoming NAHMS Equine 2015 Study. NAHMS.

Newman, P.J., 1994. The role of PECAM-1 in vascular cell biology. Ann N Y Acad Sci 714, 165-174.

Norgren, L., Hiatt, W.R., Dormandy, J.A., Nehler, M.R., Harris, K.A., Fowkes, F.G., Group, T.I.W., 2007. Inter-Society Consensus for the Management of Peripheral Arterial Disease (TASC II). J Vasc Surg 45 Suppl S, S5-67.

O'Neill, C.L., McLoughlin, K.J., Chambers, S.E.J., Guduric-Fuchs, J., Stitt, A.W., Medina, R.J., 2018. The Vasoreparative Potential of Endothelial Colony Forming Cells: A Journey Through Pre-clinical Studies. Front Med (Lausanne) 5, 273.

O'Toole, E.A., 2001. Extracellular matrix and keratinocyte migration. Clin Exp Dermatol 26, 525-530.

Ortved, K.F., Nixon, A.J., 2016. Cell-based cartilage repair strategies in the horse. Vet J 208, 1-12.

Patel, J., Donovan, P., Khosrotehrani, K., 2016. Concise Review: Functional Definition of Endothelial Progenitor Cells: A Molecular Perspective. Stem Cells Transl Med 5, 1302-1306.

Patschan, D., Kribben, A., Muller, G.A., 2016. Postischemic microvasculopathy and endothelial progenitor cell-based therapy in ischemic AKI: update and perspectives. Am J Physiol Renal Physiol 311, F382-394.

Peled, E., Boss, J., Bejar, J., Zinman, C., Seliktar, D., 2007. A novel poly(ethylene glycol)-fibrinogen hydrogel for tibial segmental defect repair in a rat model. J Biomed Mater Res A 80, 874-884.

Pelley, J.L., Daar, A.S., Saner, M.A., 2009. State of academic knowledge on toxicity and biological fate of quantum dots. Toxicol Sci 112, 276-296.

Pelosi, E., Castelli, G., Testa, U., 2014. Endothelial progenitors. Blood Cells Mol Dis 52, 186-194.

Perkins, N.R., Reid, S.W., Morris, R.S., 2005. Profiling the New Zealand Thoroughbred racing industry. 2. Conditions interfering with training and racing. N Z Vet J 53, 69-76.

Petersen, G.F., Hilbert, B., Trope, G., Kalle, W., Strappe, P., 2014. Efficient transduction of equine adipose-derived mesenchymal stem cells by VSV-G pseudotyped lentiviral vectors. Res Vet Sci 97, 616-622.

Peterson GF, H.B., Trope G, Kalle W, Strappe P, 2014. Efficient transduction of equine adipose-derived mesenchymal stem cells by VSV-G pseudotyped lentiviral vectors. Res Vet Sci 97, 616 - 622.

Pi, Q.M., Zhang, W.J., Zhou, G.D., Liu, W., Cao, Y., 2010. Degradation or excretion of quantum dots in mouse embryonic stem cells. BMC Biotechnol 10, 36.

Pias-Peleteiro, J., Campos, F., Perez-Mato, M., Lopez-Arias, E., Rodriguez-Yanez, M., Castillo, J., Sobrino, T., 2017. Endothelial progenitor cells as a therapeutic approach for intracerebral hemorrhage. Current Pharmaceutical Design 23, 1-14.

Piera-Velazquez, S., Jimenez, S.A., 2012. Molecular mechanisms of endothelial to mesenchymal cell transition (EndoMT) in experimentally induced fibrotic diseases. Fibrogenesis Tissue Repair 5, S7.

Portou, M.J., Baker, D., Abraham, D., Tsui, J., 2015. The innate immune system, toll-like receptors and dermal wound healing: A review. Vascul Pharmacol 71, 31-36.

Pradhan, S., Clary, J.M., Seliktar, D., Lipke, E.A., 2017. A three-dimensional spheroidal cancer model based on PEG-fibrinogen hydrogel microspheres. Biomaterials 115, 141-154.

Profyris, C., Tziotzios, C., Do Vale, I., 2012. Cutaneous scarring: Pathophysiology, molecular mechanisms, and scar reduction therapeutics Part I. The molecular basis of scar formation. J Am Acad Dermatol 66, 1-10; quiz 11-12.

Prokopi, M., Pula, G., Mayr, U., Devue, C., Gallagher, J., Xiao, Q., Boulanger, C.M., Westwood, N., Urbich, C., Willeit, J., Steiner, M., Breuss, J., Xu, Q., Kiechl, S., Mayr, M., 2009. Proteomic analysis reveals presence of platelet microparticles in endothelial progenitor cell cultures. Blood 114, 723-732.

Qadura, M., Terenzi, D.C., Verma, S., Al-Omran, M., Hess, D.A., 2018. Concise Review: Cell Therapy for Critical Limb Ischemia: An Integrated Review of Preclinical and Clinical Studies. Stem Cells 36, 161-171.

Rafii, S., Lyden, D., 2003. Therapeutic stem and progenitor cell transplantation for organ vascularization and regeneration. Nat Med 9, 702-712.

Richardson, M.R., Yoder, M.C., 2011. Endothelial progenitor cells: quo vadis? J Mol Cell Cardiol 50, 266-272.

Robey, T.E., Saiget, M.K., Reinecke, H., Murry, C.E., 2008. Systems approaches to preventing transplanted cell death in cardiac repair. J Mol Cell Cardiol 45, 567-581.

Romero, A., Barrachina, L., Ranera, B., Remacha, A.R., Moreno, B., de Blas, I., Sanz, A., Vazquez, F.J., Vitoria, A., Junquera, C., Zaragoza, P., Rodellar, C., 2017. Comparison of autologous bone marrow and adipose tissue derived mesenchymal stem cells, and platelet rich plasma, for treating surgically induced lesions of the equine superficial digital flexor tendon. Vet J 224, 76-84.

Rosen, A.B., Kelly, D.J., Schuldt, A.J., Lu, J., Potapova, I.A., Doronin, S.V., Robichaud, K.J., Robinson, R.B., Rosen, M.R., Brink, P.R., Gaudette, G.R., Cohen, I.S., 2007. Finding fluorescent needles in the cardiac haystack: tracking human mesenchymal stem cells labeled with quantum dots for quantitative in vivo three-dimensional fluorescence analysis. Stem Cells 25, 2128-2138.

Roxanis, I., Colling, R., Kartsonaki, C., Green, A.R., Rakha, E.A., 2018. The significance of tumour microarchitectural features in breast cancer prognosis: a digital image analysis. Breast Cancer Res 20, 11.

Rufaihah, A.J., Johari, N.A., Vaibavi, S.R., Plotkin, M., Di Thien, D.T., Kofidis, T., Seliktar, D., 2017. Dual delivery of VEGF and ANG-1 in ischemic hearts using an injectable hydrogel. Acta Biomater 48, 58-67.

Salter, M.M., Seeto, W.J., DeWitt, B.B., Hashimi, S.A., Schwartz, D.D., Lipke, E.A., Wooldridge, A.A., 2015. Characterization of endothelial colony-forming cells from peripheral blood samples of adult horses. Am J Vet Res 76, 174-187.

Sandker, M.J., Duque, L.F., Redout, E.M., Chan, A., Que, I., Lowik, C., Klijnstra, E.C., Kops, N., Steendam, R., van Weeren, R., Hennink, W.E., Weinans, H., 2017. Degradation, intra-articular retention and biocompatibility of monospheres composed of [PDLLA-PEG-PDLLA]-b-PLLA multi-block copolymers. Acta Biomater 48, 401-414.

Santos, V.H.D., Pfeifer, J.P.H., Souza, J.B., Stievani, F.C., Hussni, C.A., Golim, M.A., Deffune, E., Alves, A.L.G., 2019. Evaluation of alginate hydrogel encapsulated mesenchymal stem cell migration in horses. Res Vet Sci 124, 38-45.

Sato, T.N., Tozawa, Y., Deutsch, U., Wolburg-Buchholz, K., Fujiwara, Y., Gendron-Maguire, M., Gridley, T., Wolburg, H., Risau, W., Qin, Y., 1995. Distinct roles of the receptor tyrosine kinases Tie-1 and Tie-2 in blood vessel formation. Nature 376, 70-74.

Scharf, A., Holmes, S., Thoresen, M., Mumaw, J., Stumpf, A., Peroni, J., 2015. Superparamagnetic iron oxide nanoparticles as a means to track mesenchymal stem cells in a large animal model of tendon injury. Contrast Media Mol Imaging 10, 388-397.

Schmeisser, A., Garlichs, C.D., Zhang, H., Eskafi, S., Graffy, C., Ludwig, J., Strasser, R.H., Daniel, W.G., 2001. Monocytes coexpress endothelial and macrophagocytic lineage markers and form cord-like structures in matrigel under angiogenic conditions. Cardiovasc Res 49, 671-680.

Schmeisser, A., Graffy, C., Daniel, W.G., Strasser, R.H., 2003. Phenotypic overlap between monocytes and vascular endothelial cells. Adv Exp Med Biol 522, 59-74.

Seeto, W.J., Tian, Y., Winter, R.L., Caldwell, F.J., Wooldridge, A.A., Lipke, E.A., 2017. Encapsulation of Equine Endothelial Colony Forming Cells in Highly Uniform, Injectable Hydrogel Microspheres for Local Cell Delivery. Tissue Eng Part C Methods 23, 815-825.

Seliktar, D., 2012. Designing cell-compatible hydrogels for biomedical applications. Science 336, 1124-1128.

Seo, S.G., Yeo, J.H., Kim, J.H., Kim, J.B., Cho, T.J., Lee, D.Y., 2013. Negative-pressure wound therapy induces endothelial progenitor cell mobilization in diabetic patients with foot infection or skin defects. Exp Mol Med 45, e62.

Sharpe, A.N., Seeto, W.J., Winter, R.L., Zhong, Q., Lipke, E.A., Wooldridge, A.A., 2016. Isolation of endothelial colony-forming cells from blood samples collected from the jugular and cephalic veins of healthy adult horses. Am J Vet Res 77, 1157-1165.

Sideras, K., Galjart, B., Vasaturo, A., Pedroza-Gonzalez, A., Biermann, K., Mancham, S., Nigg, A.L., Hansen, B.E., Stoop, H.A., Zhou, G., Verhoef, C., Sleijfer, S., Sprengers, D., Kwekkeboom, J., Bruno, M.J., 2018. Prognostic value of intra-tumoral CD8(+) /FoxP3(+) lymphocyte ratio in patients with resected colorectal cancer liver metastasis. J Surg Oncol.

Siemieniuch, M.J., Szostek, A.Z., Gajos, K., Kozdrowski, R., Nowak, M., Okuda, K., 2016. Type of Inflammation Differentially Affects Expression of Interleukin 1beta

and 6, Tumor Necrosis Factor-alpha and Toll-Like Receptors in Subclinical Endometritis in Mares. PLoS One 11, e0154934.

Sieveking, D.P., Buckle, A., Celermajer, D.S., Ng, M.K., 2008. Strikingly different angiogenic properties of endothelial progenitor cell subpopulations: insights from a novel human angiogenesis assay. J Am Coll Cardiol 51, 660-668.

Slotkin, J.R., Chakrabarti, L., Dai, H.N., Carney, R.S., Hirata, T., Bregman, B.S., Gallicano, G.I., Corbin, J.G., Haydar, T.F., 2007. In vivo quantum dot labeling of mammalian stem and progenitor cells. Dev Dyn 236, 3393-3401.

Smith, R.K., Werling, N.J., Dakin, S.G., Alam, R., Goodship, A.E., Dudhia, J., 2013. Beneficial effects of autologous bone marrow-derived mesenchymal stem cells in naturally occurring tendinopathy. PLoS One 8, e75697.

Sorice, S., Rustad, K.C., Li, A.Y., Gurtner, G.C., 2016. The Role of Stem Cell Therapeutics in Wound Healing: Current Understanding and Future Directions. Plast Reconstr Surg 138, 31S-41S.

Stalhammar, G., Fuentes Martinez, N., Lippert, M., Tobin, N.P., Molholm, I., Kis, L., Rosin, G., Rantalainen, M., Pedersen, L., Bergh, J., Grunkin, M., Hartman, J., 2016. Digital image analysis outperforms manual biomarker assessment in breast cancer. Mod Pathol 29, 318-329.

Sugaya, H., Mishima, H., Gao, R., Kaul, S.C., Wadhwa, R., Aoto, K., Li, M., Yoshioka, T., Ogawa, T., Ochiai, N., Yamazaki, M., 2016. Fate of bone marrow mesenchymal stromal cells following autologous transplantation in a rabbit model of osteonecrosis. Cytotherapy 18, 198-204.

Telen, M.J., 2014. Cellular adhesion and the endothelium: E-selectin, L-selectin, and pan-selectin inhibitors. Hematol Oncol Clin North Am 28, 341-354.

Temenoff, J.S., Athanasiou, K.A., LeBaron, R.G., Mikos, A.G., 2002. Effect of poly(ethylene glycol) molecular weight on tensile and swelling properties of oligo(poly(ethylene glycol) fumarate) hydrogels for cartilage tissue engineering. J Biomed Mater Res 59, 429-437.

Theoret, C.L., Barber, S.M., Gordon, J.R., 2002. Temporal localization of immunoreactive transforming growth factor [beta]1 in normal equine skin and in full-thickness dermal wounds. Veterinary Surgery 31, 274-280.

Theoret, C.L., Barber, S.M., Moyana, T.N., Gordon, J.R., 2001. Expression of transforming growth factor [beta], [beta], and basic fibroblast growth factor in full-thickness skin wounds of equine limbs and thorax. Veterinary Surgery 30, 269-277.

Theoret, C.L., Olutoye, O.O., Parnell, L.K., Hicks, J., 2013. Equine exuberant granulation tissue and human keloids: a comparative histopathologic study. Vet Surg 42, 783-789.

Theoret, C.L., Wilmink, J.M., 2013. Aberrant wound healing in the horse: naturally occurring conditions reminiscent of those observed in man. Wound Repair Regen 21, 365-371.

Tholouli, E., Sweeney, E., Barrow, E., Clay, V., Hoyland, J.A., Byers, R.J., 2008. Quantum dots light up pathology. J Pathol 216, 275-285.

Timmermans, F., Plum, J., Yoder, M.C., Ingram, D.A., Vandekerckhove, B., Case, J., 2009. Endothelial progenitor cells: identity defined? J Cell Mol Med 13, 87-102.

Toupadakis, C.A., Wong, A., Genetos, D.C., Cheung, W.K., Borjesson, D.L., Ferraro, G.L., Galuppo, L.D., Leach, J.K., Owens, S.D., Yellowley, C.E., 2010. Comparison of the osteogenic potential of equine mesenchymal stem cells from bone marrow, adipose tissue, umbilical cord blood, and umbilical cord tissue. Am J Vet Res 71, 1237-1245.

Tracey, A.K., Alcott, C.J., Schleining, J.A., Safayi, S., Zaback, P.C., Hostetter, J.M., Reinerston, E.L., 2014. The effects of topical oxygen therapy on equine distal limb dermal wound healing. Can Vet J 55, 1146-1152.

Tsang, A.S., Dart, A.J., Sole-Guitart, A., Dart, C.M., Perkins, N.R., Jeffcott, L.B., 2017. Comparison of the effects of topical application of UMF20 and UMF5 manuka honey with a generic multifloral honey on wound healing variables in an uncontaminated surgical equine distal limb wound model. Aust Vet J 95, 333-337.

Usui, M.L., Mansbridge, J.N., Carter, W.G., Fujita, M., Olerud, J.E., 2008. Keratinocyte migration, proliferation, and differentiation in chronic ulcers from patients with diabetes and normal wounds. J Histochem Cytochem 56, 687-696.

Vasyliev, R.G., Oksymets, V.M., Rodnichenko, A.E., Zlatska, A.V., Gubar, O.S., Gordiienko, I.M., Zubov, D.O., 2017. Tissue engineered bone for treatment of combat related limb injuries. Exp Oncol 39, 191-196.

Vidal, M.A., Robinson, S.O., Lopez, M.J., Paulsen, D.B., Borkhsenious, O., Johnson, J.R., Moore, R.M., Gimble, J.M., 2008. Comparison of chondrogenic potential in equine mesenchymal stromal cells derived from adipose tissue and bone marrow. Vet Surg 37, 713-724.

Wang, P.H., Huang, B.S., Horng, H.C., Yeh, C.C., Chen, Y.J., 2018. Wound healing. J Chin Med Assoc 81, 94-101.

Wang, X.X., Yang, J.X., Pan, Y.Y., Zhang, Y.F., 2015. Protective effects of tanshinone A on endothelial progenitor cells injured by tumor necrosis factor-alpha. Mol Med Rep 12, 4055-4062.

Watts, A.E., Yeager, A.E., Kopyov, O.V., Nixon, A.J., 2011. Fetal derived embryonic-like stem cells improve healing in a large animal flexor tendonitis model. Stem Cell Res Ther 2, 4.

Werb, Z., 1997. ECM and cell surface proteolysis: regulating cellular ecology. Cell 91, 439-442.

Wilke, M.M., Nydam, D.V., Nixon, A.J., 2007. Enhanced early chondrogenesis in articular defects following arthroscopic mesenchymal stem cell implantation in an equine model. J Orthop Res 25, 913-925.

Wilmink, J.M., van Herten, J., van Weeren, P.R., Barneveld, A., 2002. Retrospective study of primary intention healing and sequestrum formation in horses compared to ponies under clinical circumstances. Equine Vet J 34, 270-273.

Wilmink, J.M., van Weeren, P.R., 2005. Second-intention repair in the horse and pony and management of exuberant granulation tissue. Vet Clin North Am Equine Pract 21, 15-32.

Wilmink, J.M., Van Weeren, P.R., Stolk, P.W.T., Van Mil, F.N., Barneveld, A., 1999. Differences in second-intention wound healing between horses and ponies: histological aspects. Equine Vet J 31, 61-67.

Winter, R.L., Seeto, W.J., Tian, Y., Caldwell, F.J., Lipke, E.A., Wooldridge, A.A., 2018. Growth and function of equine endothelial colony forming cells labeled with semiconductor quantum dots. BMC Vet Res 14, 247.

Wu, X., Liu, H., Liu, J., Haley, K.N., Treadway, J.A., Larson, J.P., Ge, N., Peale, F., Bruchez, M.P., 2003. Immunofluorescent labeling of cancer marker Her2 and other cellular targets with semiconductor quantum dots. Nat Biotechnol 21, 41-46.

Yamada, A.L.M., Alvarenga, M.L., Brandao, J.S., Watanabe, M.J., Rodrigues, C.A., Hussni, C.A., Alves, A.L.G., 2016. PRP-gel scaffold associated with mesenchymal stem cells: use in experimental chondral defect of equine models. Pesquisca Veterinaria Brasileira 36, 461-467.

Yang, J.X., Pan, Y.Y., Zhao, Y.Y., Wang, X.X., 2013. Endothelial progenitor cell-based therapy for pulmonary arterial hypertension. Cell Transplant 22, 1325-1336.

Yang, J.X., Tang, W.L., Wang, X.X., 2010. Superparamagnetic iron oxide nanoparticles may affect endothelial progenitor cell migration ability and adhesion capacity. Cytotherapy 12, 251-259.

Yasuda, T., Weisel, R.D., Kiani, C., Mickle, D.A., Maganti, M., Li, R.K., 2005. Quantitative analysis of survival of transplanted smooth muscle cells with real-time polymerase chain reaction. J Thorac Cardiovasc Surg 129, 904-911.

Yoder, M.C., Mead, L.E., Prater, D., Krier, T.R., Mroueh, K.N., Li, F., Krasich, R., Temm, C.J., Prchal, J.T., Ingram, D.A., 2007. Redefining endothelial progenitor cells via clonal analysis and hematopoietic stem/progenitor cell principals. Blood 109, 1801-1809.

Yuan, R., Rao, T., Cheng, F., Yu, W.M., Ruan, Y., Zhang, X.B., Larre, S., 2018. Quantum dot-based fluorescent probes for targeted imaging of the EJ human bladder urothelial cancer cell line. Exp Ther Med 16, 4779-4783.

Yukawa, H., Mizufune, S., Mamori, C., Kagami, Y., Oishi, K., Kaji, N., Okamoto, Y., Takeshi, M., Noguchi, H., Baba, Y., Hamaguchi, M., Hamajima, N., Hayashi, S., 2009. Quantum dots for labeling adipose tissue-derived stem cells. Cell Transplant 18, 591-599.

Zhang, G., Hu, Q., Braunlin, E.A., Suggs, L.J., Zhang, J., 2008. Enhancing efficacy of stem cell transplantation to the heart with a PEGylated fibrin biomatrix. Tissue Eng Part A 14, 1025-1036.

Zhang, L., Chang, M., Beck, C.A., Schwarz, E.M., Boyce, B.F., 2016. Analysis of new bone, cartilage, and fibrosis tissue in healing murine allografts using whole slide imaging and a new automated histomorphometric algorithm. Bone Res 4, 15037.

Zhang, M., Methot, D., Poppa, V., Fujio, Y., Walsh, K., Murry, C.E., 2001. Cardiomyocyte grafting for cardiac repair: graft cell death and anti-death strategies. J Mol Cell Cardiol 33, 907-921.

Zhang, Y., Herbert, B.S., Rajashekhar, G., Ingram, D.A., Yoder, M.C., Clauss, M., Rehman, J., 2009. Premature senescence of highly proliferative endothelial progenitor cells is induced by tumor necrosis factor-alpha via the p38 mitogen-activated protein kinase pathway. FASEB J 23, 1358-1365.

Zhang, Y., Li, Y., Wang, S., Han, Z., Huang, X., Li, S., Chen, F., Niu, R., Dong, J.F., Jiang, R., Zhang, J., 2013. Transplantation of expanded endothelial colony-

forming cells improved outcomes of traumatic brain injury in a mouse model. J Surg Res 185, 441-449.

Zhao, P., Xu, Q., Tao, J., Jin, Z., Pan, Y., Yu, C., Yu, Z., 2018. Near infrared quantum dots in biomedical applications: current status and future perspective. Wiley Interdiscip Rev Nanomed Nanobiotechnol 10, e1483.

Zhou, W.C., Zhang, Q.B., Qiao, L., 2014. Pathogenesis of liver cirrhosis. World J Gastroenterol 20, 7312-7324.

Zubin, E., Conti, V., Leonardi, F., Zanichelli, S., Ramoni, R., Grolli, S., 2015. Regenerative therapy for the management of a large skin wound in a dog. Clin Case Rep 3, 598-603.

Appendix A Preliminary Research for Mitomycin C Dose Determination

A

	Control	Mitomycin C (10 µg/mL)	Mitomycin C (20 µg/mL)
Time of Cell Seeding	500,000	500,000	500,000
24h	1,750,000	1,600,000	1,375,000
32h	3,350,000	3,200,000	3,000,000
48h	8,500,000	5,500,000	2,962,500
72h		7,000,000	2,800,000

B

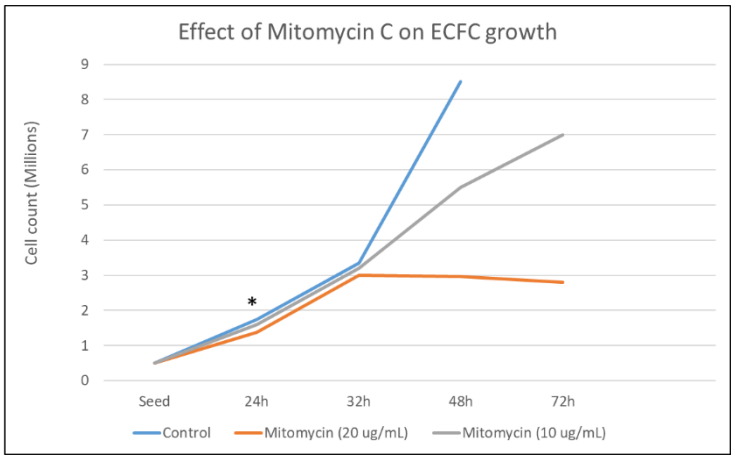

Cell growth data of equine ECFCs with and without exposure to mitomycin C. A) Total number of cells at various time points with and without mitomycin C (MMC).
B) Graphical representation of control cells and cells exposed to 10 µg/mL or 20 µg/mL MMC. * indicates time of MMC exposure.

Appendix B Variation in Relative Percentage of Wound and Non-Wound Regions from Biopsies

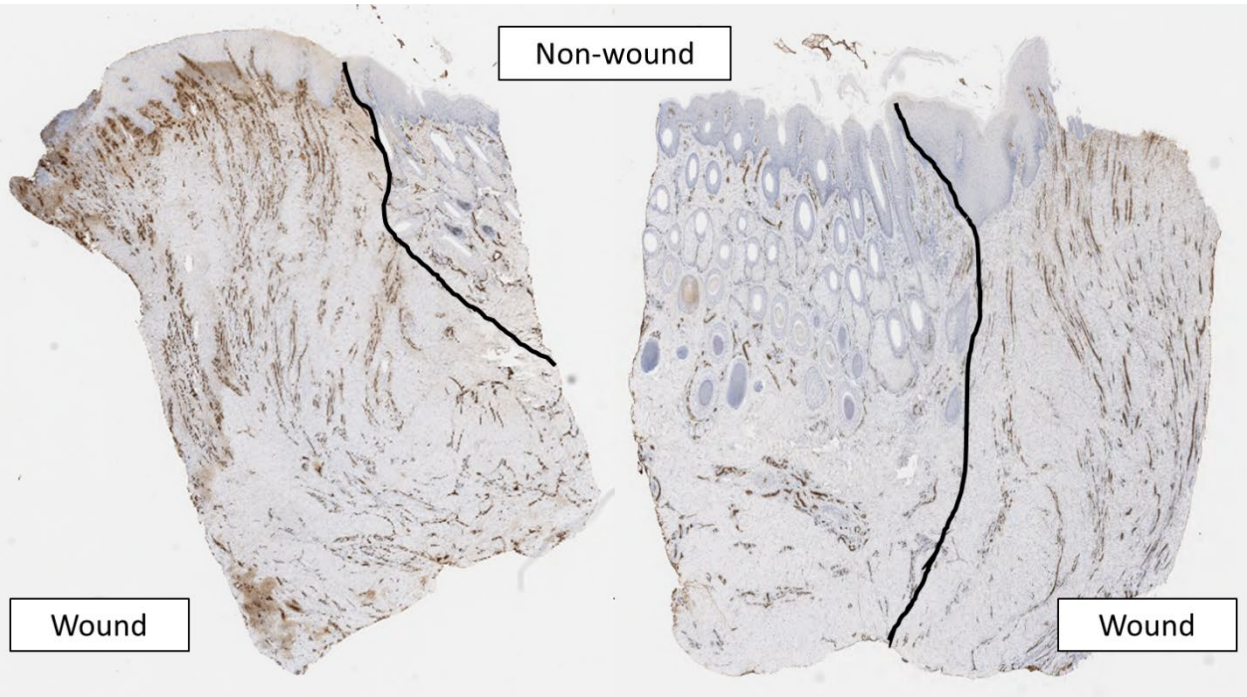

Variation in the relative percentage of Wound and Non-Wound tissue present in biopsies existed as demonstrated by these representative photomicrographs. The black line marks the demarcation between epithelialized skin at the periphery of the surgically-induced wound (Non-Wound region) and the healing wound (Wound region). In part due to this variation, 8 mm punch biopsies were obtained in the second half of the study instead of the 6 mm punch biopsies used in the first half of the study.

Appendix C Variation in Size and Staining Characteristics from Biopsies

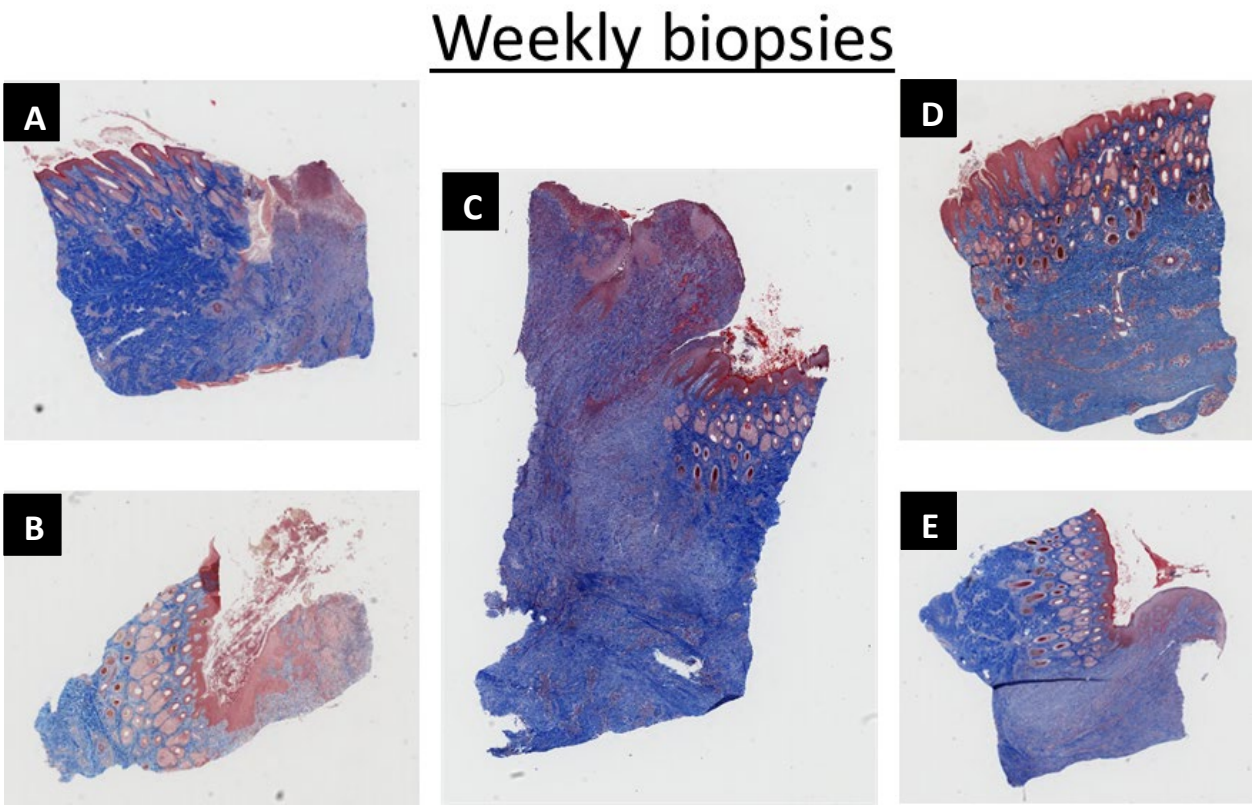

Variation in the size, shape, and staining characteristics of the biopsies is demonstrated by these representative photomicrographs. The biopsies pictured were obtained from the wound periphery at weekly intervals. Samples from week 1 (A), week 2 (B, C), week 3 (D), and week 4 (E) biopsies stained with Masson's trichrome. Although the staining variation was accounted for in the Visiopharm algorithms, this may have impacted analysis. In part due to this variation observed, 8 mm punch biopsies were obtained in the second half of the study instead of the 6 mm punch biopsies used in the first half of the study.

Appendix D Horse-specific Variation in WSA, GS, and Wound Temperature

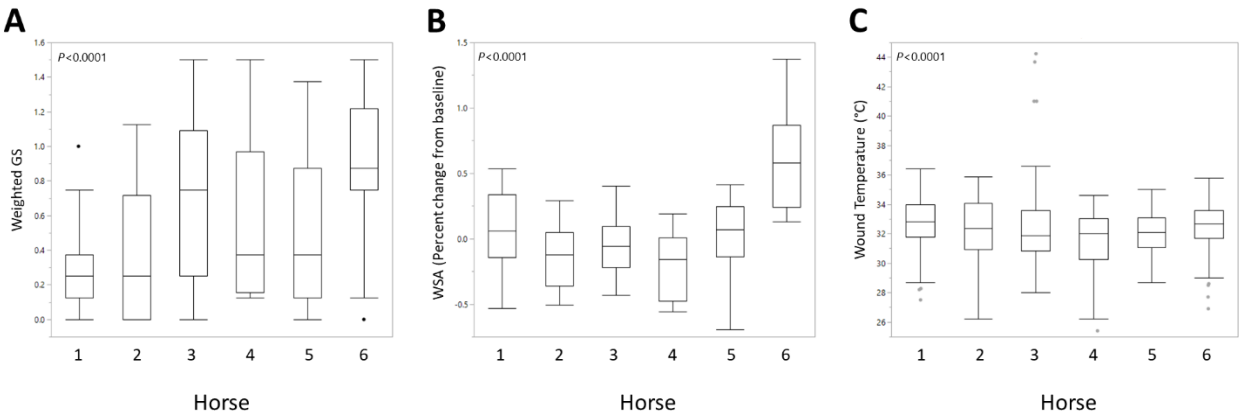

Variation in weighted granulation scores (A), wound surface area presented as percent change from baseline (B), and wound temperature in degrees Celsius (C) attributable to the individual horse. All time points are included in these figures, and there is significant variation present (P<0.0001). Data are presented as box-and-whisker plots, with median values represented by the horizontal lines and the interquartile range represented by the box. Grey dots are values that are 1.5 times the box length above the 75th percentile. The ends of the whiskers represent the smallest and largest values not classified as outliers.

Appendix E Horse-specific Variation of IHC Stain Quantification in Week 1 Biopsies

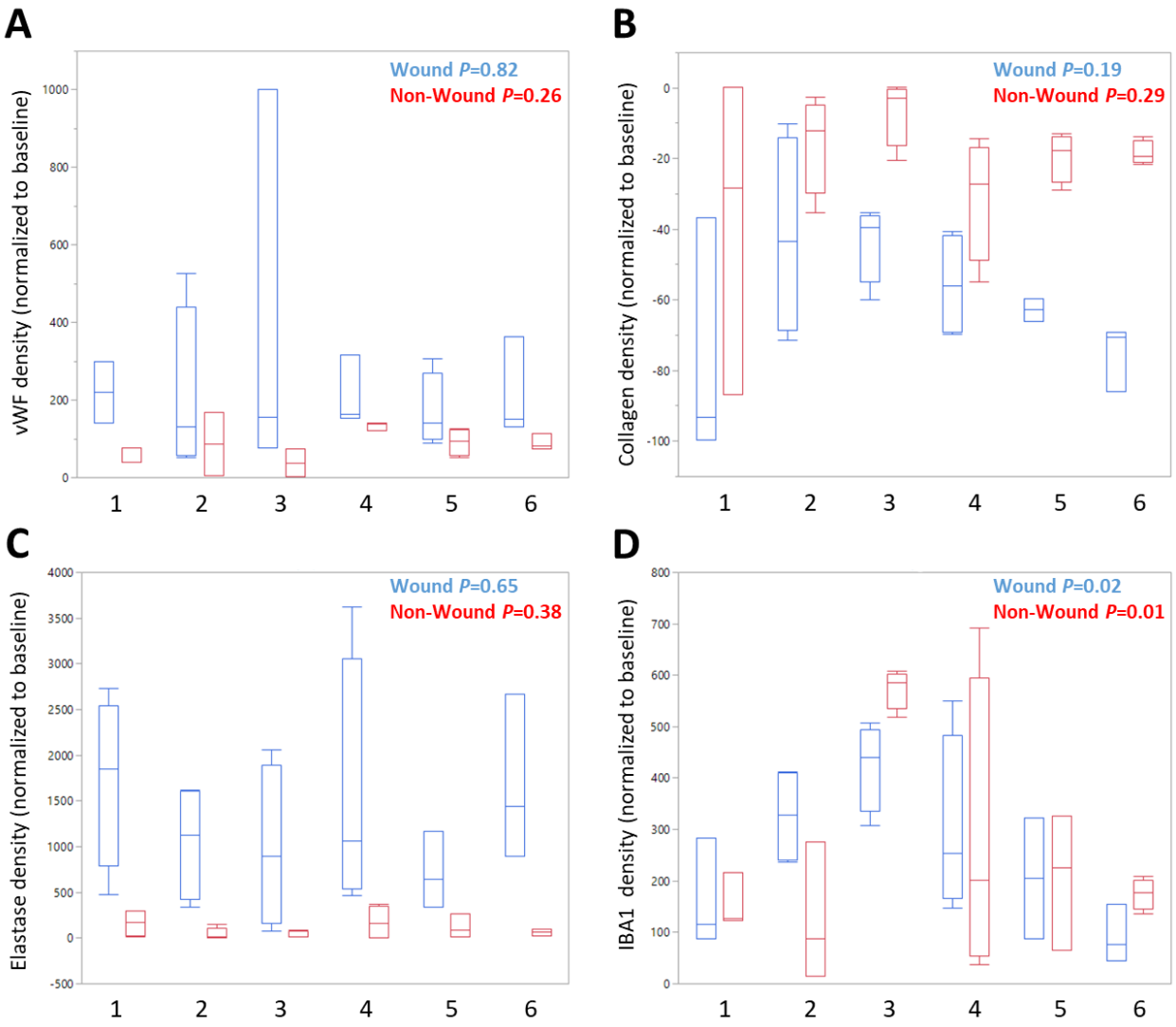

Variation in the immunohistochemical stain quantification of von Willebrand factor (A), collagen as quantified by Masson's Trichrome stain (B), Elastase (C), and IBA1 (D) attributable to the individual horse from Week 1 biopsies. Wound (blue) and Non-Wound (red) regions of analysis are presented as well as results from statistical analyses (corresponding blue and red colors). Data are presented as box-and-whisker plots, with median values represented by the horizontal lines and the interquartile range represented by the box. Grey dots are values that are 1.5 times the box length above the 75th percentile. The ends of the whiskers represent the smallest and largest values not classified as outliers.

Appendix F Horse-specific Variation of IHC Stain Quantification in Week 4 Biopsies

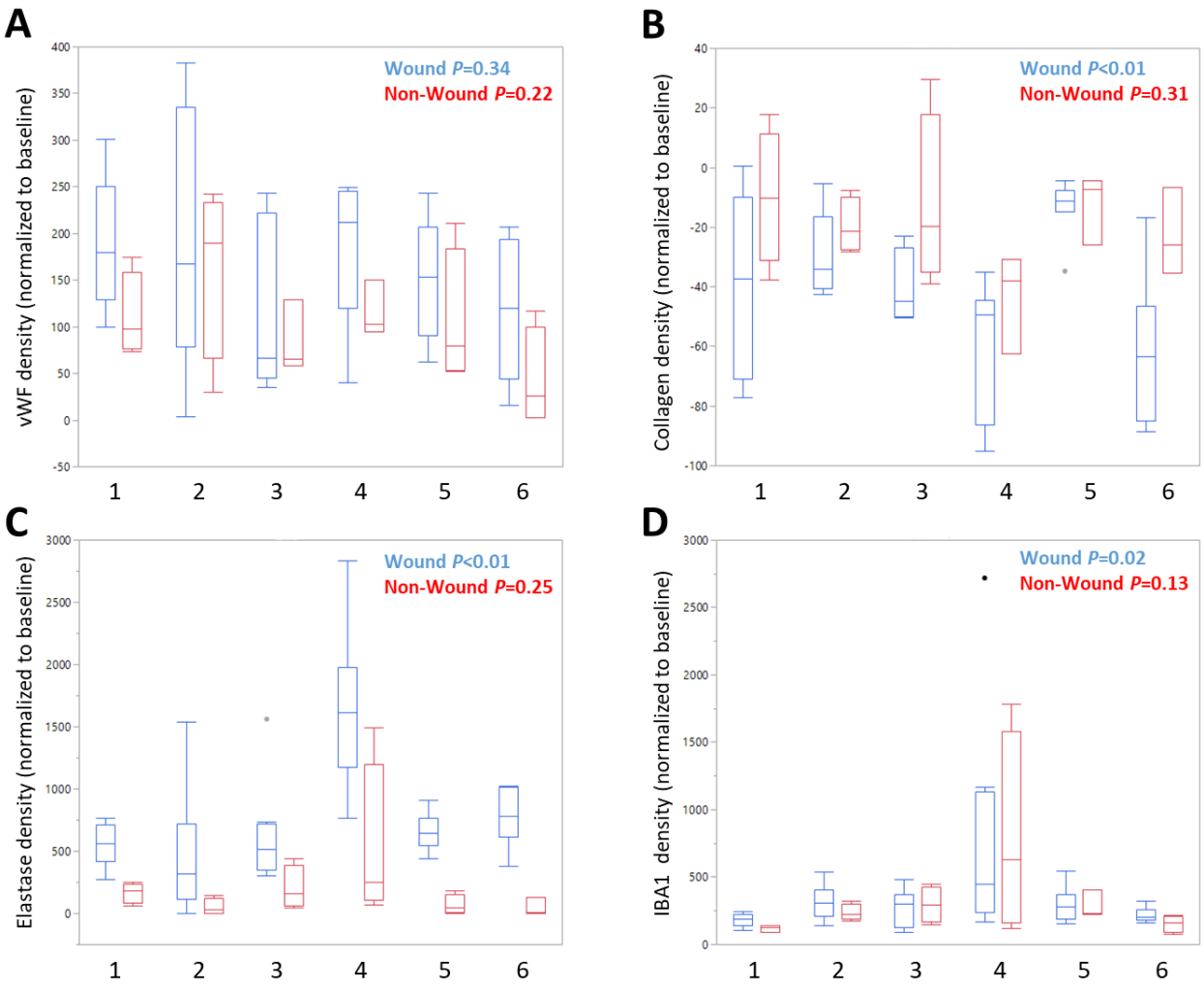

Variation in the immunohistochemical stain quantification of von Willebrand factor (A), collagen as quantified by Masson's Trichrome stain (B), Elastase (C), and IBA1 (D) attributable to the individual horse from Week 4 biopsies. Wound (blue) and Non-Wound (red) regions of analysis are presented as well as results from statistical analyses (corresponding blue and red colors). Data are presented as box-and-whisker plots, with median values represented by the horizontal lines and the interquartile range represented by the box. Grey dots are values that are 1.5 times the box length above the 75th percentile. The ends of the whiskers represent the smallest and largest values not classified as outliers.